Wissenschaftszentrum Weihenstephan für Ernährung, Landnutzung und Umwelt

Lehrstuhl Experimentelle Genetik

# Mitochondrial copper overload in a rat model for Wilson disease is paralleled by upregulated COX17 and can be restored using the bacterial peptide methanobactin

Christin Leitzinger

Vollständiger Abdruck der von der Fakultät Wissenschaftszentrum Weihenstephan für Ernährung, Landnutzung und Umwelt der Technischen Universität München zur Erlangung des akademischen Grades eines

Doktors der Naturwissenschaften

genehmigten Dissertation.

| | |
|---|---|
| Vorsitzende: | Univ.-Prof. Dr. Dr. Hannelore Daniel |
| Prüfer der Dissertation: | 1. apl. Prof. Dr. Dr. Jerzy Adamski |
| | 2. Univ.-Prof. Dr. Martin Klingenspor |

Die Dissertation wurde am 26.10.2016 bei der Technischen Universität München eingereicht und durch die Fakultät Wissenschaftszentrum Weihenstephan für Ernährung, Landnutzung und Umwelt am 03.02.2017 angenommen.

# Table of contents

**List of figures ........ XI**

**List of supplementary figures ........ XIII**

**List of tables ........ XIV**

**List of supplementary tables ........ XV**

**Summary ........ 1**

**Zusammenfassung ........ 3**

**1 Introduction ........ 7**
1.1 Wilson disease: a copper-storage disease with progressive hepatolenticular degeneration ........ 7
1.2 Mitochondria – essential copper-dependent cell organelles that are affected in Wilson disease ........ 8
1.3 Treatment of Wilson disease using copper chelators ........ 12
1.4 Methanobactin – a peptide with a very high affinity for copper ........ 13
1.5 The LPP rat as an animal model for studying mitochondrial alterations in Wilson disease ........ 14
1.6 Aim of this study ........ 15

**2 Material and Methods ........ 17**
2.1 Material ........ 17
2.1.1 Cell line ........ 17
2.1.2 Bacteria ........ 17
2.1.3 Plasmid and enzymes ........ 17
2.1.4 Oligonucleotides ........ 17
2.1.5 Media ........ 18
2.1.6 Chemicals ........ 19
2.1.7 Solutions and buffers ........ 22
2.1.8 Antibodies ........ 23
2.1.9 Kits ........ 24
2.1.10 Equipment and consumables ........ 24
2.1.11 Software ........ 28
2.2 Methods ........ 29
2.2.1 Wilson disease patient liver samples ........ 29
2.2.2 Animal experiments ........ 29
2.2.2.1 Animals ........ 29
2.2.2.2 Genotyping of LPP rats ........ 30
2.2.2.3 Examination of serum and plasma parameters and definition of animal disease states ........ 30
2.2.2.4 Animal treatments ........ 31
2.2.3 Cell culture experiments ........ 31
2.2.3.1 Cell cultivation ........ 31
2.2.3.2 Copper-histidine solution ........ 34
2.2.4 Isolation and analysis of mitochondria from liver tissue and HepG2 cells ........ 35

2.2.4.1 Subfractionation of human and rat liver tissue and isolation of liver mitochondria ........ 35
2.2.4.2 Isolation of mitochondria from HepG2 cells ........ 35
2.2.4.3 Measurement of the mitochondrial membrane fluidity ........ 35
2.2.4.4 Simultaneous measurement of MMP-loss and MPT-induction and curve sketching ........ 36
2.2.4.5 ATP synthesis ........ 37
2.2.5 Protein analyses ........ 37
2.2.5.1 Determination of mitochondrial and cellular protein concentration ........ 37
2.2.5.2 Immunoblot analyses ........ 37
2.2.5.3 Proteomic analyses of *Atp7b* rat liver mitochondria ........ 38
2.2.6 Molecular biological methods ........ 39
2.2.6.1 Knockdown of *COX17* in HepG2 cells using siRNA ........ 39
2.2.6.2 Overexpression of *COX17* in HepG2 cells ........ 39
2.2.6.3 Reverse transfection of HepG2 cells with *COX17* ........ 42
2.2.6.4 Quantitative realtime polymerase chain reaction (qRT-PCR) ........ 42
2.2.7 Chromatography of mitochondrial proteins ........ 42
2.2.7.1 Gel filtration ........ 43
2.2.7.2 Anion exchange chromatography ........ 43
2.2.8 Miscellaneous ........ 43
2.2.8.1 Immunoprecipitation ........ 43
2.2.8.2 Metal content determination ........ 44
2.2.8.3 Electron microscopy ........ 44
2.2.8.4 Immunohistochemistry ........ 45
2.2.9 Statistics ........ 45

**3 Results ........ 47**
3.1 The LPP *Atp7b*$^{-/-}$ rat – an animal model for liver failure in Wilson disease ........ 47
3.1.1 Progressing disease states in the Wilson disease LPP *Atp7b*$^{-/-}$ rat model ........ 47
3.1.2 Copper increasingly accumulates in liver homogenate and mitochondria from Wilson disease patients and *Atp7b*$^{-/-}$ rats with disease progression ........ 48
3.1.3 Structural alterations are comparable among mitochondria from Wilson disease patients and diseased *Atp7b*$^{-/-}$ rats ........ 49
3.1.4 Increasing mitochondrial copper load is paralleled by structural alterations of liver mitochondria from *Atp7b*$^{-/-}$ rats ........ 50
3.1.5 Mitochondrial membrane fluidity and swelling is reduced in *Atp7b*$^{-/-}$ rats with disease progression ........ 53
3.1.6 Mitochondrial function is increasingly harmed in *Atp7b*$^{-/-}$ rats with disease progression ........ 56
3.2 Methanobactin – a highly efficient agent to decopper liver mitochondria in a Wilson disease rat model ........ 58
3.2.1 Methanobactin efficiently decoppers HepG2 cells without severe toxic effects ........ 58
3.2.2 Short-term methanobactin treatment of *Atp7b*$^{-/-}$ rats decoppers liver mitochondria *in vivo* ........ 61
3.2.3 Acute treatment with methanobactin rescues diseased *Atp7b*$^{-/-}$ rats from liver failure ........ 65
3.2.4 A new treatment strategy for Wilson disease using methanobactin ........ 66

3.3 Increasing mitochondrial copper load is paralleled by COX17 upregulation ..... 69
3.4 COX17 upregulation is simulated in Cu-His treated HepG2 WT cells ..... 77
3.4.1 Millimolar Cu-His concentrations are toxic to HepG2 WT cells ..... 77
3.4.2 Treatment of HepG2 WT cells with rising Cu-His concentrations raises cellular and mitochondrial copper load ..... 78
3.4.3 Cu-His treatment of HepG2 WT cells increases cellular and mitochondrial COX17 abundance ..... 79
3.4.4 COX17+ cells are less susceptible towards Cu-His than COX17- cells ..... 80
3.4.4.1 Establishing *COX17* knockdown and overexpression ..... 81
3.4.4.2 *COX17* protects HepG2 cells against toxic Cu-His ..... 83

**4 Discussion ..... 85**
4.1 The LPP rat as an animal model for studying alterations of liver mitochondria in Wilson disease ..... 85
4.1.1 Liver mitochondrial damage in diseased *Atp7b*$^{-/-}$ rats is highly comparable to that observed in Wilson disease ..... 85
4.1.2 The detrimental effect of mitochondrial copper overload in *Atp7b*$^{-/-}$ rats ..... 86
4.2 Methanobactin – a highly efficient treatment prevents disease progression in a Wilson disease rat model ..... 88
4.2.1 Methanobactin efficiently decoppers HepG2 cells ..... 88
4.2.2 Short-term methanobactin treatment prevents acute liver failure in *Atp7b*$^{-/-}$ rats ..... 89
4.2.3 Methanobactin – a new treatment strategy to decopper liver mitochondria in Wilson disease ..... 90
4.3 COX17 – balancing the mitochondrial copper overload in Wilson disease ..... 91
4.3.1 COX17 upregulation for the export of excess mitochondrial copper ..... 91
4.3.2 Upregulation of *COX17* protects HepG2 cells towards Cu-His-induced damage ..... 94
4.3.3 Possible interaction partners of COX17 in Wilson disease are involved in maintaining the mitochondrial structure and energy production ..... 96

**5 Conclusions ..... 99**

**6 References ..... 101**

**Supplement ..... CXVII**

**List of publications ..... CXXV**

**Contributions ..... CXXVII**

**Proof of figures and tables taken from published articles ..... CXXIX**

**Acknowledgements ..... CXXXI**

# List of abbreviations

| | |
|---|---|
| ADP | adenosine diphosphate |
| Af | affected *Atp7b*$^{-/-}$ rat |
| ANT | adenine nucleotide transporter |
| APS | ammonium persulfate |
| AST | aspartate aminotransferase |
| ATOX1 | antioxidant 1 copper chaperone |
| ATP | adenosine triphosphate |
| bp | base pairs |
| BSA | bovine serum albumin |
| bw | body weight |
| CCCP | carbonyl cyanide m-chlorophenyl hydrazone |
| CcO | cytochrome c oxidase |
| CCS1 | copper chaperone for superoxide dismutase |
| cDNA | complementary DNA |
| CHCHD6 | coiled-coil-helix-coiled-coil-helix domain containing 6 (MICOS complex subunit Mic25) |
| Co | control *Atp7b*$^{+/-}$ rat |
| COX17 | cytochrome c oxidase assembly protein |
| COX17- | HepG2 cells with *COX17* knockdown |
| COX17+ | HepG2 cells with *COX17* overexpression |
| cp | ceruloplasmin |
| Cp | crossing point |
| CS | mitochondrial citrate synthase |
| CTR1 | copper transporter 1 |
| Cu-His | copper-histidine solution |
| CypD | cyclophilin D |
| CysA | cyclosporine A |
| Di | diseased *Atp7b*$^{-/-}$ rat |
| DMEM | Dulbecco's modified eagle medium |
| DNA | deoxyribonucleic acid |
| dNTP | deoxyribonucleotide triphosphate |
| Do | disease onset *Atp7b*$^{-/-}$ rat |
| D-PA | D-penicillamine |
| DPH | 1,6-diphenyl-1,3,5-hexatriene |
| EDTA | ethylenediaminetetraacetic acid |
| EGTA | ethylene glycol-bis(2-aminoethylether)-N,N,N′,N′-tetraacetic acid |
| EM | electron microscopy |
| em | emission |
| ex | excitation |
| f | female |

| | |
|---|---|
| FCCP | carbonyl cyanide-p-trifluoromethoxyphenylhydrazone |
| FCS | fetal calf serum |
| fw | forward |
| GAPDH | glyceraldehyde 3-phosphate dehydrogenase |
| HepG2 | human hepatocellular carcinoma cells |
| HPLC | high performance liquid chromatography |
| i.p. | intraperitoneal |
| ICP-OES | inductively coupled plasma optical emission spectrometry |
| IEX_F | ionic exchange fraction |
| IMS | intermembrane space |
| IP | isolation buffer |
| kDa | kilo dalton |
| LEC | Long-Evans-Chinnamon rat |
| LPP | crossbreed between the Long-Evans-Cinnamon (LEC) rat and the Piebald Virol Glaxo (PVG) rat, defective in *PINA* and *Atp7b* (for more information on *PINA* see [2]) |
| m | male |
| MB | methanobactin |
| MEM | minimum essential medium |
| MIA40 | mitochondrial intermembrane space import and assembly protein 40 |
| MICOS | mitochondrial contact site and cristae organisation system |
| MIM | mitochondrial inner membrane |
| MMP, $\Delta\Psi$ | mitochondrial transmembrane potential |
| Mo | moribund *Atp7b*$^{-/-}$ rat |
| MOM | mitochondrial outer membrane |
| MOPS | 4-morpholinepropanesulfonic acid |
| mPol | milli polarisation |
| MPT | mitochondrial permeability transition |
| mRNA | messenger RNA |
| NAO | nonyl acridine orange |
| NEAA | non-essential amino acids solution |
| No. | number |
| OXPHOS | oxidative phosphorylation |
| PBS | phosphate buffered saline |
| PCR | polymerase chain reaction |
| Pen/Strep | penicillin/streptomycin |
| Pi | inorganic phosphate |
| ppm | parts per million |
| PVG | Piebald Virol Glaxo rat |
| qRT-PCR | quantitative realtime polymerase chain reaction |
| rev | reverse |
| Rh123 | rhodamine 123 |
| RNA | ribonucleic acid |

| | |
|---|---|
| RPII | RNA polymerase II |
| SCO1 | cytochrome c oxidase assembly protein SCO1 |
| SDS | sodium dodecyl sulfate |
| siRNA | silencing ribonucleic acid |
| SOD1 | copper-zinc dependent superoxide dismutase |
| *Taq* | *Thermus aquaticus* |
| TBE | TRIS-borate-EDTA |
| TBS | TRIS-buffered saline |
| TBS-T | TBS with tween |
| TEMED | tetramethylethylenediamine |
| TES | N-[Tris(hydroxymethyl)methyl]-2-aminoethanesulfonic acid |
| TETA | trientine |
| TMA-DPH | 1-(4-(trimethylamino)phenyl)-6-phenylhexa-1,3,5-triene |
| TRIS | tris(hydroxymethyl)aminomethane |
| TTM | ammonium tetrathiomolybdate |
| U | untreated *Atp7b*$^{-/-}$ rat |
| UV | ultraviolet |
| w. w. | wet weight |
| WD | Wilson disease |
| WT | wild type |

# List of figures

Figure 1-1 Impairment of copper metabolism in Wilson disease patients in comparison to healthy humans [45]. 8
Figure 1-2 Structure of liver mitochondria *in situ* and isolated (rat liver). 9
Figure 1-3 Protein complexes of the oxidative phosphorylation within the mitochondrial inner membrane [96]. 10
Figure 1-4 Copper sorting and delivery within the mitochondrial intermembrane space [128]. 11
Figure 1-5 LPP rat – an animal model for studying mitochondrial alterations in Wilson disease (© photo by Christin Leitzinger). 14
Figure 3-1 Copper load in liver homogenate and liver mitochondria increases with disease progression of *Atp7b*$^{-/-}$ rats and is highly comparable to untreated WD patients. 49
Figure 3-2 Mitochondrial structure impairments are highly similar between WD patients and diseased *Atp7b*$^{-/-}$ rats *in situ*. 50
Figure 3-3 Mitochondrial structural alterations are absent in *Atp7b*$^{+/-}$ control rat livers and increase with disease progression of *Atp7b*$^{-/-}$ rats. 51
Figure 3-4 Disease progression of *Atp7b*$^{-/-}$ rats is paralleled by massive structural alterations of isolated rat liver mitochondria. 52
Figure 3-5 Mitochondrial membrane fluidity is reduced at the lipid-water interface in isolated *Atp7b*$^{-/-}$ rat liver mitochondria. 54
Figure 3-6 Mitochondrial swelling is reduced in *Atp7b*$^{-/-}$ rats with disease progression compared to *Atp7b*$^{+/-}$ rats. 55
Figure 3-7 Inhibition of calcium-induced swelling with CysA is increasingly harmed in liver mitochondria isolated from *Atp7b*$^{-/-}$ rats with disease progression compared to *Atp7b*$^{+/-}$ rats. 56
Figure 3-8 Mitochondrial transmembrane potential is less stable in liver mitochondria isolated from *Atp7b*$^{-/-}$ rats with disease progression compared to liver mitochondria from *Atp7b*$^{+/-}$ rats. 57
Figure 3-9 ATP production is increasingly harmed in liver mitochondria isolated from *Atp7b*$^{-/-}$ rats with disease progression compared to *Atp7b*$^{+/-}$ rats. 57
Figure 3-10 D-PA, TETA and MB are less toxic to HepG2 cells than TTM. 59
Figure 3-11 MB induces an intermediate loss of MMP after two hours of treatment which is recovered after six hours. 60

Figure 3-12 In contrast to TTM, D-PA and TETA, MB significantly reduces cellular copper concentration in copper-preloaded HepG2 cells. .......... 61
Figure 3-13 In contrast to D-PA and TETA, short-term MB treatment of *Atp7b*$^{-/-}$ rats reduces the liver damage marker AST. ...................................... 62
Figure 3-14 Short-term MB treatment of *Atp7b*$^{-/-}$ rats reduces copper burden in liver homogenate and isolated rat liver mitochondria. .......................... 63
Figure 3-15 Short-term MB but not D-PA or TETA treatment of *Atp7b*$^{-/-}$ rats normalises mitochondrial structure. ................................................... 64
Figure 3-16 Acute MB treatment normalises the structure of liver mitochondria in *Atp7b*$^{-/-}$ rats. ........................................................................ 65
Figure 3-17 In contrast to D-PA and TETA, short-term MB treatment reverses ATP production in liver mitochondria isolated from *Atp7b*$^{-/-}$ rats. .......... 66
Figure 3-18 Short-term MB treatment postpones the onset of liver failure in *Atp7b*$^{-/-}$ rats for at least two weeks. .................................................. 67
Figure 3-19 Subfractionated *Atp7b*$^{-/-}$ rat liver mitochondria have an increased copper load compared to *Atp7b*$^{+/-}$ rats. ............................................... 70
Figure 3-20 Protein amount of mitochondrial COX17 increases with disease progression of *Atp7b*$^{-/-}$ rats and is comparable to that from WD patients. .................................................................................. 73
Figure 3-21 Amount of COX17 positive liver cells increases in liver tissue with disease progression of *Atp7b*$^{-/-}$ rats. ................................................... 74
Figure 3-22 ACAD11 and CHCHD6 are possible interaction partners of COX17 in situations with elevated copper, such as Wilson disease. ................. 76
Figure 3-23 Millimolar Cu-His concentrations are toxic to HepG2 WT cells. ........... 77
Figure 3-24 Treatment of HepG2 WT cells with increasing Cu-His concentrations induces a raise in cellular and mitochondrial copper load. ........................................................................................ 79
Figure 3-25 Treating HepG2 WT cells with increasing Cu-His concentrations raises cellular and mitochondrial abundance of COX17. ...................... 80
Figure 3-26 Knockdown of *COX17* in HepG2 cells reduces *COX17* level for up to 95% relative to the nonsilencing control. ........................................ 81
Figure 3-27 Overexpression of *COX17* in HepG2 cells increases cellular COX17 level up to 2.5-fold relative to the vector control. ..................... 82

# List of supplementary figures

Supplementary Figure 1 Treatment of HepG2 cells with MB reduces cellular copper load for approximately 50% compared to untreated control cells. ............................ CXVII

Supplementary Figure 2 Single cell-based analysis shows an increase of COX17 positive liver cells with disease progression of *Atp7b*$^{-/-}$ rats. ......................................... CXVIII

Supplementary Figure 3 COX17- cells are more susceptible towards Cu-His compared to non-transfected HepG2 WT cells and COX17+ cells. ............................................... CXIX

# List of tables

Table 2-1 Oligonucleotides ..... 17
Table 2-2 Media and additives for subcultivation of HepG2 cells ..... 18
Table 2-3 Media composition for subcultivation and treatment of HepG2 cells ..... 19
Table 2-4 Chemicals ..... 19
Table 2-5 Solutions and buffers ..... 22
Table 2-6 Antibodies used for immunoblot analysis and immunohistochemistry ..... 23
Table 2-7 Commercially available kits ..... 24
Table 2-8 Equipment ..... 25
Table 2-9 Tools ..... 26
Table 2-10 Consumables ..... 27
Table 2-11 Software ..... 28
Table 2-12 Treatment of LPP *Atp7b*$^{-/-}$ rats ..... 31
Table 2-13 Concentration and respective dose of Cu-His used for several assays ..... 34
Table 2-14 Inducers for measurement of MMP and swelling in mitochondria ..... 37
Table 2-15 Endonuclease treatment ..... 41
Table 3-1 Serum AST and bilirubin values enable the definition of different disease states of *Atp7b*$^{-/-}$ rats. ..... 47
Table 3-2 A new treatment regimen, consisting of intense MB treatment (3x/d i.p.) cycles interrupted by drug-free observation periods, postpones the disease onset in *Atp7b*$^{-/-}$ rats to more than 166 days of age. ..... 69
Table 3-3 Proteomic analysis of subfractionated rat liver mitochondria presents COX17 as an important protein for balancing the mitochondrial copper overload in *Atp7b*$^{-/-}$ rat liver mitochondria. ..... 71
Table 3-4 15 µM Cu-His reduces cellular proliferation and vitality of HepG2 WT cells for approximately 30%. ..... 78
Table 3-5 COX17- cells are more susceptible towards Cu-His treatment than COX17+ cells. ..... 84

# List of supplementary tables

Supplementary Table 1 Copper concentrations in liver homogenate and liver mitochondria progressively increase with disease progression of *Atp7b*$^{-/-}$ rats. ................................ CXX
Supplementary Table 2 Different treatment regimens enhance MB-induced mitochondrial decoppering in *Atp7b*$^{-/-}$ rats. ........................................................................ CXXI
Supplementary Table 3 The copper-binding proteins COX11 and SCO1 are up- or downregulated in one of the two subfractions of rat liver mitochondria. ............................ CXXII

# Summary

Wilson disease (WD) is an autosomal recessively inherited disorder of the copper metabolism. A loss-of-function mutation in the copper-transporting ATPase ATP7B impairs biliary copper excretion, causing progressive copper accumulation and damaging the liver and liver mitochondria, finally leading to fulminant hepatitis. In this thesis, liver mitochondria from LPP *Atp7b*$^{-/-}$ rats – an animal model for WD carrying the same genetic defect causing WD in humans – were investigated to further understand mitochondrial impairments in WD.

As liver mitochondria from human WD patients and *Atp7b*$^{-/-}$ rats show comparable copper loads and structural alterations, this animal model can be used for studies of mitochondrial impairments in WD. The liver damage markers serum aspartate aminotransferase and bilirubin define progressing disease states in *Atp7b*$^{-/-}$ rats. Increasing liver and mitochondrial copper load is observed with disease progression of untreated *Atp7b*$^{-/-}$ rats. The following impairments are found in liver mitochondria of these rats with disease progression and rising copper load: structural alterations, a decreasing fluidity of mitochondrial membranes, an impaired capacity to undergo large amplitude swelling (MPT) and a decreasing ability to block MPT by the addition of cyclosporine A and finally, the stability of the mitochondrial transmembrane potential decreases, leading to an impaired ATP production. Thus, reducing the mitochondrial copper load by copper chelating agents is the prime requirement for an effective treatment in this WD animal model.

Currently available copper chelation treatments in WD target mobilisation of liver copper and its excretion via the urine. D-penicillamine (D-PA) and trientine (TETA) – to be taken lifelong several times a day – have an intermediate copper affinity, mobilising copper from the liver tissue. This copper is excreted via the urine, but a part of it may possibly reach the brain leading to secondary neurologic damages. Decoppering of the liver using D-PA fails in 10–50% of WD patients, leaving liver transplantation the only available treatment possibility. Thus, it would be desirable to have a copper chelating agent with a higher copper affinity to avoid secondary brain damage, and a better efficiency to decopper liver mitochondria to avoid liver failure. Using the bacterial peptide methanobactin (MB) – produced by *Methylosinus trichosporium* OB3b and having a very high affinity for copper – the question is addressed whether it decoppers hepatocytes and liver mitochondria more efficient than D-PA or TETA. In contrast to D-PA, TETA and ammonium tetrathiomolybdate (TTM), MB significantly reduces the copper load in HepG2 cells for 30% within 24 hours without inducing cellular and mitochondrial toxicity. *Atp7b*$^{-/-}$ rats were treated short-term either intraperitoneally with

MB or orally with D-PA or TETA. Short-term MB treatment reduces initially elevated liver damage markers, paralleled by an efficient decoppering of whole liver and especially liver mitochondria. Further, MB restores the mitochondrial structure and ATP production. Using D-PA or TETA, liver damage markers cannot be reduced and mitochondrial decoppering is less efficient compared to MB. Mitochondrial decoppering by MB lasts several weeks and avoids disease progression in *Atp7b*$^{-/-}$ rats. These data indicate a possible new treatment strategy in WD: In contrast to the lifelong treatment in humans using D-PA or TETA, MB could be used for short, but intense decoppering phases followed by several drug-free weeks.

In liver mitochondria isolated from *Atp7b*$^{-/-}$ rats, copper load increases with disease progression. Elevated liver mitochondrial copper loads can be balanced up to approximately 7 nmol copper per mg mitochondrial protein, thereafter, the mitochondrial structure and function break down. Up to now, it is unknown how liver mitochondria deal with high copper concentrations in WD. To address this issue, protein abundances were analysed in copper-rich fractions from liver mitochondria isolated from both, either *Atp7b*$^{+/-}$ or *Atp7b*$^{-/-}$ rats. Using proteomic analyses, the copper-binding protein COX17 is identified to be upregulated in *Atp7b*$^{-/-}$ rats compared to *Atp7b*$^{+/-}$ rats. COX17 increases with rising mitochondrial copper load and this upregulation may be protective for mitochondria – an issue addressed in the last part of this thesis.

A cell culture model was established to analyse whether upregulation of COX17 is protective for copper-loaded *Atp7b*$^{-/-}$ rat liver mitochondria. Treating human hepatocytes (HepG2 cells) with copper-histidine (Cu-His) leads to an increase in cellular and mitochondrial copper and a parallel upregulation of COX17. Using this model, COX17 upregulation as observed in *Atp7b*$^{-/-}$ rats can be simulated. This model is further used to up- and downregulate *COX17* to analyse whether COX17 upregulation has a protective or damaging function in situations of copper overload. Downregulating *COX17* increases cellular susceptibility towards rising Cu-His concentrations and prolonged treatment with low Cu-His concentrations. HepG2 cells with upregulated *COX17* are less sensitive towards Cu-His. These data suggest that COX17 upregulation is protective in copper-loaded liver mitochondria.

# Zusammenfassung

Die Wilsonsche Erkrankung (Morbus Wilson) ist eine autosomal rezessiv vererbte Störung des Kupferstoffwechsels. Der genetische Defekt liegt in der kupfertransportierenden ATPase ATP7B und führt zu einer beeinträchtigten Ausscheidung von Kupfer über die Galle. Dies bewirkt eine erhebliche Akkumulation von Kupfer in der Leber und den Lebermitochondrien, die unbehandelt zu einer fulminanten Leberentzündung führt. In der vorliegenden Arbeit wurden Lebermitochondrien aus LPP *Atp7b*$^{-/-}$ Ratten untersucht, um mitochondriale Beeinträchtigungen der Wilsonschen Erkrankung besser zu verstehen. Bei der LPP *Atp7b*$^{-/-}$ Ratte handelt es sich um ein Tiermodell für Morbus Wilson, welches den gleichen genetischen Defekt trägt, der Morbus Wilson im Menschen hervorruft.

Es wird gezeigt, dass Lebermitochondrien von humanen Wilson-Patienten und *Atp7b*$^{-/-}$ Ratten eine vergleichbare Kupferbelastung und ähnliche strukturelle Veränderungen aufweisen. Daher ist dieses Tiermodell geeignet, um mitochondriale Beeinträchtigungen der Wilsonschen Erkrankung zu untersuchen. Steigende Marker für Leberschäden (Serum Aspartataminotransferase- und Bilirubin-Werte) definieren fortschreitende Krankheitsstadien in *Atp7b*$^{-/-}$ Ratten. Mit fortschreitendem Krankheitsstadium und zunehmender Kupferbelastung wurden folgende Beeinträchtigungen der Lebermitochondrien unbehandelter *Atp7b*$^{-/-}$ Ratten gefunden: zunehmende strukturelle Veränderungen, eine reduzierte Fluidität der mitochondrialen Membranen, der mitochondriale Permeabilitätsübergang (MPT) ist gestört und das Ausmaß des Anschwellens der Mitochondrien reduziert. Normalerweise kann der MPT durch die Zugabe von Cyclosporin A verhindert werden, jedoch ist diese Wirkung mit zunehmendem Krankheitsstadium der *Atp7b*$^{-/-}$ Ratten beeinträchtigt. Schließlich ist auch das mitochondriale Transmembranpotential weniger zeitstabil und geht mit einer gestörten ATP-Produktion einher. Daher ist die mitochondriale Entkupferung unter Verwendung hochaffiner kupferbindender Substanzen eine wichtige Voraussetzung, um *Atp7b*$^{-/-}$ Ratten zu therapieren.

Die aktuell verfügbare Therapie der Wilsonschen Erkrankung zielt darauf ab, das in der Leber vorhandene Kupfer zu mobilisieren und es über den Urin auszuscheiden. D-Penicillamin (D-PA) oder Trientin (TETA) müssen lebenslang mehrfach täglich eingenommen werden. Beide Substanzen haben eine mittlere Kupferaffinität und können somit das Kupfer in der Leber mobilisieren. Dieses Kupfer wird über den Urin ausgeschieden, wobei jedoch ein Teil dieser Komplexe möglicherweise zum Gehirn transportiert wird und zu sekundären neurologischen Schäden führt. Bei 10–50 % der Wilson-Patienten ist die Entkupferung der Leber unter Verwendung von D-PA ineffizient, sodass eine Lebertransplantation notwendig ist. Daher ist die Frage, ob andere Substanzen mit einer höheren Kupferaffinität Lebermitochondrien effizienter entkupfern, um sekundäre neurologische Schäden und Leberversagen zu verhindern. Unter Verwendung von Methanobactin (MB) – einem Peptid, welches von *Methylosinus trichosporium* OB3b produziert wird und eine sehr hohe Affinität für Kupfer aufweist – wurde diese Fragestellung bearbeitet. Im Gegensatz zu D-PA, TETA und Ammoniumtetrathiomolybdat (TTM) reduziert MB die Kupferbelastung in HepG2-Zellen innerhalb von 24 Stunden signifikant um 30 %. Toxische Effekte von MB werden im verwendeten Dosisbereich nicht beobachtet. Daher erhielten *Atp7b*$^{-/-}$ Ratten in einer Kurzzeitbehandlung intraperitoneal MB oder oral D-PA oder TETA. MB ist in der Lage, anfänglich erhöhte Marker für Leberschäden zu reduzieren, dabei die Leber und die Lebermitochondrien effektiv zu entkupfern und damit die mitochondriale Struktur und ATP-Produktion wieder herzustellen. D-PA und TETA können einen Leberschaden nicht reduzieren und die mitochondriale Entkupferung ist im Vergleich zu MB weniger effizient. Die mitochondriale Entkupferung durch MB bleibt für mehrere Wochen stabil und verhindert das Fortschreiten der Erkrankung im Tiermodell. Daher ist eine neue Behandlungsstrategie für die Wilsonsche Erkrankung denkbar: Im Gegensatz zu einer lebenslangen Behandlung mit D-PA oder TETA, könnte MB für eine intensive Kurzzeitbehandlung verwendet werden. Anschließend wären mehrere Wochen einer Behandlungspause möglich.

In Lebermitochondrien von *Atp7b*$^{-/-}$ Ratten wurde mit fortschreitender Erkrankung eine zunehmende Kupferbelastung gemessen. Die steigende Kupferbelastung können die Lebermitochondrien bis zu etwa 7 nmol Kupfer pro mg mitochondriales Protein regulieren. Übersteigt die mitochondriale Kupferbelastung diesen kritischen Punkt, kommt es zu einer irreversiblen Beeinträchtigung der mitochondrialen Struktur und Funktion. Gegenwärtig ist unbekannt, wie die Lebermitochondrien mit der hohen Kupferbelastung in der Wilsonschen Erkrankung umgehen. Um diese Frage zu untersuchen, wurden die Häufigkeiten verschiedener Proteine in kupferreichen Fraktionen der Lebermitochondrien von *Atp7b*$^{+/-}$ und *Atp7b*$^{-/-}$ Ratten analysiert. Anhand einer Proteomanalyse wurde das kupferbindende Protein COX17 identifiziert, welches im Vergleich zu *Atp7b*$^{+/-}$ Ratten in *Atp7b*$^{-/-}$ Ratten deutlich vermehrt vorkommt. Darüber hinaus steigt die Menge von COX17 mit zunehmender mitochondrialer Kupferbelastung an. Diese erhöhte Menge von COX17 könnte ein Schutzmechanismus für Mitochondrien vor hohen Kupferbelastungen sein – ein Aspekt, der im letzten Teil der Arbeit untersucht wird.

Ob die zunehmende Menge von COX17 einen Schutzmechanismus für kupferbelastete *Atp7b*$^{-/-}$ Rattenlebermitochondrien darstellt oder schädlich ist, wurde anhand eines

Zellkulturmodells untersucht. Durch die Behandlung von humanen Leberzellen (HepG2-Zellen) mit Histidin gebundenem Kupfer (Cu-His) konnte eine zum Tier vergleichbare zelluläre und mitochondriale Kupferbelastung und Erhöhung von COX17 simuliert werden. Anschließend wurde dieses Modell verwendet, um die Expression von *COX17* zu reduzieren und zu verstärken. Die Reduktion der *COX17* Expression erhöht die Empfindlichkeit der HepG2-Zellen gegenüber steigenden Cu-His-Konzentrationen und einer verlängerten Exposition gegenüber niedrigen Cu-His-Konzentrationen. HepG2-Zellen mit einer verstärkten Expression von *COX17* sind weniger empfindlich gegenüber Cu-His wie anhand der verbesserten Vitalität der Zellen dargestellt wird. Diese Ergebnisse deuten an, dass die steigende Menge von COX17 mit zunehmender Kupferbelastung der Lebermitochondrien zellprotektiv ist.

# 1 Introduction

## 1.1 Wilson disease: a copper-storage disease with progressive hepatolenticular degeneration

Wilson disease (WD) was first characterised by Samuel Alexander Kinnear Wilson in 1912 [3]. It is an autosomal recessively inherited disorder [4] of the copper metabolism [5]. Copper is an essential trace element [6, 7] that functions as a cofactor for several enzymes, for example the copper-zinc dependent superoxide dismutase (SOD1) or the mitochondrial cytochrome c oxidase (CcO) [7-15], being important for metabolic processes, such as antioxidative defense and mitochondrial respiration [16-22]. Approximately 2 mg copper per day is taken up via the nutrition [23-25]. It is actively absorbed by enterocytes [26, 27], bound to albumin or amino acids, especially histidine [28-30], and via the portal circulation it is transported to the liver [28, 31-33]. The copper transporter CTR1, located in the basolateral membrane of hepatocytes [34-36], mediates reduction of Cu(II) to Cu(I) at the plasma membrane [37] and the uptake of Cu(I) into liver cells (Figure 1-1) [25, 38]. Copper chaperones like ATOX1, COX17 and metallothioneins bind this copper in the cytosol [10-13, 39]. ATOX1 transports copper to the secretory pathway of hepatocytes through direct interactions with the P-type ATPase ATP7B (Figure 1-1) [39-42]. Depending on the cytosolic copper concentration, ATP7B changes its localisation and fulfils two functions [14]: Low copper concentrations stabilise the copper-binding at the trans-golgi network and provide the incorporation of copper into apoceruloplasmin [14, 43]. This leads to the production of functional ceruloplasmin which is excreted into the bloodstream [14, 44-46]. Due to increasing cellular copper load, dynactin [47] mediates the redistribution of ATP7B to vesicular compartments near the bile duct membranes, leading to biliary copper excretion [14]. Whole liver contains approximately 6–12 mg copper in human adults [48] and excessive copper is excreted via the bile [25, 49]. In WD, mutations of *ATP7B* lead to a loss-of-function of the protein [50-57], on the one hand causing an impaired copper insertion into apoceruloplasmin and hence reduced serum ceruloplasmin concentrations and on the other hand these mutations affect biliary copper excretion [53]. Especially in the liver and liver mitochondria [58-60], copper accumulates about 15-fold [5, 33, 50, 51, 53, 61, 62], inducing mitochondrial, plasma membrane [34, 45] and hepatocyte damage [5] and leading to chronic and fulminant hepatitis, progressive liver cirrhosis and liver failure [3, 50, 63, 64]. The damage of hepatocytes may lead to the spillover of liver copper into the bloodstream and thus to deleterious effects in the brain [33, 34, 65, 66]. Neurologic and psychiatric manifestations are comparable with these of Parkinson patients and include behavior changes, deteriorated handwriting, dystonia, hypertonia, muscle spasms or polyneuropathies [3, 33, 67-69].

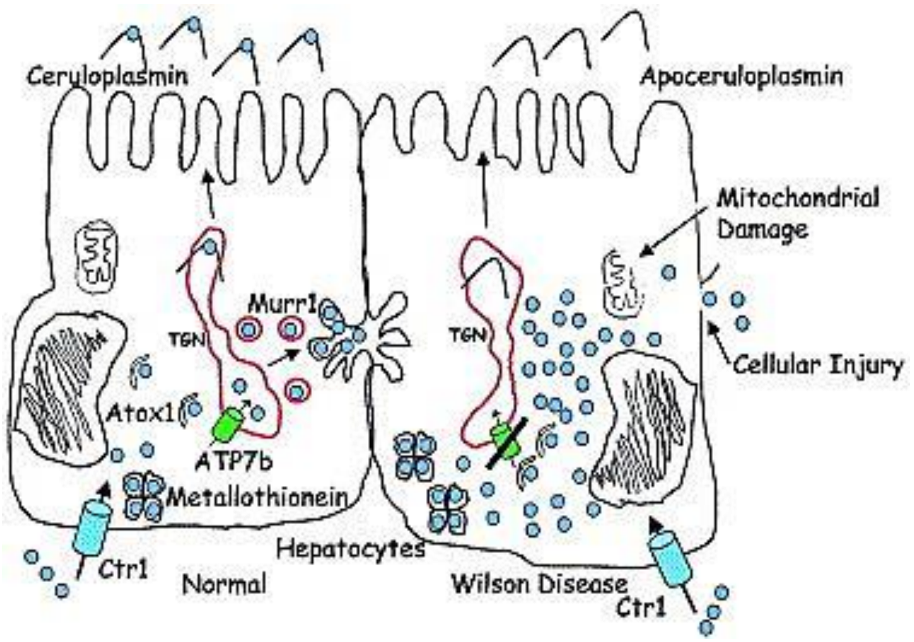

Figure 1-1 Impairment of copper metabolism in Wilson disease patients in comparison to healthy humans [45].

*Copper transporter 1 (*CTR1*) mediates copper uptake (blue circles) into hepatocytes. Copper (Cu) is subjected to copper-binding and -transporting proteins, such as metallothioneins or* ATOX1*.* ATOX1 *transports Cu to the secretion system of the cell:* ATP7B *(left). At normal cellular Cu concentrations,* ATP7B *is located at the trans-golgi network (TGN), mediating the incorporation of Cu into ceruloplasmin (cp) which is excreted into the blood. Increasing cellular copper concentrations lead to the retranslocation of* ATP7B *to the late endosome, incorporation of Cu into vesicles and excretion of these via the bile. Loss-of-function mutations of ATP7B like in Wilson disease (right) lead to impairments of copper excretion via the bile and incorporation of Cu into cp. Apoceruloplasmin (Cu-free cp) is released into the blood. Cu accumulates in the cytosol of hepatocytes, inducing mitochondrial and membrane damages. Reused with kind permission. From: Ting Y. Tao and Jonathan D. Gitlin (2003) Hepatic Copper Metabolism: Insights From Genetic Disease. Hepatology. 2003 Jun;37(6):1241-7 [45].*

## 1.2 Mitochondria – essential copper-dependent cell organelles that are affected in Wilson disease

In WD, mitochondria are one major target for liver copper accumulation, leading to structural and functional impairments of these organelles [59, 70-73].

Mitochondria are ubiquitous and essential organelles, promoting vital functions in most eukaryotes [74-76]. The development of mitochondria is described by the endosymbiotic theory [77]. According to this theory, prokaryotes were taken up via endocytosis by eukaryotes and developed to cell organelles over time – the mitochondria [77, 78]. Due to this endocytosis, mitochondria have two membranes, dividing the organelles into four compartments [79, 80]: the protein-rich and electron-dense mitochondrial matrix, separated by the mitochondrial inner membrane (MIM) [75] from the intermembrane space (IMS) which finally is bounded by the mitochondrial outer membrane (MOM) (Figure 1-2) [79, 80]. The MIM has many invaginations called cristae [75], leading to an increase of the inner membranes surface [81, 82].

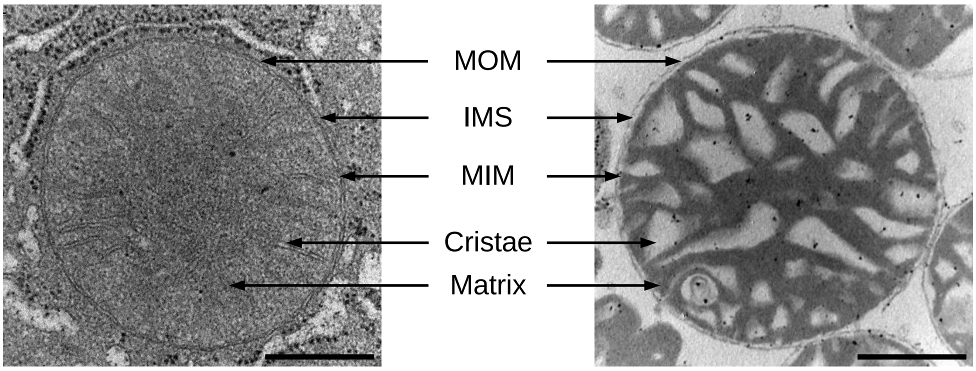

Figure 1-2 Structure of liver mitochondria *in situ* and isolated (rat liver).

*Mitochondria in situ and isolated have a double membrane: the mitochondrial outer membrane (MOM), which is the boundary to the cytosol, and the mitochondrial inner membrane (MIM), which separates the mitochondrial matrix from the mitochondrial intermembrane space (IMS). MIM is folded, leading to the formation of cristae. Whereas mitochondria in situ (left) appear in the orthodox phenotype, isolated mitochondria (right) appear in the condensed conformation [83]. Scale bar: 500 nm.*

The MOM separates the mitochondria from the cellular cytosol [75]. Pores within the MOM (voltage-dependent anion channel, VDAC) [84] allow free diffusion of molecules up to the size of 5 kDa from the cytosol to the IMS [84-90]. The mitochondrial inner membrane is impermeable for molecules and ions such as $H^+$ [87, 91, 92], being essential for the characteristic function of the MIM that is the generation of ATP by oxidative phosphorylation (OXPHOS) [91, 93-96]. The MIM has a very high protein content of approximately 76% [97] most importantly due to the four protein complexes of the mitochondrial respiratory chain and the ATP synthase ($F_OF_1$ ATP synthase, complex V) (Figure 1-3) [98, 99]. The coupling of these five complexes is termed oxidative phosphorylation [81, 91, 95, 100, 101]. This process describes the stepwise transfer of electrons from electron donors, such as NADH, $FADH_2$ or succinate to oxygen via complexes I to IV [95, 99, 101-104]. The flow of electrons is paralleled by the proton transport from the matrix into the IMS via complexes I, III and IV, leading to the formation of an electrochemical proton gradient (Figure 1-3) [91, 95, 101] and to a difference in charge across the MIM of approximately -180 mV [91, 96, 105, 106]. This gradient is called mitochondrial transmembrane potential (MMP, $\Delta\Psi$) [92, 101, 106] and is used by complex V ($F_OF_1$ ATP synthase) for ATP production as protons are re-translocated into the matrix [91, 101]. ATP is synthesised out of ADP and inorganic phosphate (Pi) [107]. The adenine nucleotide transporter (ANT) is located at the MIM and enables the exchange of ATP and ADP across this membrane [108, 109], linking cytosolic energy consumption and mitochondrial energy formation [110-112].

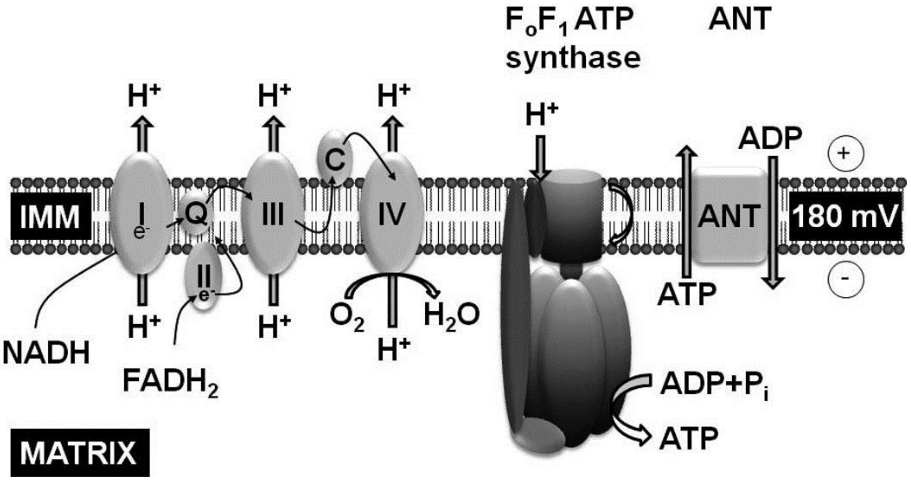

Figure 1-3 Protein complexes of the oxidative phosphorylation within the mitochondrial inner membrane [96].

*The electron transfer chain is located in the mitochondrial inner membrane (MIM, here abbreviated IMM) and contains four complexes (complexes I to IV) that are coupled to complex V ($F_OF_1$ ATP synthase). During electron ($e^-$) transfer, protons are pumped from the matrix into the IMS, leading to the formation of an electrochemical proton gradient (mitochondrial transmembrane potential, MMP, ΔΨ). This gradient is used by complex V for ATP production from ADP and inorganic phosphate.* ANT *enables the exchange of ATP and ADP across the MIM. Reused with kind permission. After: R. J. Gazmuri, J. Radhakrishnan (2012) Protecting mitochondrial bioenergetic function during resuscitation from cardiac arrest. Critical care clinics. 2012 Apr;28(2):245-70* [96].

For the activity of complexes I to IV, several prosthetic groups are necessary [99, 113]. Typically, these are iron-sulfur-clusters or hem groups, containing metals as cofactor for oxidation processes [99, 113]. Complex IV – the cytochrome c oxidase (CcO) – is of special interest as copper is necessary for the assembly and function of this complex [114-126]. Each CcO complex has three copper ions [125, 127]: two of which are located in the CuA (subunit II) and one is located in the CuB (subunit I) center [120, 128]. The CuB center stepwise reduces oxygen to water during OXPHOS [126, 129, 130]. The cytochrome c oxidase assembly protein SCO1 metalates CcO subunit II [120, 128, 131] and COX11 metalates the CcO subunit I (Figure 1-4) [132]. Copper loading of SCO1 and COX11 is mediated by the cytochrome c oxidase assembly protein COX17 [118]. The unstructured N-terminal domain of COX17 can assume several foldings and enables the interaction with SCO1 [133] and COX11 [118, 134], thereby mediating copper transfer [122, 123, 134-136].

CCS1 (copper chaperone for SOD1) is responsible for copper transport to the mitochondria [137]. Copper is driven into mitochondria and to the respective binding partners via their individual affinities for copper [138]. Approximately 60–85% of the mitochondrial copper is bound to a ligand (CuL, its molecular identity is unknown) within the mitochondrial matrix [139, 140], possibly serving as reserve for the metalation of newly synthesised CcO and SOD1 under changing physiological conditions [141]. The CcO is the most important copper-binding enzyme in mitochondria and contains 10–40% of the mitochondrial copper [131, 140]. A smaller amount of copper is bound to mitochondrial copper chaperones, such as the cytochrome c oxidase assembly protein COX17 which is located in the IMS but also in the cellular cytosol [11, 133, 139].

In yeast, Cox17 is involved in the biogenesis of the mitochondrial contact site and cristae organisation system (MICOS) [142]. The MICOS complex is important for an intact structure of the MIM and cristae formation [142]. Cox17 is either involved in assembly and stabilisation of the MICOS complex or in transport of copper ions to the complex, thereby regulating the level of mature MICOS complexes [142]. Up to now, the clear mechanism of MICOS assembly is unknown, however, Cox17 and copper are involved in MICOS biogenesis [142].

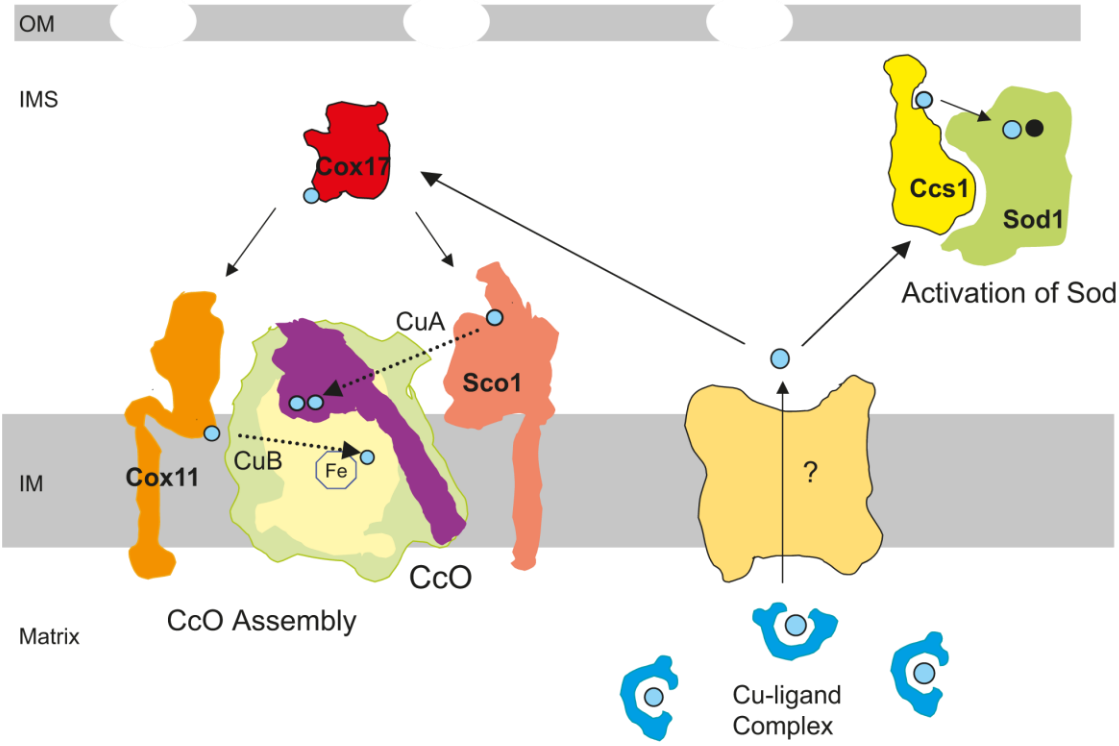

Figure 1-4 Copper sorting and delivery within the mitochondrial intermembrane space [128].

*The two major mitochondrial cuproenzymes are the cytochrome c oxidase (CcO) and the copper-zinc dependent superoxide dismutase (*SOD1*).* COX17 *transports copper to* COX11 *for incorporation into the CuB site of the CcO and to* SCO1 *for incorporation into the CuA site of the CcO.* CCS1 *provides copper for* SOD1*. The majority of the mitochondrial copper is bound to a ligand within the matrix. An unknown transporter is involved in the delivery of copper to the IMS for usage by* COX17 *and* CCS1*. Reused with kind permission. After: Paul A. Cobine, Fabien Pierrel, Dennis R. Winge (2006) Copper trafficking to the mitochondrion and assembly of copper metalloenzymes. Biochim Biophys Acta. 2006 Jul;1763(7):759-72* [128].

In WD, copper accumulated in the liver and liver mitochondria induces mitochondrial impairments [59, 70-73]. These include structural alterations, such as altered size (giant mitochondria), structure (increased electron density, separation of inner and outer mitochondrial membrane, abnormal folding of the mitochondrial inner membrane with dilation of mitochondrial cristae) and numerous inclusions like lipids [33, 58, 70-72, 143-145]. Moreover, mitochondrial fatty acid catabolism is impaired [70, 71, 145-148] and enzyme activities of the OXPHOS complexes are reduced [59, 70, 149]. Impairment of the mitochondrial aconitase [59, 149] leads to increased oxidative damages of mitochondrial DNA and impaired capacity of repair mechanisms [73, 150]. Rat liver mitochondria triggered with copper undergo swelling (unfolding of the MIM) [19, 151], leading to MOM rupture [152] and depletion of the MMP [153].

## 1.3 Treatment of Wilson disease using copper chelators

Due to the loss-of-function of ATP7B, copper accumulates within the liver and liver mitochondria [33, 50, 51, 53, 60-62]. To decrease copper uptake, for WD patients, it is recommended to avoid copper-rich foods like seafood, nuts, mushrooms or chocolate [33, 154-157]. For treatment of WD, copper chelating agents are necessary to prevent or reduce liver copper accumulation [158, 159] and reverse mitochondrial impairments [72]. Dimercaprol (BAL), introduced for WD around 1948 [5, 160], mediates copper excretion via the urine [161, 162], thereby improving symptoms of WD [163]. For dimercaprol, large volumes have to be injected intramuscularly [164] and therefore, it is not longer used for clinical application [165]. Currently, the treatment of choice is the orally applicated D-penicillamine (D-PA) [158, 166]. Lifelong daily doses of up to 1500 mg D-PA have to be taken [158]. D-PA reduces the mitochondrial copper load *in vivo* [58, 152] and reverses the mitochondrial structure [72, 152]. Bound copper is excreted via the urine [158]. For most WD patients, D-PA is an effective therapy [33, 158, 166, 167]. If treatment starts before the onset of advanced liver and neurologic damage, D-PA will improve clinical symptoms of WD patients [168, 169]. About 10–50% of WD patients cannot be treated long-term using D-PA [33, 66, 170, 171] as they develop severe side effects like fever, dermal injuries, thrombocytopenia, hypersensitivity reactions, nephrotic syndrome or neurologic damages [46, 155, 165, 166, 168, 172, 173]. Neurologic deterioration call for termination of D-PA treatment, leading to reaccumulation of copper as well as liver damages [33, 167, 174]. Alternatively, similar doses of trientine (TETA) can be applicated orally every day and lifelong [33, 166-168, 172, 175, 176]. TETA decreases the intestinal copper absorption for up to 80% [175] and increases urinary copper excretion [33, 175]. Compared to D-PA, TETA has fewer side effects, such as rashes, gastritis, sideroblastic anemia or Lupus-like reactions [33, 155, 166, 171].

In case of a non-acute manifestation or for maintenance therapy, treatment with lower doses of copper chelating agents and/or zinc may prevent disease progression [33, 177-180]. Zinc salts induce metallothioneins in enterocytes [159, 178, 181-183]. These cysteine-rich proteins have a higher affinity for copper than for zinc [33, 184, 185], functioning as endogenous chelator for copper [33]. This prevents entrance of copper into portal circulation [33] and leads to shedding of the intestinal cells through the faeces [33, 178].

Tetrathiomolybdate, which is applicated orally [186, 187], is still in the exploratory phase [33, 155], and it forms unsoluble complexes with copper-metallothionein that will be deposited in the liver [33, 188, 189]. In case of acute liver failure, fulminant hepatitis or if patients do not respond to other treatments, liver transplantation is necessary [155, 190, 191], correcting the metabolic defect of WD [155, 190, 192-194]. An anti-copper treatment is not longer required, but lifelong immunosuppression [192, 194-196].

Despite these treatment options, other agents are necessary for an efficient decoppering of the liver. Zinc salts are not recommended for initial therapy [170]. D-PA and TETA can mobilise copper from tissues [197], but as they have an only intermediate copper affinity [198], the copper complexes released into the blood may often cause secondary effects in the brain and treatment has to be discontinued [199-202]. Moreover, D-PA and TETA often are not able to prevent liver copper accumulation, leading to liver failure [33, 66, 169]. Therefore, for successful treatment of WD, new agents with a higher affinity for copper are necessary.

## 1.4 Methanobactin – a peptide with a very high affinity for copper

A very promising candidate compound to reverse the mitochondrial copper overload in WD is methanobactin (MB). MB is a small, copper-binding chromopeptide (1154 Da) excreted by the methane-oxidising bacterium *Methylosinus trichosporium* OB3b [203, 204]. These bacteria use methane as only carbon and energy source [204-206]. For methane oxidation, copper is required [204]. To ensure sufficient copper uptake under copper-limiting conditions, specific copper uptake mechanisms have been evolved [204, 207]. Methanotrophic bacteria excrete MB that binds the copper with a very high affinity ($>10^{-21}$ M) and these complexes are then re-internalised [205-209]. Inside, copper regulates expression of methane-monooxygenases and methane oxidation [204]. MB has a much higher affinity for copper compared to the known affinities of copper-binding proteins in eukaryotic cells ($10^{-12}$–$10^{-15}$ M) [138]. Due to this high affinity of MB for copper, this agent was used for long-term treatment of *Atp7b*$^{-/-}$ rats and compared to the long-term treatment using D-PA [152]. Both copper chelators diminish the mitochondrial copper load in *Atp7b*$^{-/-}$ rats for approximately 70% [152], but also a short-term treatment of *Atp7b*$^{-/-}$ rats with MB reduces whole liver copper for approximately 50% [210]. Thus, alternatively to D-PA, MB may possibly be used for treatment of human WD patients [1, 210]. Nevertheless, as MB is a bacterial peptide, an immune response could be developed against the MB peptide [1].

## 1.5 The LPP rat as an animal model for studying mitochondrial alterations in Wilson disease

In this thesis, an animal model is used to analyse mitochondrial impairments and mitochondrial decoppering in WD. This animal model is the LPP rat (Figure 1-5), which is a crossbreed between the Long-Evans-Cinnamon (LEC) rat and the Piebald Virol Glaxo (PVG) rat [2]. The LPP rat has a 13 kb deletion in *Atp7b* – the gene affected in human WD [2]. Due to the recessive inheritance, heterozygous and wild type LPP rats have a normal phenotype showing no copper accumulation and therefore, these rats served as controls [152]. Homozygous LPP $Atp7b^{-/-}$ rats show a progressive liver copper accumulation with increasing age [152]. At an age of approximately 90 days, these rats develop fulminant liver damages, indicated by increased serum values of aspartate aminotransferase (AST) and bilirubin, leading to liver failure and death [152]. Rat liver mitochondria show a massive copper accumulation and structural alterations, such as enlarged cristae and an altered shape, leading to loss-of-function of these organelles [152, 211]. Similar mitochondrial alterations (see section 1.2) have been reported in WD patients [70, 71, 144, 145] and other animal models for WD, such as the $Atp7b^{-/-}$ mouse, the Jackson toxic milk mouse and LEC rats [58, 212, 213]. Mitochondrial changes in $Atp7b^{-/-}$ rats can be efficiently reversed by long-term treatment with copper chelators if treatment starts before the onset of clinically apparent liver damage [152].

© Christin Leitzinger

Figure 1-5 LPP rat – an animal model for studying mitochondrial alterations in Wilson disease (© photo by Christin Leitzinger).

## 1.6 Aim of this study

The aim of this work is to further characterise and understand mitochondrial impairments in WD. The LPP *Atp7b*$^{-/-}$ rat model is used to compare the copper concentrations in liver homogenate and liver mitochondria as well as the mitochondrial structure in LPP rats and human WD patients. Moreover, a detailed analysis of mitochondrial alterations depending on the disease state of LPP *Atp7b*$^{-/-}$ rats is addressed in this work, including mitochondrial structure and function as well as biochemical characteristics.

The prime requirement for an effective treatment of WD is to reduce elevated liver mitochondrial copper load by using copper chelating agents. This second part of the thesis focuses on analysing the toxicity and decoppering efficiency of MB – an agent with a high affinity for copper – on HepG2 cells *in vitro* and liver mitochondria from LPP *Atp7b*$^{-/-}$ rats *in vivo* in comparison to the low affinity copper chelators D-PA and TETA. A treatment scheme consisting of repetitive MB injections is analysed whether this can improve the decoppering efficiency in liver mitochondria from *Atp7b*$^{-/-}$ rats.

Copper load increases in liver mitochondria from LPP *Atp7b*$^{-/-}$ rats with disease progression. Isolated rat liver mitochondria, containing approximately 7 nmol copper per mg mitochondrial protein, show massive structural but slight functional alterations [58, 152]. These data indicate that mitochondria can balance the rising copper load up to this concentration, thereafter the mitochondria break down. The third part of this work addresses the question how mitochondria deal with elevated copper concentrations in WD. That is why the abundance of mitochondrial proteins is analysed in subfractionated copper-loaded rat liver mitochondria by using mass spectrometry.

COX17 is found to be upregulated in liver mitochondria isolated from LPP *Atp7b*$^{-/-}$ rats compared to *Atp7b*$^{+/-}$ rats and as it is a copper-binding protein, it seems to be an important protein for balancing elevated mitochondrial copper loads. The fourth aim of this thesis is to analyse whether COX17 upregulation in LPP *Atp7b*$^{-/-}$ rats is protective or damaging for mitochondria. To elucidate this question, a cell culture model using HepG2 cells is established for up- and downregulating *COX17*.

# 2 Material and Methods

## 2.1 Material

### 2.1.1 Cell line

For cell culture experiments, HepG2 cells obtained from ATCC (ATCC® HB-8065) were used [214]. This cell line is a human hepatocellular carcinoma cell line taken from a 15 years old male Caucasian [214].

### 2.1.2 Bacteria

Chemo-competent *Escherichia coli* Top10 (Thermo Fisher Scientific) were used for transfection and amplification of plasmids.

### 2.1.3 Plasmid and enzymes

For overexpression of *COX17* in HepG2 cells, the plasmid pcDNA3.1(+) (Thermo Fisher Scientific, kindly provided by Dr. Michelle Vincendeau and Dr. Karl Kenji Schorpp, Helmholtz Center Munich, Institute of Molecular Toxicology and Pharmacology, Neuherberg, Germany) was used.

For endonuclease treatment of plasmid and DNA isolated from HepG2 cells, NheI and PmeI, obtained from New England Biolabs, were used.

### 2.1.4 Oligonucleotides

Oligonucleotides used in this thesis are listed in Table 2-1. Synthesis of PCR primers was done by Eurofins MWG GmbH, Ebersberg, Germany. SiRNAs were obtained from Eurogentec S.A., Seraing, Belgium.

Table 2-1 Oligonucleotides

| Name | Length | Sequence in 5’-3’-direction | Gene | Application |
|---|---|---|---|---|
| JBJB611[a] | 28 bp | CCCATACGTATACAAACACCAAACTAGA | *Atp7b*<br>(intron 15) | Genotyping of LPP rats<br>(primer mix 1) |
| JBJB616[a] | 30 bp | CTTTGAACTTTGGACTTCTATCATTGTTGA | | |
| JBJB618[a] | 30 bp | ACCAGGTCAGCTACGTGAGCCAAGTCTCTC | *Pina5.1,*<br>accession #AF120492 | Genotyping of LPP rats<br>(primer mix 2) |
| JBJB619[a] | 30 bp | TGGGTGCTGCCTGACTCCAGCCTTTGTGGG | | |

Table 2-1 Oligonucleotides

| Name | Length | Sequence in 5’-3’-direction | Gene | Application |
|---|---|---|---|---|
| COX17-siRNA_fwd | 18 bp | GCCGGGTCTGGTTGACTC | *COX17* | qRT-PCR *COX17* HepG2 cells |
| COX17-siRNA_rev | 20 bp | CTAGGGCTCTCATGCATTCC | | |
| RPII s | 19 bp | GCACCACGTCCAATGACAT | *RPII* | qRT-PCR *RPII* HepG2 cells |
| RPII as | 18 bp | GTGCGGCTGCTTCCATAA | | |
| siRNA 1 | 21 bp | GGAGAAGAACACTGTGGACAT | *COX17* | Knockdown of *COX17* |
| siRNA 2 | 21 bp | GCCCACAAGGAATGCATGAGA | *COX17* | |
| siRNA 3 | 21 bp | GAACACTGTGGACATCTAATT | *COX17* | |
| NHE-3xFLAG_COX17 (fw)[b] | 111 bp | TTCGATGCTAGCATGGACTACAAGGATGATGATGACAAGGACTACAAGGATGATGATGACAAGGACTACAAGGATGATGATGACAAGGCTAGCATGCCGGGTCTGGTTGAC | *COX17* | Overexpression of *COX17* in HepG2 cells<br>pcDNA3.1(+) vector without flag |
| PmeI (rev)[b] | 47 bp | TTCGATGTTTAAACTCATATTTTAAATCCTAGGGCTCTCATGCATTC | *COX17* | pcDNA3.1(+) vector without flag |

[a] These oligonucleotides were described by Ahmed *et al.* [2].

[b] These oligonucleotides were designed by Dr. Michelle Vincendeau.

### 2.1.5 Media

Media and additives used for cell culture are listed in Table 2-2. Media compositions for subcultivation (10% FCS) and treatment experiments (2% FCS) are listed in Table 2-3. MEM medium was used for experiments shown in section 3.2, whereas DMEM medium was used for experiments shown in section 3.4.

Table 2-2 Media and additives for subcultivation of HepG2 cells

| Medium | Manufacturer | Order No. |
|---|---|---|
| Antibiotic-Antimycotic (100X) | Life Technologies | 15240-062 |
| DMEM (high glucose) | Life Technologies | 31966-021 |
| Dulbecco's balanced salt solution (DPBS), no calcium, no magnesium | Life Technologies | 14190-094 |
| Fetal calf serum (FCS) | Biochrom | S 0115 |
| MEM non-essential amino acids solution (100X) (NEAA) | Life Technologies | 11140-035 |
| MEM, no glutamine, no phenol red | Life Technologies | 51200-046 |
| Opti-MEM® | Life Technologies | 31985-070 |
| Penicillin-Streptomycin (10 000 U/ml) (Pen/Strep) | Life Technologies | 15140-122 |
| Sodium pyruvate (100 mM) | Life Technologies | 11360-070 |
| Trypsin-EDTA (0.05%), phenol red | Life Technologies | 25300-054 |

Table 2-3 Media composition for subcultivation and treatment of HepG2 cells

| Medium | 10% FCS medium | 2% FCS medium |
|---|---|---|
| MEM | | |
| - Antibiotic-Antimycotic | 5.7 ml | 5.3 ml |
| - Sodium pyruvate | 5.7 ml | 5.3 ml |
| - NEAA | 5.7 ml | 5.3 ml |
| - FCS | 57.0 ml | 10.5 ml |
| DMEM glucose | | |
| - Penicillin-Streptomycin | 5.6 ml | 5.2 ml |
| - FCS | 56.0 ml | 10.3 ml |
| Transfection experiments | DMEM without Pen/Strep | - |

### 2.1.6 Chemicals

Table 2-4 Chemicals

| Chemical | Company | Application |
|---|---|---|
| 2,4,6-Tris(dimethylamino-methyl)phenol (DMP30) | Serva | Electron microscopy analysis |
| 2-Mercaptoethanol | Sigma | Immunoblot analysis |
| 2-Propanol | VWR | Immunoblot analysis |
| 30% Acrylamide solution | Roth | Immunoblot analysis |
| Acetic acid | Merck | Destaining buffers |
| Adenosine diphosphate (ADP) | Sigma | ATP assay |
| Agar agar (Lennox) | Roth | LB agar plates |
| Agarose | Biozym | Gel electrophoresis |
| Albumin Fraction V, fatty acid free | Roth | $IP^+$ buffer |
| Ammonium acetate | Sigma | Anion exchange chromatography |
| Ammonium tetrathiomolybdate (TTM) | Gift from K.T. Suzuki (Chiba University, Japan) | Cell culture experiments |
| Ammonium persulfate (APS) | Sigma | Immunoblot analysis |
| Ampicillin | Sigma | Cultivation of bacteria |
| ATP Bioluminescence Assay Kit | Roche | ATP assay |
| ATP Bioluminescence Standard | Roche | ATP assay |
| Boric acid | Roth | TBE buffer |
| Bromphenol blue | Sigma | Gel electrophoresis |
| BSA standard | Sigma | Bradford |
| Calciumchloride ($CaCl_2$) | Roth | MMP/MPT |
| Carbonyl cyanide m-chloro-phenylhydrazone (CCCP) | Sigma-Aldrich | Cell culture experiments |
| Cell extraction buffer | Life Technologies | Cell lysis |
| Complete Mini (Protease inhibitor cocktail tablets) | Roche Diagnostics GmbH | Cell culture sample preparation for immunoblot analysis |
| Copper (II) sulfate * $5H_2O$ ($CuSO_4$) | VWR | MMP/MPT |
| Copper (II) chloride dihydrate | Sigma | Copper-histidine solution |

Table 2-4 Chemicals

| **Chemical** | **Company** | **Application** |
|---|---|---|
| Cyclosporine A (CysA) | Fluka | MMP/MPT |
| n-Dodecyl β-D-maltoside (DDM) | Sigma | Proteomic analysis |
| DEPC water | Carl Roth GmbH | PCR |
| Diethylaminoethyl-Sephacel | Sigma-Aldrich | Anion exchange chromatography |
| Dimethylsulfoxide (DMSO) | Sigma | Polarisation expriments |
| Dodecenylsuccinic anhydride (DDSA) | Serva | Electron microscopy analysis |
| D-penicillamine hydrochloride (D-PA) | Laborchemie Apolda | Treatment of LPP rats, cell culture experiments |
| DPH (1,6-diphenyl-1,3,5-hexatriene) | Sigma | Polarisation expriments |
| EGTA (Ethylene glycol-bis(2-amino-ethylether)-N,N,N′,N′-tetraacetic acid) | Fluka | Isolation buffer |
| Ethanol | Merck | Electron microscopy |
| Ethidiumbromide | AppliChem | Gel electrophoresis |
| FCCP (Carbonyl cyanide-p-trifluoromethoxyphenylhydrazone) | Sigma | MMP/MPT |
| Glutaraldehyde (2.5%) in 0.1 M Sodium Cacodylate buffer | EMS Science Services | Electron microscopy analysis |
| Glycerol | Sigma | Immunoblot analysis |
| Glycidether | Serva | Electron microscopy analysis |
| Glycine | Sigma | Immunoblot analysis |
| Heparin (25 000 U/ml) | Roche | Inhibition of blood coagulation |
| Hoechst 33342 | Life Technologies | Cell culture (fluorescence staining) |
| Hydrochloric acid | Merck | pH adjustment |
| Isoflurane | Abbott Laboratories | Inhalation anesthesia of rats |
| LB medium (Lennox) | Roth | LB medium |
| L-Histidine | Sigma | Copper-histidine solution |
| Magnesium chloride ($MgCl_2$) | Sigma | ATP assay |
| Methanobactin from *Methylosinus trichosporium* OB3b | Kindly provided by Alan A. DiSpirito | Treatment of LPP rats, cell culture experiments |
| Methanol | Fluka | Immunoblot analysis |
| Methylnadic anhydride (MNA) | Serva | Electron microscopy analysis |
| MitoTracker® Deep red | Molecular Probes Inc. | Fluorescence imaging of HepG2 cells |
| Molecular sieve 4 Å | Roth | Electron microscopy analysis |
| MOPS (4-Morpholinepropanesulfonic acid) | Fluka | MMP/MPT |
| Neutral red | Sigma-Aldrich | Neutral red assay |
| Nitric acid 65% | Merck | Wet ashing of samples for copper determination |
| Nonidet™ P 40 Substitute (NP40) | Sigma Life Science | COX17 immunoprecipitation |
| Nonyl acridine orange (NAO) | Molecular Probes Inc. (Invitrogen) | Fluorescence imaging of HepG2 cells |
| Nuclease-free water | PeqLab | PCR, transfection experiments |
| Nycodenz® | Axis Shield | Density gradient |

Table 2-4 Chemicals

| Chemical | Company | Application |
|---|---|---|
| o-Dianisidine dihydrochloride | Sigma | Ceruloplasmin oxidase activity |
| Osmium tetroxide | EMS Science Services | Osmic acid |
| PBS (Phosphate buffered saline) | Merck | Cell culture |
| Percoll® | GE Healthcare | Density gradient |
| Phosphoric acid | Sigma | Swelling buffer |
| Pierce 660 nm Protein Assay | Thermo Scientific | Pierce protein determination |
| Poly-D-Lysine hydrobromide | Sigma | Cell culture |
| Ponceau S | Sigma | Immunoblot analysis |
| Potassium chloride (KCl) | Merck | ATP assay |
| Potassium dichromate | Sigma | Osmic acid |
| Potassium ferrocyanide * $3H_2O$ | Sigma | ATP assay |
| Potassium hydroxide (KOH) | Merck | Osmic acid, isolation buffer |
| Powdered milk | Roth | Immunoblot analysis |
| Propylenoxid | Serva | Electron microscopy |
| Protease Inhibitor Cocktail | Sigma | COX17 immunoprecipitation |
| Rhodamine 123 (Rh123) | Invitrogen | MMP |
| Rotenone | Sigma | MMP/MPT, ATP assay |
| Roti®-Nanoquant | Roth | Bradford protein determination |
| SDS (10X) | Roth | Immunoblot analysis |
| SDS (sodium salt) | Serva | Immunoblot analysis |
| S.O.C. medium | Invitrogen | Transformation (*COX17* overexpression) |
| Sodium acetate | Sigma | Ceruloplasmin oxidase activity |
| Sodium Cacodylate buffer 0.2 M, pH 7.4 | EMS Science Services | Electron microscopy analysis |
| Sodium chloride (NaCl) | Sigma | Rinse of rat liver, osmic acid, MB, copper-histidine solution |
| Sodium hydroxide solution (NaOH) | Fluka | pH adjustment |
| Succinate $Na_2$-Salt * $6H_2O$ | Sigma | ATP assay |
| Sucrose | Fluka | Preparation of mitochondria |
| Sulfuric acid | Merck | Ceruloplasmin oxidase activity |
| TEMED | Sigma | Immunoblot analysis |
| TES | Sigma | Isolation buffer |
| Tetrahydrofurane | Roth | Polarisation expriments |
| TMA-DPH (1-(4-(trimethylamino) phenyl)-6-phenylhexa-1,3,5-triene) | Sigma | Polarisation expriments |
| Toluidin blue | Roth | Staining of semi-thin cuts |
| Total Protein Reagent | Sigma | Protein determination |
| Trientine (TETA) | Sigma-Aldrich | Treatment of LPP rats, cell culture experiments |
| TRIS | VWR | Immunoblot analysis |
| Triton X-100 | Sigma | Polarisation expriments |
| Trypan blue | Sigma-Aldrich | Cell culture (life/dead-staining) |

Table 2-4 Chemicals

| Chemical | Company | Application |
|---|---|---|
| Tween 20 | Sigma-Aldrich | Immunoblot analysis |
| Uranyl acetate (1%) | Science Services | Staining of ultrathin cuts (EM) |
| Zinc acetate | Sigma | Zinc-MB |
| Zinc sulfate | Sigma | Treatment of LPP rats |

## 2.1.7 Solutions and buffers

Table 2-5 Solutions and buffers

| Solution | Composition |
|---|---|
| Blocking solution | 5 g powdered milk per 100 ml 1X TBS-T |
| Buffer for osmic acid | 6 ml 2.5 N KOH + 50 ml 5% potassium dichromate |
| Density gradient | |
| - Percoll | 60 ml IPP buffer (0.1% BSA) + appropriate amount of sucrose:<br>solution A: 1.435 g sucrose<br>solution B: 2.56 g sucrose<br>solution C: 9.24 g sucrose<br>18% Percoll: solution A + 5.4 ml Percoll<br>30% Percoll: solution B + 9.0 ml Percoll<br>60% Percoll: solution C + 18.0 ml Percoll |
| - Nycodenz | 40%: 40 ml Nycodenz + 60 ml 10 mM TRIS pH 7.4<br>33%: 33 ml 40% + 67 ml 10 mM TRIS pH 7.4<br>28%: 84 ml 40% + 216 ml 10 mM TRIS pH 7.4<br>27%: 54 ml 40% + 146 ml 10 mM TRIS pH 7.4<br>24%: 48 ml 40% + 152 ml 10 mM TRIS pH 7.4 |
| Destaining solution | Immunoblot: 10% acetic acid, 40% technical ethanol, 50% $H_2O$<br>Neutral red assay: 1% acetic acid, 50% technical ethanol, 49% $H_2O$ |
| Developer solution | Per 10 ml: each 500 µl ECL 1 and 2 + 9 ml $H_2O$ |
| Epon 812 | 130.5 g glycidether, 81.5 g Methylnadic anhydride (MNA), 61.5 g dodecenylsuccinic anhydride (DDSA), 3.75 ml 2,4,6-tris(dimethylamino-methyl)phenol (DMP30) (according to [215]) |
| IPP buffer | Per 0.5 L: 51.4 g sucrose (final 300 mM), 1146 mg TES (final 10 mM), 38 mg EGTA (final 0.2 mM), 0.5 g BSA (fatty acid free), pH 6.9 with 5 M KOH |
| Isolation buffer (IP buffer) | $IP^-$: per 1 L 102.8 g sucrose (final 300 mM), 1146 mg TES (final 5 mM), 76 mg EGTA (final 0.2 mM), pH 7.2 with 5 M KOH<br>$IP^+$ (with 0.1% BSA): 1 L $IP^-$ + 1 g fatty acid free BSA |
| Laemmli buffer | 4X, per 50 ml: 10 ml 1 M TRIS/HCl pH 6.8 (final 200 mM), 4 g SDS (final 8%), 0.2 g bromphenol blue (final 0.4%), 20 ml glycerol (final 40%)<br>For usage: 500 µl laemmli buffer + 25 µl 2-mercaptoethanol |
| LB agar plates | Per 1 L: 20 g LB broth (Lennox), 15 g agar agar, 100 µg/ml ampicillin |
| Lysis buffer | 5 ml cell extraction (CE) buffer + ½ tablet proteinase inhibitor cocktail |
| Lysis buffer (Immunoprecipitation COX17) | 300 mM NaCl, 10 mM TRIS/HCl pH 8.0, 0.5% Nonidet™ P 40 Substitute (NP40), 5 µl protease inhibitor cocktail, add to 500 µl MilliQ-$H_2O$ |
| MOPS-TRIS | 21 g per 200 ml $H_2O$, pH 7.4 with 2 M TRIS |
| Osmic acid | 30 ml 4% osmium tetroxide, 30 ml MilliQ-$H_2O$, 30 ml 3.4% NaCl, 30 ml buffer (KOH + 5% potassium dichromate; pH 7.2) |

Table 2-5 Solutions and buffers

| Solution | Composition |
|---|---|
| Ponceau S | Per 1 L: 1% Ponceau S (weight per volume), 5% acetic acid |
| Potassium dichromate | 5% = 2.5 g/50 g |
| SDS lysis buffer | 2% SDS, 50 mM TRIS/HCl pH 7.4, 150 mM NaCl |
| Separating gel | For two gels, 15%: 3.76 ml 1 M TRIS pH 8.8, 5 ml 30% acrylamide, 50 µl 20% SDS, 50 µl 10% APS, 5 µl TEMED, 1.2 ml $H_2O$ |
| Sodium acetate | 0.1 M: 8.2 g sodium acetate, 2.6 ml 100% acetic acid, add to 1 L with MilliQ-$H_2O$ |
| Stacking gel | For two gels: 1.25 ml 1 M TRIS pH 6,8, 1.33 ml 30% acrylamide, 50 µl 20% SDS, 50 µl 10% APS, 10 µl TEMED, 7.2 ml $H_2O$ |
| Stripping buffer | Per 1 L: 20 g SDS, 50 ml 1 M TRIS/HCl, pH 6.8<br>For usage: 50 ml stripping buffer + 350 µl 2-mercaptoethanol |
| Swelling buffer (SWP1) | Per 500 ml: 34.23 g 1 M sucrose (final 0.2 M), 10 ml 0.5 M MOPS-TRIS (final 10 mM), 10 ml 0.25 M succinate (final 5 mM), 500 µl 1 M Pi (final 1 mM), 100 µl 50 mM EGTA (final 10 µM), 500 µl 2 mM rotenone (final 2 µM) |
| TBE buffer | 20X: 121.14 g TRIS + 61.83 g boric acid + 40 ml 0.5 M ethylenediaminetetraacetic acid (EDTA), add to 1 L MilliQ-$H_2O$ (pH 8.3) |
| TBS | 10X, per 1 L: 100 ml 1 M TRIS/HCl pH 8.0, 87.75 g NaCl (final 1.5 M) |
| TBS-T | 100 ml 10X TBS, 900 ml MilliQ-$H_2O$, 500 µl Tween 20 |
| Transfer buffer | Per 2 L: 2.5 ml 20% SDS (final 0.025%), 5.8 g glycine (final 39 mM), 11.6 g TRIS (final 48 mM) |
| TRIS/HCl | 1 M: 60.57 g TRIS per 500 ml MilliQ-$H_2O$<br>pH adjusted to 6.8, 7.4 or 8.8, respectively, using 32% HCl |
| Urea buffer | 8 M urea in 0.1 M TRIS/HCl pH 8.5 |
| Washing buffer | Washing buffer 1: 150 mM NaCl, 10 mM TRIS/HCl pH 8.0<br>Washing buffer 2: 300 mM NaCl, 10 mM TRIS/HCl pH 8.0 |
| Zinc-methanobactin | 20 mM MB + 20 mM zinc acetate |

## 2.1.8 Antibodies

Table 2-6 Antibodies used for immunoblot analysis and immunohistochemistry

| Antibody | Order number | Company | Dilution |
|---|---|---|---|
| Anti-Biotin | #7075 | Cell Signaling | 1 : 1000 |
| Anti-Mouse | #7076 | Cell Signaling | 1 : 1000 |
| Anti-Mouse | 710029 | KPL | Ready to use |
| Anti-Rabbit | #7074 | Cell Signaling | 1 : 1000 |
| COX17 | C12231<br>sc-100521 | Assay Biotech<br>Santa Cruz | 1 : 1000 (immunoblot HepG2 cells)<br>1 : 100 (immunoblot rat liver mitochondria)<br>1 : 1000 (immunohistochemistry staining of rat liver tissue) |
| GAPDH | 2118 | Cell Signaling | 1 : 2000 |
| HSP60 | 611563 | BD | 1 : 5000 |
| Mitochondrial citrate synthase | NBP2-13878 | Novus biologicals | 1 : 1000 |
| β-Actin | A4700 | Sigma | 1 : 1000 |

## 2.1.9 Kits

Table 2-7 Commercially available kits

| **Description** | **Manufacturer** | **Application** |
|---|---|---|
| 20X LumiGLO® Reagent and 20X Peroxide | Cell Signaling | Immunoblot Analysis |
| 2-log DNA ladder | New England Biolabs | Gel electrophoresis |
| ATP Bioluminescence Assay Kit CLS II | Roche | ATP assay |
| Biotinylated Protein Ladder Detection Pack | Cell Signaling | Immunoblot analysis |
| CellTiterGlo® 2.0 Assay | Promega | Measurement of ATP content (cell culture) |
| DirectPCR® Lysis Reagent Tail/Ear | PeqLab | DNA isolation from rat tails or ears |
| DNA ligation kit | Thermo Fisher Scientific | Ligation of vector and insert (*COX17* overexpression) |
| dNTPs | Qiagen | PCR – genotyping of LPP rats |
| Expand High Fidelity PCR system | Roche | Amplification of cDNA |
| FuGENE® HD Transfection Reagent | Promega | *COX17* overexpression |
| Gene Ruler DNA ladder 100 bp | Fermentas | Gel electrophoresis |
| Lipofectamine® RNAiMAX Transfection Reagent | Invitrogen | *COX17* knockdown |
| NucleoSpin® Gel and PCR Clean-up | Macherey-Nagel | PCR clean up and gel extraction |
| NucleoSpin® Plasmid | Macherey-Nagel | Preparation of plasmid DNA (small scale) |
| One Step SYBR® PrimeScript™ RT PCR Kit II | TaKaRa Clontech | qRT-PCR |
| peqGold Proteinase K | Peqlab | DNA isolation from rat tails or ears |
| Plasmid Maxi Kit | Qiagen | Preparation of plasmid DNA (large scale) |
| Precision Plus Protein™ Dual Color Standards | Bio-Rad | Immunoblot analysis |
| Protein G Sepharose 4 Fast Flow | GE Healthcare Life Sciences | COX17 immunoprecipitation |
| QIAshredder | Qiagen | RNA isolation from HepG2 cells |
| RNAse free DNAse set | Qiagen | RNA isolation from HepG2 cells |
| RNeasy Micro Kit | Qiagen | RNA isolation from HepG2 cells |
| *Taq* DNA-Polymerase (250 units) | Qiagen | PCR – genotyping of LPP rats |
| Verso cDNA Synthesis Kit | Thermo Fisher Scientific | Translation of RNA in cDNA |

## 2.1.10 Equipment and consumables

Equipment, tools and consumables used in this thesis are listed in Table 2-8, Table 2-9 and Table 2-10.

Table 2-8 Equipment

| Equipment | Name | Manufacturer |
|---|---|---|
| Absorbance measurement | | |
| - Photometer | BioPhotometer | Eppendorf |
| - UV Spectrophotometer | UV-1800 | Shimadzu |
| - Spectrophotometer | NanoDrop 2000 | Thermo Scientific |
| Anesthetic vaporizer (isoflurane) | Sigma Delta | Penlon |
| Autoclave | VX-95 | Systec |
| Cell Viability Analyzer | Vi-Cell™ XR | Beckman Coulter |
| Centrifuges | Avanti J-26S XP | Beckman Coulter |
| | L-70 ultracentrifuge | Beckman Coulter |
| | Optima Max 130 Ultracentrifuge | Beckman Coulter |
| | Centrifuge 5415 D | Eppendorf |
| | Centrifuge 5417 R | Eppendorf |
| | Centrifuge 5810 R | Eppendorf |
| | 1K15 | Sigma |
| | 3K15 | Sigma |
| | 3-30K | Sigma |
| Contrasting device | QG-3100 Automated TEM Stainer | RMC |
| Diagnostic system | Reflotron® Plus | Roche |
| Electrophoresis Power Supply | Consort EV243 | Sigma |
| | PowerPac™ Basic | Bio-Rad |
| Heating block | HB-130 | Unitek |
| Homogenizer | Potter S | B. Braun Melsungen AG |
| Imaging systems | | |
| - Gel imaging | Gel iX20 | Intas |
| - Immunoblot imaging | ChemoCam Imager 3.2 | Intas |
| - UV transilluminator | UST-30M-8R | VWR |
| Incubator | | |
| - 37 °C, 5% $CO_2$ (cells) | BBD 6220 | Heraeus Instruments |
| - 37 °C, 5% $CO_2$ (bacteria) | Function Line | Heraeus Instruments |
| - 60 °C (electron microscopy) | UNB400 | Memmert |
| - 37 °C, shaker (bacteria) | Shaker Series I 26 | New Brunswick Scientific |
| Light Cycler | LightCycler® 480 II | Roche |
| Magnetic mixer | Combimag RCT | IKA |
| Microplate reader | | |
| - Multi-Mode reader | Synergy 2 | Biotek |
| - Fluorescence imaging | Operetta | PerkinElmer |
| - Luminescence | Centro LB 960 | Berthold Technologies |
| - Absorbance | Spectra Max 340 | Molecular Devices |
| Microscopes | | |
| - Transmitted-light microscope | Labovert | Leitz |
| - Fluorescence microscope | EVOS FL | Life Technologies |
| - Transmission electron microscope | EM10 | Zeiss |
| PCR cycler | Mastercycler gradient | Eppendorf |
| | GeneAmp PCR System 9700 | Applied Biosystems |
| pH meter | PB-11 | Sartorius |
| Precision pump | Pump 11 Elite | Harvard Apparatus |

Table 2-8 Equipment

| Equipment | Name | Manufacturer |
|---|---|---|
| Printer | DPU-414 | Seiko Instruments GmbH |
| Rotors | 12024-H<br>12154-H<br>12156-H<br>12349<br>19776-H<br>70.1 Ti<br>JA25-50<br>JA10<br>JA12<br>Swing out SW55Ti | Sigma<br>Sigma<br>Sigma<br>Sigma<br>Sigma<br>Beckman Coulter<br>Beckman Coulter<br>Beckman Coulter<br>Beckman Coulter<br>Beckman Coulter |
| Sample trimmer | EM TRIM 2 | Leica |
| Shaker | REAX 2000<br>Rotatory Mixer<br>Shaker DRS-12<br>Thermomixer comfort<br>Titramax 100<br>VF2<br>Vibrax-VXR | Heidolph<br>Kisker<br>Neolab<br>Eppendorf<br>Heidolph<br>IKA<br>IKA |
| Tissue stainer | DISCOVERY XT | Ventana Medical System, Roche |
| Ultramicrotome | Ultracut E | Reichert-Jung |
| Ultrapure water system | Purelab Flex | Elga Veolia |
| Ultrasonic device | UP400S | Hielscher |
| Waterbath | GFL 1002 (37 °C) | GFL |
| Weighing scale | Kern 440-47N<br>Kern PCB<br>AB204<br>PB3002-S/PH<br>PE3000 | Kern & Sohn GmbH<br>Kern & Sohn GmbH<br>Mettler TOLEDO<br>Mettler TOLEDO<br>Mettler |
| Work bench | UVF 6.18 S | BDK |

Table 2-9 Tools

| Tool | Manufacturer |
|---|---|
| Blotting chamber Mini PROTEAN® Tetra Cell | Bio-Rad |
| Cell Homogenizer with tungsten carbide sphere | Isobiotec |
| Centrifuge tubes | Nalgene, Beckman Coulter |
| Diamond knives for semi and ultra thin cuts | Diatome |
| Dissecting set (tweezers, sciccors, scalpel) | Various |
| Electrophoresis system Novex® Mini-Cell | Invitrogen |
| Laboratory glass ware | Schott |
| Migration chamber | Bio-Rad |
| Mini trans-blot module | Bio-Rad |
| Neubauer haemocytometer | Marienfeld |

Table 2-9 Tools

| **Tool** | **Manufacturer** |
|---|---|
| Pipettes | |
| - Accu-jet® Pro | Brand, Wertheim |
| - Research Plus (0.1–2.5 µl) | Eppendorf |
| - Research (0.5–10 µl, 2–20 µl, 10–100 µl, 20–200 µl, 100–1000 µl) | Eppendorf |
| - Finnpipette 12x 50–300 µl | Thermo Labsystems |
| S.G.E. Gas Tight Luer Lock Syringe 1 ml | Sigma-Aldrich |
| Spatula | Various |
| Storage box for grids | Plano GmbH |
| Telfon-glass homogenizer with compatible pestles (15 ml, 30 ml) | B. Braun Biotech Melsungen |

Table 2-10 Consumables

| **Consumable** | **Manufacturer** |
|---|---|
| BEEM capsules, size 00 | PLANO GmbH |
| Combitips advanced | Eppendorf, Hamburg |
| Conical Centrifuge Tubes (15 ml, 50 ml) | Falcon |
| Dropping bottles | Bürkle |
| Easy Embedding Mold, Size 3 | Science Services |
| EconoPac® 10 DG Columns | Bio-Rad |
| Gel cassettes 1.0 mm | Novex Life Technologies |
| Griffin beakers, PP | Bürkle |
| Multiwell plates | |
| - 12-well | Falcon |
| - 96-well, clear, V shape | Nunc |
| - 96-well, clear, flat bottom | Falcon |
| - 96-well, white, flat bottom | Thermo Fisher Scientific |
| - 96-well, black, clear flat bottom | Greiner Bio-One |
| - 96-well, black, clear glass bottom | PerkinElmer |
| - Light Cycler Plates (Frame Star® 480) | 4titude |
| Parafilm | Sigma |
| Pasteur pipettes | |
| - Glass | Hirschmann |
| - PE | Brand |
| Petri dishes (5 cm, 10 cm) | Falcon |
| Pipette tips | |
| - 0.01–10 µl, 2–200 µl, 50–1000 µl | Eppendorf |
| - 10 µl, 20 µl, 200 µl, 1000 µl (filter) | Starlab |
| - Gel loading tips multiflex | Roth |
| - Pipettes sterile (5 ml, 10 ml, 25 ml, 50 ml) | Greiner Bio-One |
| Polypropylene Round-Bottom Tubes (14 ml) | Falcon |
| Polyvinyldifluoride (PVDF) membranes | Bio-Rad |
| Razor blades | Apollo |

Table 2-10 Consumables

| Consumable | Manufacturer |
|---|---|
| Reaction vessels | |
| - 0.2 ml, clear, thinwall (PCR) | Eppendorf |
| - 0.5 ml, clear, safe lock, biopur | Eppendorf |
| - 1.5 ml; 2.0 ml, clear, non-sterile | Sarstedt |
| - 1.5 ml, 2.0 ml, clear, safe lock, biopur | Eppendorf |
| - 1.5 ml, black | Roth |
| - 5.0 ml, clear, safe lock, non-sterile | Eppendorf |
| Reflotron test stripes (AST, bilirubin) | Roche |
| Screw thread vials (glass) with caps | Neolab |
| Semi-micro cuvette, PS, capacity 1.5 ml | Brand |
| Single-use hypodermic needles (size 18; 25) | B. Braun |
| Single-use spatula | Heathrow Scientific |
| Sterile filter 0.22 µm | GE Healthcare |
| Sterile hypodermic syringes Injekt® Solo (1 ml, 2 ml, 5 ml, 10 ml, 20 ml) | B. Braun |
| TEM Grids, Formvar Film coated, 1000 µm, Single Hole, Cu | Science Services |
| Transparencies for immunoblots | 5star |
| Vials of polyethylen Minis 2001 scintillation tubes | ZINSSER ANALYTIC |
| Whatman Gel Blotting Paper GB005, 58x58 cm | VWR |

## 2.1.11 Software

Table 2-11 Software

| Program | Application |
|---|---|
| Adobe Photoshop CS6 | Image editing |
| BioEdit 7.1.11 | Sequence analysis |
| ChemoStar Imager | Chemiluminescent imaging of immunoblots |
| UV Probe 2.43 | Ceruloplasmin measurement |
| Curve Analyst; Evaluator;<br>MATLAB Compiler Runtime 7.17 | Analysis of mitochondrial transmembrane potential and mitochondrial permeability transition |
| Definiens Tissue Studio 3 | Quantification of immunohistochemistry staining for COX17 |
| Endnote X5 | Citation of literature |
| Gen5 | Synergy 2 Biotek Reader |
| GraphPad Prism 7 | Statistical analysis |
| ImageJ 149 | Quantification of immunoblots |
| Light Cycler® 480 Software Release 1.5.0 SP4 | Quantitative Realtime PCR |
| MicroWin 2010, Version 5.17 | ATP assay |
| Harmony 3.5.2 | Immunofluorescence analysis |
| Scaffold 4 | Analysis of proteomic data |
| SoftMaxPro 5.2 | Determination of protein content in cell culture samples |
| Vi-Cell XR 2.04 | Growth curves |

## 2.2 Methods

### 2.2.1 Wilson disease patient liver samples

**WD patient liver samples were kindly provided by Karl-Heinz Weiss, University Hospital Heidelberg, Germany.**

Patients were enrolled by giving their informed consent, and the study protocol conformed to the ethical guidelines of the 1975 Declaration of Helsinki as reflected in the a priori approval by the ethical committee of the Medical University of Heidelberg.

Four WD patients with liver failure, transplanted at the University Hospital Heidelberg for Wilson disease, were included in this thesis. Two patients (no. 1 and 2, sections 3.1.2, 3.1.3 and 3.3) were not treated with copper chelators, while two patients (no. 3 and 4) underwent liver failure after D-penicillamine (D-PA) treatment [1]. After explantation, WD patient livers were shock frozen in liquid nitrogen and stored at -80 °C [1]. Thawed tissue samples were immediately fixed for electron microscopy analysis using glutaraldehyde [1].

### 2.2.2 Animal experiments

**All parts of animal experiments were done together with Josef Lichtmannegger and Tamara Rieder.**

Animal experiments were verified by the Ausschuss für Tierversuche und Versuchstierhaltung (ATV) at the Helmholtz Center Munich, Neuherberg, Germany, and approved by the ethical committee of the Regierung von Oberbayern, Munich [1].

#### 2.2.2.1 Animals

The LPP rat strain was provided by Jimo Borjigin, University of Michigan, Ann Arbor, Michigan, USA [1, 2, 152]. The LPP rat is a crossbreed between LEC rats, carrying a deletion in the *Atp7b* gene, and PVG rats [2, 152]. Rats had access to an *ad libitum* Altromin 1314 diet (Altromin Spezialfutter GmbH, copper content of the rat diet was 13 mg/kg) and tap water [1, 152]. All rats were housed under the guidelines for the care and use of laboratory animals of the Helmholtz Center Munich, Neuherberg, Germany [152]. In this study, heterozygous *Atp7b*$^{+/-}$ rats served as controls [1].

### 2.2.2.2 Genotyping of LPP rats

Genotyping of LPP rats was done as described previously [2] with slight modifications. In brief, DNA isolation was performed from rat tailes or ear punches using DirectPCR® Lysis Reagent Tail or Ear Kit from Peqlab according to the manufacturer's instructions. Polymerase chain reaction was done using 2.5 µl 10X PCR buffer (Qiagen), 0.5 µl dNTPs (Qiagen), each 1 µl primer mix 1 and 2 as described in section 2.1.4, 0.12 µl *Taq* DNA polymerase (Qiagen), 17.88 µl PCR water (Sigma), and 2.0 µl of isolated DNA per sample. PCR program includes 15 minutes at 95 °C for initial denaturation, 35 cycles of 30 seconds at 94 °C for denaturation, 30 seconds at 57 °C for primer annealing, and one minute at 72 °C for DNA synthesis, and finally ten minutes at 72 °C for terminal DNA synthesis. PCR product was loaded on a 1% agarose gel with ethidium bromide and analysed against 100 bp DNA ladder obtained from Fermentas.

If PCR result was not unambigous, sublingual sampled blood obtained from the rats was mixed with 5 µl heparin and centrifuged for two minutes at 16 100 rcf to gain plasma. Plasma was analysed regarding ceruloplasmin oxidase activity as described by Schosinsky *et al.* [216]. In common with WD patients, LPP *Atp7b*$^{-/-}$ rats show no ceruloplasmin oxidase activity in comparison to heterozygous and homozygous wild type rats [217].

### 2.2.2.3 Examination of serum and plasma parameters and definition of animal disease states

For determination of serum or plasma aspartate aminotransferase (AST) and bilirubin concentrations, sublingual blood (during monitoring) or blood from vena cava (final blood sampling) was collected in 1.5 ml reaction vessels without or with 5 µl heparin (25 000 U/ml), mixed, and centrifuged for two minutes at 16 100 rcf for gaining serum or plasma. Based on the staining of the test stripes, reflection measurement of blood values was done using Reflotron® Plus according to the manufacturer's instructions (Roche Diagnostics, Germany). Increased AST (>200 U/L) and bilirubin values (>0.5 mg/dl) are indicators for liver disease. The following parameters were defined for several disease states of LPP *Atp7b*$^{-/-}$ rats: affected (AST <200 U/L, bilirubin <0.5 mg/dl), disease onset (AST >200 U/L, bilirubin <0.5 mg/dl), diseased (AST >200 U/L, bilirubin >0.5 mg/dl) and moribund (AST >200 U/L, bilirubin >8 mg/dl) [1].

#### 2.2.2.4 Animal treatments

*Atp7b*$^{-/-}$ rats were treated with D-PA [152, 165, 218], trientine (TETA) [219] or methanobactin (MB) with or without zinc (Zn) [1] as summarised in Table 2-12. For D-PA, the long-term oral application of 100 mg/kg bw/d successfully prevents the onset of hepatitis in LEC rats [165, 218]. The oral application of 3000 ppm TETA via the drinking water revealed no toxicity in subchronic toxicity studies in rats [1, 219]. At the age of treatment start (about day 85), *Atp7b*$^{-/-}$ rat livers have a copper content of approximately 250 µg/g w.w. [1, 152]. As an *Atp7b*$^{-/-}$ rat liver of 8 g w.w. contains around 31.5 µmol copper, single MB doses were applicated equimolar to this copper amount [1]. The copper chelators were applied at a molar ratio of MB 1 : D-PA 4.3 : TETA 17.4 [1]. MB was kindly provided by Alan A. DiSpirito. Agents were dissolved in drinking water (D-PA, TETA) or sodium chloride (MB).

Table 2-12 Treatment of LPP *Atp7b*$^{-/-}$ rats

| **Agent** | **Treatment** | **Dosage** | **Application** | **Rats** |
|---|---|---|---|---|
| D-PA | 4 d | 100 mg/kg bw/d [165, 218] | Orally (drinking water) | 4 |
| TETA | 4 d | 480 mg/kg bw/d [219] | Orally (drinking water) | 4 |
| MB | 3 d, 1x/day | 150 mg/kg bw/injection | Intraperitoneally | 3 |
| MB | 5 d, 1x/day | 150 mg/kg bw/injection | Intraperitoneally | 6 |
| MB + Zinc | 5 d, 1x/day + 2–3 weeks Zn | 150 mg/kg bw/injection + 80 mg/kg bw/d | Intraperitoneally (MB), orally (food, Zn) | 3 |
| MB | 8 d, 2x/day | 150 mg/kg bw/injection | Intraperitoneally | 4 |
| MB | 5 d, 3x/day + observation periods | 150 mg/kg bw/injection | Intraperitoneally | 4 |

### 2.2.3 Cell culture experiments

#### 2.2.3.1 Cell cultivation

For cell culture experiments, HepG2 cells with different genetic background were used. HepG2 cells without any genetic alterations are named as wild type (WT), whereas HepG2 cells with *COX17* knockdown or overexpression are named as COX17- and COX17+, respectively. WT cells were passaged twice a week and not longer used than 20 passages. For subcultivation, medium containing 10% FCS (standard subcultivation condition) was used, whereas for all treatments, medium containing 2% FCS (termed as “control”) was used.

### *Subcultivation*

For subcultivation of HepG2 cells, cells were washed once with PBS without calcium and magnesium and trypsinised for six minutes at 37 °C and 5% carbon dioxide (standard subcultivation conditions). Trypsination was stopped using warmed 10% FCS containing medium. After centrifugation for five minutes at 200 xg, cell pellets were resuspended in medium with 10% FCS and cells were separated using a hallow needle. Cell number was determined using a Neubauer haemocytometer. Differentiation between live and dead cells was done using trypan blue.

### *Cell proliferation*

Growth curves were done to analyse proliferation and viability of HepG2 cells. $1 \times 10^5$ cells per 1 ml DMEM supplemented with 10% FCS were seeded per well of a 12-well plate and grown for 24 hours. Afterwards, for the 24 hour value, supernatant from one well per condition was collected and the well was washed once using PBS without $Ca^{2+}$ and $Mg^{2+}$. Cells were trypsinised with 250 µl trypsin for five minutes at 37 °C and 5% $CO_2$. Trypsination was stopped by adding 250 µl DMEM with 10% FCS. Wells were rinsed with another 500 µl DMEM with 10% FCS. Cell counting was done using live-dead staining with trypan blue in a Cell Viability Analyzer (Beckman Coulter). Remaining wells were used for medium shift to 1 ml of fresh DMEM with 10% FCS (standard subcultivation condition), DMEM with 2% FCS (control) or 15 µM copper-histidine (Cu-His) in DMEM with 2% FCS and allowed to grow for another 24 to 48 hours.

### *Neutral red assay*

For cellular cytotoxicity analyses, neutral red assay was performed as described by Repetto *et al.* with slight modifications [220]. The uncharged dye neutral red is taken up by endocytosis into the acidic lysosomes and protonated, preventing the dyes release from the cells [220]. Not viable cells do not take up neutral red and are not stained [220]. $2 \times 10^4$ HepG2 cells per well were seeded in columns one to eleven of a sterile clear 96-well flat bottom plate and grown for 24 hours at 37 °C and 5% $CO_2$. Column twelve just contains medium without cells as it functions as background. Afterwards, growth medium was discarded from four wells and 100 µl DMEM with 1.6 µM Hoechst 33342 was added for 20 minutes at 37 °C and 5% $CO_2$ for nucleus staining. Nuclei were counted using fluorescence microscope EVOS FL (Life Technologies) to ensure a similar cell amount among repeated neutral red assays. For treatment, 100 µl of the agents diluted in MEM (D-PA, TETA, MB, TTM, CCCP, Figure 3-10) or DMEM (Cu-His, section 3.4) supplemented with 2% FCS were added and incubated for 24 hours. Medium was removed and 100 µl of freshly prepared and filtrated neutral red solution was added for two hours at 37 °C and 5% $CO_2$. Cells were washed once with 150 µl PBS and neutral red was removed from cells using 150 µl destain solution by shaking for ten minutes at room temperature and 5 rpm. Fluorescence was measured at ex 520/25 nm and em 620/40 nm. Amount of viable cells from several treatments was calculated relative to the control.

### *Cellular ATP content*

For the analysis of the cellular ATP content of HepG2 cells, bioluminescence signals of luciferase was measured using CellTiterGlo Assay Kit according to the manufacturer's instructions [221]. Living cells produce ATP, whereas dead cells do not [221]. $2 \times 10^4$ HepG2 cells per well were seeded in white 96-well plates and grown for 24 hours at 37 °C and 5% $CO_2$. Medium was displaced by 100 µl agent (increasing concentrations of copper-histidine) diluted in DMEM supplemented with 2% FCS and incubated for 24 hours in a 37 °C incubator. Wells were washed twice with PBS. ATP standard was diluted in PBS from 4 µM to 0.05 µM. From each standard dilution step 100 µl were pipetted in two wells. Finally, luminescence was measured after adding 30 µl of CellTiterGlo reagent to each well, shaking for two minutes at 5 rpm and room temperature as well as incubation for ten minutes at room temperature. ATP content was calculated according to the standard measured in parallel and referred relative to the control.

### *Immunofluorescence stainings*

Immunofluorescence analyses of HepG2 cells were done using black poly-d-lysine coated 96-well plates with clear glass bottom. $2 \times 10^4$ HepG2 cells were seeded into each well and grown for 24 hours at 37 °C and 5% $CO_2$ [1]. Medium was displaced by 100 µl agent (medium, 500 µM MB, 10 µM TTM, 250 µM CCCP) diluted in MEM supplemented with 2% FCS and incubated for two to six hours in a 37 °C incubator [1]. Cells were stained for 40 minutes at 37 °C and 5% $CO_2$ with 1.6 µM Hoechst 33342 (ex 360–400 nm, em 410–480 nm), 300 nM MitoTracker® Deep Red (ex 620–640 nm, em 650–760 nm) and 1 µM nonyl acridine orange (NAO, ex 460–490 nm, em 500–550 nm) [1]. Finally, cells were washed twice using MEM without phenolred and measured using operetta fluorescence imaging system [1].

### *Treatment of HepG2 cells for metal content determination*

For determination of copper values, 3 x $10^6$ HepG2 cells were seeded into 10 cm plates and incubated for 24 hours at 37 °C and 5% $CO_2$. Cells were treated for 24 hours with 500 µM MB. Moreover, cells were first treated for 24 hours with 15 µM Cu-His and for another 24 hours with medium (control), 500 µM MB, 10 µM TTM, 1000 µM D-PA or 1000 µM TETA (cells in MEM medium, Figure 3-12). HepG2 cells were trypsinised as described above and counted using a haemocytometer. 2.5 x $10^6$ HepG2 cells were wet ashed using 65% $HNO_3$ and analysed for copper content.

### 2.2.3.2 Copper-histidine solution

Copper-histidine solution (Cu-His) was prepared as described by Hoppe-Tichy [222]. In brief, 0.108 g Cu(II)chloride dihydrate and 0.3666 g L-histidine were mixed, solved in 80 ml 0.9% sodium chloride, pH was adjusted to 7.4 at 37 °C using 0.2 N sodium hydroxide, and finally, volume was added to 100 ml with 0.9% sodium chloride. Solution was sterile filtrated and stored in 10 ml aliquots at 4 °C.

For analysis of cellular proliferation, treatment of HepG2 cells for isolation of mitochondria and *COX17* knockdown and overexpression experiments, a dose of 0.2 nmol Cu-His per $10^5$ cells was used (marked in *italics*, Table 2-13). This dose is determined to be non-toxic to HepG2 cells, but significantly increases cellular copper load (see section 3.4).

Table 2-13 Concentration and respective dose of Cu-His used for several assays

*A dose of 0.2 nmol Cu-His per $10^5$ cells (marked in italics) was used for analysis of cellular proliferation, treatment of HepG2 cells for isolation of mitochondria and COX17 knockdown and overexpression experiments.*

| **Assay** | **Neutral red, ATP content** | **Metal content determination** | **Dose [nmol/$10^5$ cells]** |
|---|---|---|---|
| Plate | 96-well | 10 cm | |
| Cell number | 2 x $10^4$/well | 3 x $10^6$/plate | |
| Treatment volume | 100 µl | 5 ml | |
| Cu-His [µM] | 0.02 | 0.03 | 0.0004 |
| | 2 | 3 | 0.04 |
| | *10* | *15* | *0.2* |
| | 200 | 300 | 4 |
| | 1000 | - | 20 |
| | 2000 | - | 40 |

## 2.2.4 Isolation and analysis of mitochondria from liver tissue and HepG2 cells

Freshly isolated rat liver mitochondria were used for analyses of swelling (mitochondrial permeability transition, MPT), mitochondrial transmembrane potential (MMP), membrane fluidity, ATP synthesis and fixed with glutaraldehyde for subsequent electron microscopy analyses [1]. Stored frozen mitochondria were used for metal and immunoblot analyses.

### 2.2.4.1 Subfractionation of human and rat liver tissue and isolation of liver mitochondria

LPP rats were sacrificed according to the ethical guidelines and national legislation using overdose of isoflurane [223]. After opening of the abdomen, vena cava was cutted and liver was rinsed using 10 ml physiologic sodium chloride. Remaining fat and diaphragm were removed and liver was weighed. Mitochondria were derived from freshly prepared rat liver homogenate by differential centrifugation and density gradient as described previously [152, 224]. Isolated rat liver mitochondria from MB and zinc treated LPP *Atp7b*$^{-/-}$ rats were purified using percoll density gradient as described elsewhere [1, 225]. For all other animals, nycodenz density gradient was used [1].

Human liver mitochondria were isolated from frozen explanted WD patient livers as described previously [1, 152, 224].

### 2.2.4.2 Isolation of mitochondria from HepG2 cells

Isolation of mitochondria from HepG2 cells was performed as described by Schmitt *et al.* with slight modifications [226, 227]. In brief, 7 x $10^6$ HepG2 cells/ml were pumped four times with a speed of 1400 µl/minute through the cell homogenizer. Mitochondria (without purification via a density gradient) were collected and used for metal content determination and immunoblot analysis.

### 2.2.4.3 Measurement of the mitochondrial membrane fluidity

The mitochondrial membrane fluidity was measured by fluorescence polarisation using DPH and TMA-DPH as described previously [228-230]. Both compounds insert into biological membranes like the MIM: DPH in the membrane inner lipid phase and TMA-DPH in the lipid-water interface [230-232]. Excitation of the fluorophores with a defined wavelength leads to the emission of polarised light, whereby polarisation depends on the rotation of fluorophores within the membrane and thus on the membrane fluidity [233]. Less rotation leads to stronger polarised light, indicating less membrane fluidity, and strong motion ejects wider spread signals, indicating more fluid membranes [233]. 1500 µg of isolated rat liver mitochondrial protein were incubated with 50 µM DPH solved in tetrahydrofurane or 20 µM TMA-DPH solved in anhydrous dimethylsulfoxide for 30 minutes at 37 °C [1]. To a 96-well plate containing 175 µl standard swelling buffer, 75 µg mitochondrial protein was added. Measurement was done for three hours in three minute intervals at 37 °C in a fluorescence reader (Synergy 2, BioTek, Germany) with ex 366 nm and em 425 nm [1]. For measurement of fluorescence polarisation, excitation was done with vertically polarised monochromatic light [228]. Emission intensity was detected through an analyser oriented parallel ($I_{\parallel}$) or perpendicular ($I_{\perp}$) to the direction of polarisation of the excitation light [228]. Polarisation was calculated in mPol using the formula $P = (I_{\parallel} - G * I_{\perp}) / (I_{\parallel} + G * I_{\perp})$, whereby $G = 0.89$ is a correction factor for the optical system [1, 230].

#### 2.2.4.4 Simultaneous measurement of MMP-loss and MPT-induction and curve sketching

MMP of freshly isolated rat liver mitochondria was measured using the fluorescence dye rhodamine 123 (Rh123) [234, 235]. Intact mitochondria take up Rh123, leading to self-quenching of the dyes fluorescence [234, 235]. If MMP becomes impaired, the dye is released, leading to increasing fluorescence signals [235]. Swelling was measured to analyse the mitochondrias ability to unfold their inner membrane. Treating isolated mitochondria with cations [236] depolarises the MMP and uncouples OXPHOS from mitochondrial ATP production [237-239]. This induces an unspecific increase in the permeability of the MIM [237, 240] and molecules and ions for up to 1.5 kDa can enter the matrix [236, 238, 240]. The increasing ion concentration within the matrix is accompanied by an increased influx of water, leading to matrix swelling [237, 241], unfolding of the MIM and finally to mitochondrial outer membrane permeabilisation (MOMP) and rupture [239, 241, 242]. A 96-well plate containing 75 µg per well freshly isolated rat liver mitochondria in standard swelling buffer supplemented with Rh123 was parallel monitored for MMP-loss (fluorescence, ex 485/20 nm, em 528/20 nm) [1, 243] and MPT (light scattering, decrease of $OD_{540\,nm}$) [1, 244] in a Synergy2 plate reader (BioTek, 180 minutes, three minute intervals, 37 °C) [1]. Detailed conditions are summarised in Table 2-14. Appropriate curve slopes were calculated using MATLAB software as described by Schulz *et al.* [245]. For calculation, in cases with onset but not finished MMP depletion, end values were set to 180 minutes [1]. MPT extent was calculated by using the optical density from the respective end time of the MPT process (obtained by MATLAB software) in % relative to the optical density at the start of MPT induction.

Table 2-14 Inducers for measurement of MMP and swelling in mitochondria

| **Inducer** | **Analysed Parameter** |
|---|---|
| SWP1 | Stability of MMP |
| 100 µM $Ca^{2+}$ | Induction of mitochondrial swelling (ability of the mitochondria to unfold their inner membrane, swelling extent) |
| 100 µM $Ca^{2+}$ + 5 µM CysA | Inhibition of calcium-induced mitochondrial swelling |
| 100 µM $Cu^{2+}$ | Induction of mitochondrial swelling (ability of the mitochondria to unfold their inner membrane, swelling extent) |
| 1 µM FCCP | Disruption of the MMP |

#### 2.2.4.5 ATP synthesis

ATP synthesis from freshly isolated rat liver mitochondria was measured by bioluminescence using firefly luciferase from ATP Bioluminescence Assay Kit CLS II, Roche, according to the manufacturer's instructions [1].

### 2.2.5 Protein analyses

#### 2.2.5.1 Determination of mitochondrial and cellular protein concentration

Protein concentration of isolated mitochondria was determined by the method of Bradford [246]. Pierce reagent was used for the measurement of the protein concentration in lysates from cell culture samples similar to the manufacturer's instructions for microplate procedure [247]. In detail, 75 µl Pierce reagent and 5 µl of sample were used for measurement.

#### 2.2.5.2 Immunoblot analyses

Immunoblot analyses of proteins were performed according to Towbin *et al.* with slight modifications [248]. 20 µg protein were subjected to SDS-PAGE and separated proteins were transferred onto a polyvinyldifluoride (PVDF) membrane at 4 °C. Ponceau S staining was used to control protein transfer. Protein binding sites were saturated with 5% milk in TBS-T for 30 minutes at 4 °C. Binding of the primary (over night) and secondary antibody (one hour) was done at 4 °C and chemiluminescence signals were detected using ChemoCam Imager 3.2. Chemiluminescence signals were quantified using ImageJ and normalised to the following house keeping enzymes: mitochondrial citrate synthase (CS) for isolated mitochondria (Figure 3-20, Figure 3-25B) or β-actin (Figure 3-25A) or GAPDH (Figure 3-26B, Figure 3-27B) for HepG2 cell lysates. To detect several proteins, primary and secondary antibodies were removed from the membrane with SDS according to Kar *et al.* [249].

### 2.2.5.3 Proteomic analyses of *Atp7b* rat liver mitochondria

#### *Sample preparation*

Proteomic analyses of isolated rat liver mitochondria and mitochondrial subfractions were done to identify mitochondrial proteins that are involved in copper metabolism in WD. 100 µg mitochondrial protein were solubilised in 100 µl 1% weight per volume n-Dodecyl β-D-maltoside (DDM) for 30 minutes at 4 °C on a rotator. 10 µg were diluted 1 : 5 in IP$^-$ buffer. Each 5 µg from the two fractions with the highest copper content from anion exchange chromatography were collected as described in section 2.2.7.

For the identification of interaction partners of COX17, samples were prepared as described in section 2.2.8.1.

#### *Liquid-chromatography-mass spectrometry/mass spectrometry (LC-MS/MS)*

**Proteomic analyses, protein identification and quantification were done by Dr. Christine von Törne, Helmholtz Center Munich, Research Unit Protein Science, Neuherberg, Germany. Comparative analyses of protein abundances were done by myself and are shown in section 3.3.**

**MS sample preparation and mass spectrometry**

Mitochondria and subfractions were lysed at 70 °C in 2% SDS lysis buffer and sonicated on ice six times for 15 seconds. 10 µg protein were diluted in urea buffer and reduced by dithiothreitol (DTT) at 60 °C. Samples were centrifuged on a 30 kDa cut-off filter device (PALL). Proteins were proteolytically cleaved for two hours at room temperature using 1 µg lysyl endopeptidase (Lys-C; Wako) and for 16 hours at 37 °C using 2 µg trypsin (Promega). Peptides were collected by centrifugation and analysed by LC-MS/MS analysis on a LTQ-Orbitrap XL (Thermo Scientific) [250]. Samples were loaded onto a nano trap column (300 µm inner diameter × 5 mm, packed with Acclaim PepMap100 C18, 5 µm, 100 Å; LC Packings, Sunnyvale, CA) and peptides were separated by reversed phase chromatography (PepMap, 25 cm, 75 µm ID, 2 µm/100 Å pore size, LC Packings) on a nano-HPLC (Ultimate 3000, Dionex) using a nonlinear LC gradient from 5–31% of 98% acetonitrile, followed by a 31–95% gradient of 98%

acetonitrile and equilibration for 15 minutes to starting conditions. The ten most abundant peptide ions from the MS prescan were fragmented in the linear ion trap if exceeding an intensity of 200 counts and being at least doubly charged. The MS spectrum was acquired in the Orbitrap with a mass range from 300 to 1500 Da.

**Protein identification and label-free relative quantification**

The RAW files (Thermo Scientific) were analysed using the Progenesis LC-MS (v4.1, Nonlinear Dynamics) as described previously [250, 251], with the following changes: Spectra were searched using the search engine Mascot (Version 2.4, Matrix Science) against the Ensembl rat database (release 75; 25724 sequences). Search parameters used were: 10 ppm peptide mass tolerance, 0.6 Da fragment mass tolerance, one missed cleavage allowed, carbamidomethylation as fixed and methionine oxidation as well as asparagine or glutamine deamidation as variable modifications. Using the Percolator algorithm (score cut-off 15, significance threshold $p<0.05$), an average peptide false discovery rate of <1% was calculated. Normalised abundances of all unique peptides were summed up and allocated to the respective protein.

### 2.2.6 Molecular biological methods

**Knockdown and overexpression of *COX17* in HepG2 cells was done under the supervision of Dr. Michelle Vincendeau, Helmholtz Center Munich, Institute of Molecular Toxicology and Pharmacology, Neuherberg, Germany.**

#### 2.2.6.1 Knockdown of *COX17* in HepG2 cells using siRNA

For all knockdown experiments with siRNA, sterile filter tips were used. Inducing knockdown of *COX17* in HepG2 cells was done using Lipofectamin® RNAiMAX reagent from Life Technologies according to the reverse transfection protocol of the manufacturer. Knockdown was proofed by both, immunoblot analyses and quantitative realtime PCR (qRT-PCR, see section 2.2.6.2). Three different siRNAs with the sequences listed in Table 2-1 and synthesised by eurogentec were tested. SiRNA 3 showed the best knockdown results without inducing massive cell death and was therefore used for all following experiments.

#### 2.2.6.2 Overexpression of *COX17* in HepG2 cells

**RNA isolation from HepG2 cells**

RNA isolation from HepG2 cells was performed using RNeasy® Micro Kit from Qiagen according to the manufacturer’s instructions. For cell disruption, $5 \times 10^5$ HepG2 cells were resuspended in 350 µl RLT supplemented with 3.5 µl 2-mercaptoethanol, added to a Qiashredder column and centrifuged for one minute at 16 100 rcf. RNA was isolated from HepG2 WT cells for establishing overexpression of *COX17* and from transfected HepG2 cells (nonsilencing RNA, COX17-, empty pcDNA3.1(+) vector, COX17+) for qRT-PCR. RNA content was measured using NanoDrop 2000.

### Translation of RNA to cDNA

For translation of RNA into cDNA, Verso cDNA Synthesis Kit from Thermo Scientific was used. 4 µl 5X cDNA synthesis buffer, 2 µl dNTPs, each 1 µl random hexamer primer, RT enhancer and Verso enzyme mix, and 1 µg RNA added to 20 µl with nuclease-free water were incubated for 30 minutes at 42 °C and two minutes at 95 °C.

### Amplification of cDNA

Amplification of cDNA was done using Expand High Fidelity PCR system (Roche). Primers (NHE-3xFLAG_COX17 (forward) and PmeI (reverse)) were diluted to 20 µM with nuclease-free water. PCR samples contained 5 µl 10X reaction buffer with $MgCl_2$, 1 µl 10 mM dNTPs, each 1 µl 20 µM primer forward and reverse, 1 µl cDNA or water (control) and 0.75 µl *Taq* DNA polymerase added to 50 µl with nuclease-free water.

PCR cycling conditions were as follows: initial denaturation for five minutes at 95 °C, 30 cycles at 95 °C for 30 seconds denaturation, 60 °C for 30 seconds annealing of primers and 72 °C for one minute for elongation. Final elongation was done for seven minutes at 72 °C.

### Agarose gel electrophoresis

Gels containing 1.5% agarose and 1 : 10 000 diluted 1% ethidium bromide (dissolved in 1X TBE buffer) were used for electrophoresis at 110–120 V. As standard, 2-log DNA ladder from New England Biolabs was used. Bands with respective size were cutted using a scalpel.

### Isolation of DNA from agarose gels

DNA isolation from agarose gels was done using NucleoSpin Gel and PCR Clean-up Kit from Macherey-Nagel according to the manufacturer’s instructions.

### Endonuclease treatment

Endonuclease treatment of DNA and plasmid was done for 90 minutes at 37 °C as summarised in Table 2-15.

Table 2-15 Endonuclease treatment

| **Component** | **Plasmid pcDNA3.1(+)** | ***COX17* cDNA (NheI/PmeI)** |
|---|---|---|
| Template amount | 1.5 µg | 10 µl |
| Buffer | 5 µl Cut Smart | 5 µl Cut Smart |
| Enzyme 1 | 1 µl NheI | 1 µl NheI |
| Enzyme 2 | 2 µl PmeI | 2 µl PmeI |
| Nuclease-free $H_2O$ | Add to 50 µl | Add to 50 µl |

### Ligation of vector and insert

For ligation, an insert to vector ratio of three to one was used. Amount of insert was calculated using the formula: Insert [ng] = (50 ng vector x 0.2 kb insert) / (x kb vector). For the pcDNA3.1(+) vector, 5.5 ng of insert was used. Ligation was performed for 30 minutes using the following approach from the Rapid DNA Ligation Kit (Thermo Fisher Scientific): 5 µl dilution buffer, 5 µl ligation buffer, 0.75 µl T4 DNA ligase as well as the respective amount of vector and insert. Vector-insert constructs were sequenced by Eurofins MWG GmbH, Ebersberg, Germany and analysed using BioEdit 7.1.11.

### Plasmid amplification

*Escherichia coli* Top10 cells were thawed on ice for five to ten minutes. Either 1 µg pcDNA3.1(+) plasmid or whole ligation approach was added to the bacteria and chilled on ice for 30 minutes. Heat shock was done for 45 seconds at 42 °C and subsequently hold on ice for two minutes. After addition of 250 µl S.O.C. medium, bacteria were incubated at 37 °C and 800 rpm for one hour. Transformation samples were shortly centrifuged, 100 µl of the supernatant discarded, the remaining samples were plated to LB agar plates with antibiotic (ampicillin for pcDNA3.1(+)) and these were incubated upside down over night at 37 °C.

### Minipreparation of plasmid DNA

For mini culture, single colonies from plasmid amplification were transferred to 5 ml LB medium containing 1 : 1000 diluted ampicillin as antibiotic and shaked over night at 37 °C and 180 rpm. Isolation of plasmid DNA from *Escherichia coli* was performed using NucleoSpin® Plasmid Kit from Macherey-Nagel according to the manufacturer’s instructions.

### Maxipreparation of plasmid DNA

For maxi culture, 150 ml LB medium with 1 : 1000 diluted antibiotic (ampicillin) and 500 µl of mini culture were shaked over night at 37 °C and 180 rpm. Maxipreparation was done using Qiagen® Plasmid Maxi Kit according to the manufacturer’s instructions.

Sequence of vector and insert was reexamined by Eurofins MWG GmbH, Ebersberg, Germany and analysed using BioEdit 7.1.11.

#### 2.2.6.3 Reverse transfection of HepG2 cells with *COX17*

For overexpression of *COX17* in HepG2 cells, per 1 x $10^5$ cells 40 µl Optimem, 200 ng of the vector with or without insert and 1.2 µl Fugene transfection reagent were incubated according to the manufacturer's instructions. The respective amount and cells were added to the plates, mixed and allowed to grow for 24 hours before treatment started.

#### 2.2.6.4 Quantitative realtime polymerase chain reaction (qRT-PCR)

For analysis of *COX17* expression level relative to *RNA Polymerase II* (*RPII*) in knockdown and overexpression experiments, One Step SYBR® PrimeScript™ RT-PCR Kit II (Perfect Real Time) from TaKaRa was used. In brief, 12.5 µl 2X One Step SYBR RT-PCR Buffer IV, 1 µl PrimeScript 1 step Enzyme Mix II, each 0.5 µl 20 µM forward and reverse primer, and 25 ng RNA added to 25 µl with MilliQ-$H_2O$ were incubated as follows: Reverse transcription was done with each one cycle of five minutes at 42 °C and ten seconds at 95 °C, amplification was done at 95 °C for five seconds, 60 °C for 20 seconds and 72 °C for 15 seconds, repeated 40 times, during this step quantification was done, and finally, melting curves were recorded in one cycle at 95 °C for one second and 65 °C for 15 seconds.

Expression level of *COX17* normalised to the housekeeping gene *RPII* [252] was calculated according to the formula: Expression = $2^{(-(Cp_{COX17}-Cp_{RPII}))}$. Cp values are crossing points (the cycle number upon which fluorescence of SYBR green is significantly higher than the background fluorescence by the staining solution SYBR green) derived by the LightCycler® 480 Software (Roche) [253, 254]. *COX17* levels normalised to *RPII* were referred to the nonsilencing RNA for *COX17* knockdown or vector control for *COX17* overexpression, respectively.

### 2.2.7 Chromatography of mitochondrial proteins

The following methods were used for mitochondrial protein separation.

Isolated mitochondria were thawed on ice, shortly centrifuged and two aliquots of each 400 µl were taken in 1.5 ml reaction tubes. For subfractionation and enrichment of soluble proteins from the mitochondrial matrix and intermembrane space, after sonication (five bursts, cycle 0.9, amplitude 80), an 18-hour ultra-centrifugation at 100 000 xg and 4 °C was done. Membranous proteins were not analysed in this study.

#### 2.2.7.1 Gel filtration

After centrifugation, the supernatants from the duplicates were pooled. Each sample was added on an $IP^-$ equilibrated EconoPac® 10 DG Column (as specified by the manufacturer of this size exclusion column, proteins with a molecular weight of more than 6 kDa were collected). After the samples had moved into the filter, 10 ml $IP^-$ buffer were added to the column and ten fractions of each 1 ml were collected. From each sample 50 µl were used for determination of the copper concentration.

#### 2.2.7.2 Anion exchange chromatography

For anion exchange chromatography, buffer was removed from the columns, 5 ml diethylaminoethyl-Sephacel was added and the filter was inserted. The column was washed using 20 ml 20 mM ammonium acetate. The two fractions from gel filtration with the highest copper concentrations (fractions two and three) were pooled and added to the column. Upon sample entry, the column was washed twice using 20 ml 20 mM ammonium acetate. Elution was done using 10 ml 1 M ammonium acetate (ten fractions, each 1 ml). Finally, copper concentrations from the ten fractions were determined. For proteomic analyses (see section 2.2.5.3), the two fractions with the highest copper concentrations were used.

### 2.2.8 Miscellaneous

#### 2.2.8.1 Immunoprecipitation

Immunoprecipitation was done using isolated and purified rat liver mitochondria according to the method established by the working group of Dr. Alexander Wolf, Helmholtz Center Munich, Institute of Molecular Toxicology and Pharmacology, Neuherberg, Germany, and modified as follows. 1500 µg mitochondrial protein was pelleted by centrifugation for ten minutes at 9000 xg. Pellet was resuspended in 500 µl lysis buffer (containing detergent Nonidet™ P 40 Substitute) and incubated for 30 minutes on ice by shaking every ten minutes. 30 µl Sepharose G Beads were equilibrated by washing three times for two minutes at 5000 xg with 500 µl washing buffer 1. 500 µl washing buffer 1 was added to lysed mitochondria and centrifuged for twelve minutes at 13 000 xg. 100 µl of the supernatant were supplemented with 100 µl 2X laemmli and 1 µl 2-mercaptoethanol, boiled for five minutes at 95 °C, and stored as “input fraction” at -20 °C. Equilibrated beads were incubated for 15 minutes at 4 °C with 100 µl of the antibody (COX17, Santa Cruz) and, after addition of the remaining supernatant, the mixture was incubated for three hours at 4 °C on a rotator. After centrifugation for two minutes and 5000 xg, 100 µl from the supernatant were supplemented with 100 µl 2X laemmli and 1 µl 2-mercaptoethanol, boiled for five minutes at 95 °C, and stored as “flow fraction” at -20 °C. The COX17-antibody-beads containing pellet was washed twice with 500 µl washing buffer 1 and once with 500 µl washing buffer 2, each for two minutes at 5000 xg. Bead fraction was resuspended in 50 µl 1X laemmli with 3.75 µl 2-mercaptoethanol, boiled for five minutes at 95 °C and stored at -20 °C until proteomic analysis. All centrifugation steps were done at 4 °C.

### 2.2.8.2 Metal content determination

**Metal content determination was done by Peter Grill, Helmholtz Center Munich, Research Unit Analytical BioGeoChemistry, Neuherberg, Germany.**

Copper concentrations were measured in rat liver homogenates, mitochondria, mitochondrial subfractions (see section 2.2.7), cell lysates of HepG2 WT cells and mitochondria isolated from HepG2 WT cells. All solutions used for cell culture experiments were analysed for metal content to avoid unwanted copper carryover. Analyses were done by inductively coupled plasma optical emission spectrometry (ICP-OES; Ciros Vision, SPECTRO Analytical Instruments GmbH, Kleve, Germany) after wet ashing of samples with 65% nitric acid (Merck KGaA, Darmstadt, Germany) [1].

### 2.2.8.3 Electron microscopy

**Electron microscopy was done together with Carola Eberhagen (Helmholtz Center Munich, Institute of Molecular Toxicology and Pharmacology, Neuherberg, Germany), Dr. Bastian Popper (Ludwig-Maximilian-University Munich, Institute of Anatomy, Planegg-Martinsried, Germany), Gabriele Mettenleiter and Dr. Michaela Aichler (Helmholtz Center Munich, Institute of Pathology, Neuherberg, Germany).**

Liver tissue from WD patients and rats was cutted in 1 x 1 x 1 mm pieces in 2.5% glutaraldehyde. Electron microscopy from isolated mitochondria and human as well as rat liver tissue was done as described previously [1, 244, 255]. Briefly, samples were fixed in 2.5% glutaraldehyde and postfixed and prestained using 1% osmium tetroxide. After dehydration with ethanol and propylene oxide, samples were embedded in Epon 812

[255]. Ultrathin sections were negative stained with uranyl acetate and lead citrate and examined with an EM 10 CR transmission electron microscope (Zeiss, Germany).

For structural analyses, isolated rat liver mitochondria were grouped into four categories: (1) normal structured mitochondria of the “condensed” type [256], (2) mitochondria with minor alterations like slightly increased cristae, (3) mitochondria with massively increased cristae and (4) mitochondria with massive matrix condensations, matrix vacuolisation, detachments of the inner boundary membrane and severe cristae deformations [1]. For quantification, mitochondria from six figures of the 20 000-fold magnification per rat were counted.

#### 2.2.8.4 Immunohistochemistry

**Immunohistochemical staining of LPP rat liver tissue for COX17 was done in close collaboration with Claudia-Mareike Pflüger and Dr. Michaela Aichler; Dr. Annette Feuchtinger did the quantification of tissue staining, all from Helmholtz Center Munich, Institute of Pathology, Neuherberg, Germany.**

Immunohistochemical staining of rat liver tissue was done using DISCOVERY XT (Ventana Medical System, Roche, Mannheim, Germany) according to the manufacturer’s instructions. Primary antibody was COX17 (Santa Cruz) and the secondary antibody was anti-mouse (KPL). Quantification of tissue staining was done using Definiens Tissue Studio 3. Regions of interest were annotated manually and single cell-based analysis was done. Depending on the staining intensity of the cells, four categories were defined and their relative amount was calculated according to Feuchtinger *et al.* [257].

### 2.2.9 Statistics

In this thesis, “N” equals the number of biological replicates (analysed animals or cell culture experiments, respectively) and “n” the number of measurements or technical replicates [1]. Data are presented as mean ± standard deviation or mean and 25% as well as 75% quartile. If more than four technical replicates were available, Grubbs outlier test (ESD method, extreme studentized deviate) was performed with a significance level of $\alpha = 0.05$ [1]. If comparing three or more sample sets, statistical significance was analysed using one-way ANOVA with Tukey’s multiple comparisons test (GraphPad Prism 7) [1]. For comparison between two groups, the unpaired two-tailed Student’s t-test with Welch’s correction was used (GraphPad Prism 7) [1]. Throughout this study statistically significant p-values are: $^*p<0.05$, $^{**}p<0.01$, $^{***}p<0.001$, $^{****}p<0.0001$.

# 3 Results

## 3.1 The LPP *Atp7b*$^{-/-}$ rat – an animal model for liver failure in Wilson disease

The animal model used in this study is the LPP rat [2]. This rat strain carries a 13 kb deletion in *Atp7b* [2], the homologous gene affected in human Wilson disease (WD) [2].

### 3.1.1 Progressing disease states in the Wilson disease LPP *Atp7b*$^{-/-}$ rat model

Liver copper accumulation promotes progressive liver damage, finally leading to liver failure and death of *Atp7b*$^{-/-}$ rats [152]. This raises the question of whether different disease states can be defined in *Atp7b*$^{-/-}$ rats. To address this issue, the liver damage markers aspartate aminotransferase (AST) and bilirubin [71, 190] were measured in serum from *Atp7b*$^{+/-}$ and *Atp7b*$^{-/-}$ rats (Table 3-1). As WD is an autosomal recessively inherited disorder [1, 4], *Atp7b*$^{+/-}$ rats are comparable to wild type rats and served as controls [152]. AST is below 200 U/L and bilirubin is below 0.5 mg/dl in serum from *Atp7b*$^{+/-}$ rats (termed as "control") [1]. In serum from *Atp7b*$^{-/-}$ rats, AST and bilirubin levels lower and greater than 200 U/L or 0.5 mg/dl, respectively, are measured allowing the definition of the following disease states: *Atp7b*$^{-/-}$ rats with serum AST <200 U/L and bilirubin values <0.5 mg/dl are defined as "affected" [1]. These affected *Atp7b*$^{-/-}$ rats present with massive copper accumulation (see 3.1.2) but no apparent clinical signs of liver damage. *Atp7b*$^{-/-}$ rats with serum AST values >200 U/L but serum bilirubin values <0.5 mg/dl are defined as "disease onset" and *Atp7b*$^{-/-}$ rats with serum AST values >200 U/L and serum bilirubin values >0.5 mg/dl as "diseased" (Table 3-1) [1].

Table 3-1 Serum AST and bilirubin values enable the definition of different disease states of *Atp7b*$^{-/-}$ rats.

| **Disease state** | **Control** | **Affected** | **Disease onset** | **Diseased** |
|---|---|---|---|---|
| ***Atp7b* genotype** | **+/-** | **-/-** | **-/-** | **-/-** |
| Number of animals | 33 | 14 | 11 | 9 |
| AST [U/L] | 116 ± 28 | 142 ± 33 | 276 ± 60 | 463 ± 107 |
| Bilirubin [mg/dl] | <0.5 | <0.5 | <0.5 | 6.3 ± 6.5 |

### 3.1.2 Copper increasingly accumulates in liver homogenate and mitochondria from Wilson disease patients and *Atp7b*$^{-/-}$ rats with disease progression

The copper concentrations in liver homogenate and isolated liver mitochondria obtained from *Atp7b*$^{+/-}$ and *Atp7b*$^{-/-}$ rats with progressing disease states were measured spectrometrically by ICP-OES. Figure 3-1 shows low copper concentrations in liver homogenate and mitochondria from *Atp7b*$^{+/-}$ control rats (Co). In comparison, increasing copper accumulation in liver homogenate and liver mitochondria isolated from *Atp7b*$^{-/-}$ rats is observed with disease progression compared to *Atp7b*$^{+/-}$ rats [1]. To compare the rat liver and mitochondrial copper load to humans, four WD patients were included in these analyses: two of the WD patients received no treatment (Figure 3-1, no. 1 and 2) and the other two received unsuccessful D-PA treatment (Figure 3-1, no. 3 and 4) [1]. Due to acute liver failure, all four WD patients underwent liver transplantation [1]. Figure 3-1 demonstrates that copper load is comparable in liver homogenate and liver mitochondria obtained from untreated WD patients and the *Atp7b*$^{-/-}$ rats [1]. D-PA treatment reduces copper load in liver homogenate and mitochondria approximately three- to fourfold compared to untreated WD patients, nevertheless, copper loads are still four- to 30-fold higher compared to *Atp7b*$^{+/-}$ control rats [1]. D-PA often reduces liver copper load, but neurologic deterioration requires termination of D-PA treatment, leading to copper reaccumulation and acute liver failure [33, 158, 166, 167, 174]. Regarding the liver and mitochondrial copper load, the *Atp7b*$^{-/-}$ rat is a valid animal model for studying mitochondrial alterations in WD.

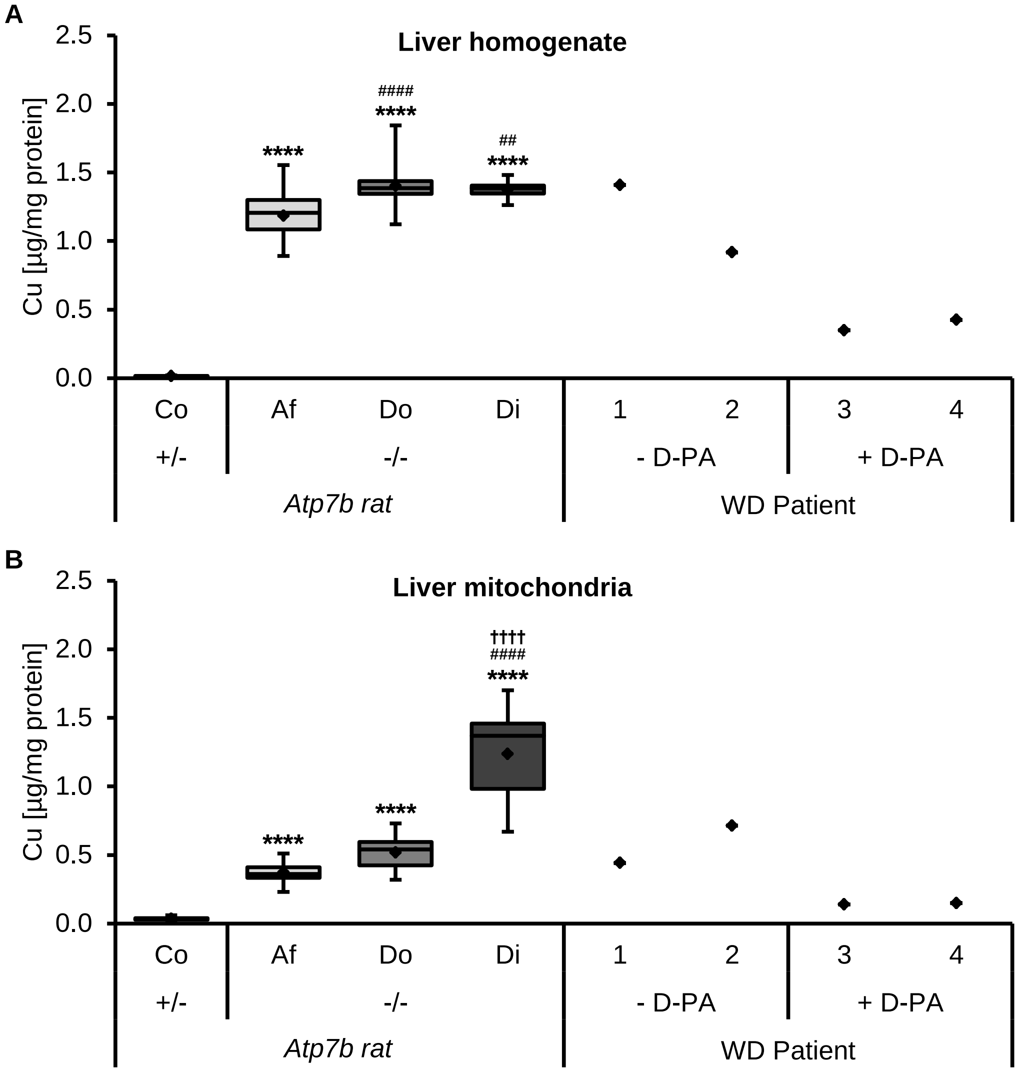

Figure 3-1 Copper load in liver homogenate and liver mitochondria increases with disease progression of *Atp7b*$^{-/-}$ rats and is highly comparable to untreated WD patients.

*Atp7b*$^{+/-}$ *control rats (Co) have a low copper load in liver homogenate (A) and liver mitochondria (B). Copper concentrations increase in both compartments of affected Atp7b*$^{-/-}$ *rats (Af) and further increase with disease progression of Atp7b*$^{-/-}$ *rats. Liver homogenate and liver mitochondria from untreated WD patients (no. 1 and 2) show copper loads comparable to Atp7b*$^{-/-}$ *rats. WD patients that received D-PA treatment before acute liver failure (no. 3 and 4) have lower copper concentrations in both compartments compared to WD patients that received no treatment prior to liver transplantation. (Co) control Atp7b*$^{+/-}$*: N=34; (Af) affected Atp7b*$^{-/-}$*: N=14; (Do) disease onset Atp7b*$^{-/-}$*: N=11; (Di) diseased Atp7b*$^{-/-}$*: N=8. WD patients: 1 and 2 untreated, 3 and 4 D-PA pretreated. Data are outlier corrected. One-way ANOVA with Tukey's multiple comparisons test. *Significant to control,* $^{\#}$*significant to affected,* $^{\dagger}$*significant to disease onset, **p<0.01, ****p<0.0001. ▬ median, ♦ mean value, 25% and 75% quartile are indicated. Adapted from Josef Lichtmannegger et al. (2016) Methanobactin reverses acute liver failure in a rat model of Wilson disease. J Clin Invest. 2016 Jul;126(7): p. 2721-35* [1]*.*

### 3.1.3 Structural alterations are comparable among mitochondria from Wilson disease patients and diseased *Atp7b*$^{-/-}$ rats

WD is characterised by massive structural alterations of liver mitochondria [33, 58, 70-72, 143-145]. The structure of liver mitochondria from WD patients was compared to diseased *Atp7b*$^{-/-}$ rats using electron miscroscopy (Figure 3-2). Liver mitochondria *in situ* from

WD patients and diseased *Atp7b*$^{-/-}$ rats show similar structural alterations. These include separation of inner and outer mitochondrial membrane, cristae dilations as well as brightening and vacuolisation of the normally electron-dense matrix [1], depicting the typical WD mitochondrial phenotype [33, 58, 70-72, 143-145]. Liver mitochondria from D-PA pretreated WD patients show heterogenous structure impairments compared to mitochondria from untreated WD patients (Figure 3-2B) [1]. Some areas contain intact mitochondria with a brightened matrix, whereas others show mitochondria with massive structural alterations [1]. These differences probably result from zonal differences as liver tissue from WD patients is highly fibrotic [1].

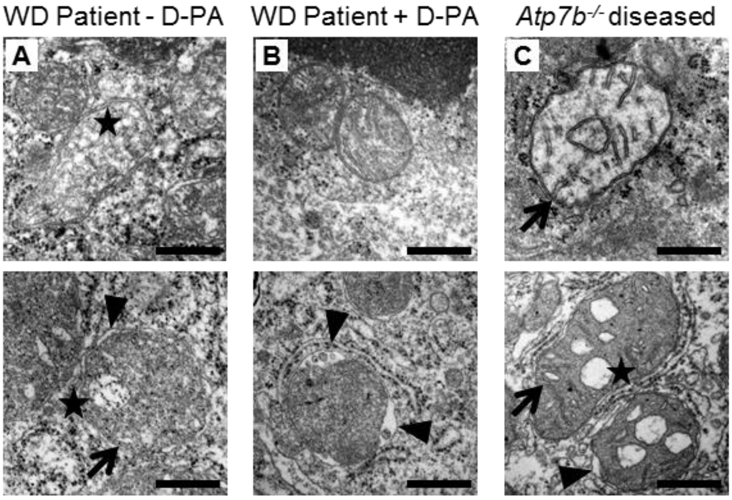

Figure 3-2 Mitochondrial structure impairments are highly similar between WD patients and diseased *Atp7b*$^{-/-}$ rats *in situ*.

*Liver mitochondria (in situ) from WD patients with acute liver failure (A: untreated, and B: D-PA pretreated prior to liver transplantation) show similar structural alterations as liver mitochondria from diseased Atp7b*$^{-/-}$ *rats (C). Separation of inner and outer boundary membrane (arrowhead), cristae dilations (arrow) as well as brightening of normally electron-dense matrix and transparent vacuoles of varying sizes (asterisk) can be observed. Some liver mitochondria from D-PA pretreated WD patients are relatively intact (upper panel), whereas others demonstrate severe structural impairments (bottom panel). Scale bar: 500 nm. Adapted from Josef Lichtmannegger et al. (2016) Methanobactin reverses acute liver failure in a rat model of Wilson disease. J Clin Invest. 2016 Jul;126(7): p. 2721-35* [1].

### 3.1.4 Increasing mitochondrial copper load is paralleled by structural alterations of liver mitochondria from *Atp7b*$^{-/-}$ rats

Are the structural alterations of *Atp7b*$^{-/-}$ rat liver mitochondria related to the respective disease states of these animals? To address this issue, liver mitochondria from *Atp7b*$^{-/-}$ rats with progressing disease states were analysed *in situ* using electron microscopy (Figure 3-3). Liver mitochondria from *Atp7b*$^{+/-}$ control rats are normally structured, whereas liver mitochondria from *Atp7b*$^{-/-}$ rats show increasing impairments with disease progression (Figure 3-3) [1]. In affected *Atp7b*$^{-/-}$ rat liver mitochondria, detachment of the inner (MIM) and outer mitochondrial membrane (MOM) can be observed. In liver mitochondria from disease onset and diseased *Atp7b*$^{-/-}$ rats, the distance between MIM and MOM increases. Liver mitochondria from diseased *Atp7b*$^{-/-}$ rats show further massive structural alterations, such as cristae dilations as well as brightening and vacuolisation of the normally electron-dense matrix [1].

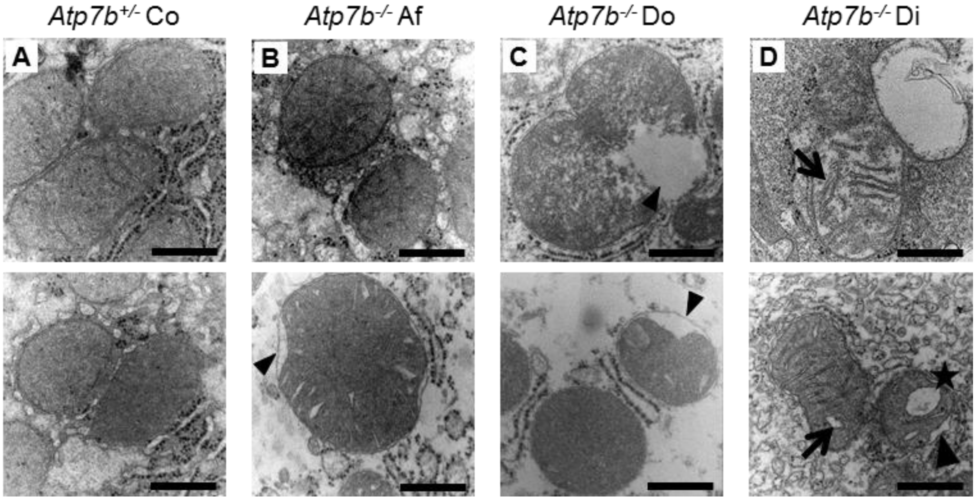

Figure 3-3 Mitochondrial structural alterations are absent in *Atp7b*$^{+/-}$ control rat livers and increase with disease progression of *Atp7b*$^{-/-}$ rats.

*Liver mitochondria in situ from Atp7b*$^{+/-}$ *control (Co) rats show no structural alterations (A). Liver mitochondria from affected Atp7b*$^{-/-}$ *rats (Af) present with structural impairments (B) that further increase with disease progression of Atp7b*$^{-/-}$ *rats (C and D, disease onset (Do) and diseased (Di), respectively). Liver mitochondria from Atp7b*$^{-/-}$ *rats present with separation of inner and outer boundary membrane (arrowhead), cristae dilations (arrow) as well as brightening of normally electron-dense matrix and transparent vacuoles of varying sizes (asterisk). Scale bar: 500 nm. Adapted from Josef Lichtmannegger et al. (2016) Methanobactin reverses acute liver failure in a rat model of Wilson disease. J Clin Invest. 2016 Jul;126(7): p. 2721-35* [1].

To quantify mitochondrial structural impairments in different disease states from *Atp7b*$^{-/-}$ rats, freshly isolated rat liver mitochondria were analysed using electron microscopy. Four classes of mitochondria are defined (Figure 3-4A): (1) normal structured mitochondria, no cristae dilations, no membrane detachment, electron-dense matrix, (2) slight structural alterations indicated by mild cristae dilation, (3) intermediate alterations with increasing cristae dilation and (4) mitochondria with massive cristae dilation, detachment of inner and outer mitochondrial membranes, matrix deformation as well as electron-dense deposits within the mitochondrial intermembrane space (IMS) [1]. For quantification, types 1 and 2 are summarised as “normal”, whereas types 3 and 4 are combined as “altered”. About 85% of the mitochondria from *Atp7b*$^{+/-}$ rats have a normal structure and approximately 15% show structural alterations. In affected *Atp7b*$^{-/-}$ rats, approximately 40% of the liver mitochondria show massive structural alterations, such as detachment of MIM and MOM and cristae dilations. These alterations increase with disease progression of *Atp7b*$^{-/-}$ rats [1]. Especially the mitochondrial membranes are affected with disease progression of *Atp7b*$^{-/-}$ rats (see increased cristae and ruptured MOM in type 4 mitochondria).

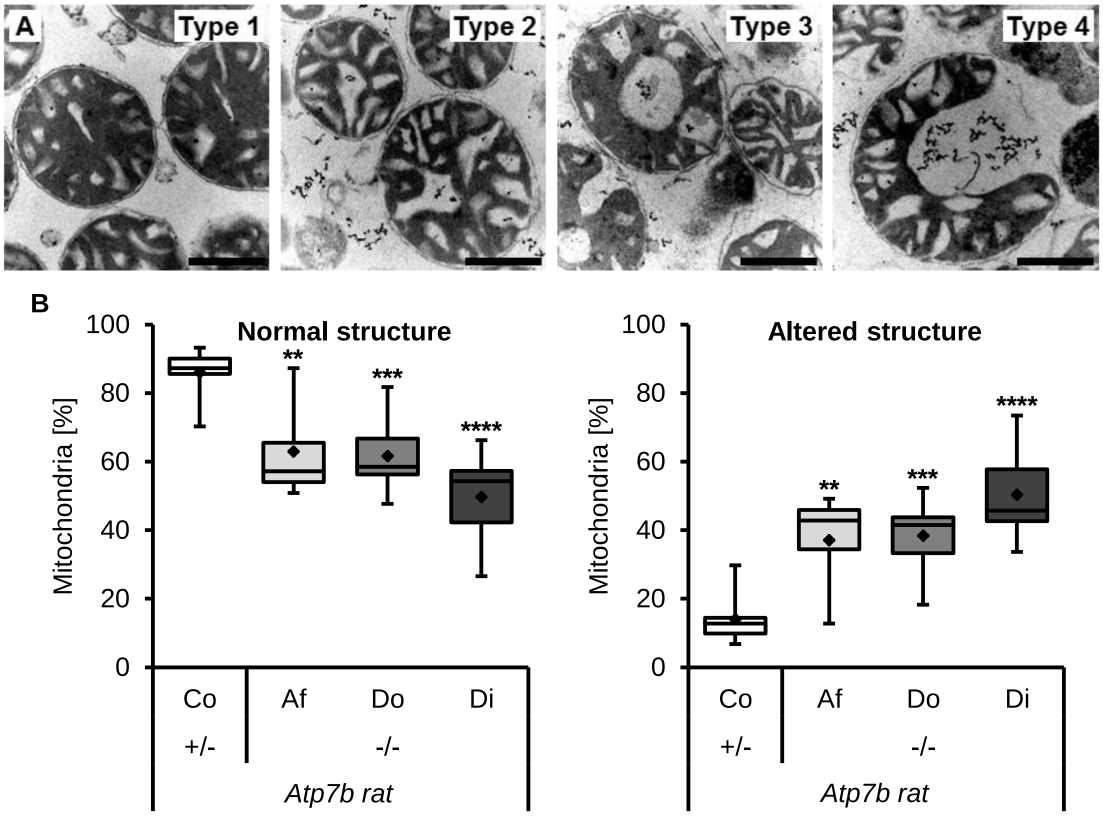

Figure 3-4 Disease progression of *Atp7b*$^{-/-}$ rats is paralleled by massive structural alterations of isolated rat liver mitochondria.

(A) *Four classes of mitochondrial structural alterations are defined: (1) normal, no structural alterations, no cristae dilations, no separation of inner and outer mitochondrial membrane, electron-dense matrix, (2) slight structural alterations characterised by mild cristae dilations, (3) intermediate alterations shown by increasing cristae dilation, (4) mitochondria with massive cristae enlargement and separation of inner and outer mitochondrial membrane. Scale bar: 500 nm.*

(B) *Structural alterations of isolated rat liver mitochondria are quantified from Atp7b*$^{+/-}$ *and progressing disease states of Atp7b*$^{-/-}$ *rats. Types 1 and 2 are summarised as "normal" and types 3 and 4 as "altered" (see (A)). Atp7b*$^{+/-}$ *rat liver mitochondria mainly show a normal structure. In affected Atp7b*$^{-/-}$ *rats, isolated liver mitochondria show structural alterations that further increase with disease progression of Atp7b*$^{-/-}$ *rats. (Co) control Atp7b*$^{+/-}$*: 75–146 d, N=8, n=1413; (Af) affected Atp7b*$^{-/-}$*: 66–93 d, N=9, n=1283; (Do) disease onset Atp7b*$^{-/-}$*: 80–107 d, N=8, n=1284; (Di) diseased Atp7b*$^{-/-}$*: 84–107 d, N=6, n=1119. N=number of rats, n=number of analysed mitochondria. One-way ANOVA with Tukey's multiple comparisons test. *Significant to control, **p<0.01, ***p<0.001, ****p<0.0001. ▬ median, ♦ mean value, 25% and 75% quartile are indicated.*

*Adapted from Josef Lichtmannegger et al. (2016) Methanobactin reverses acute liver failure in a rat model of Wilson disease. J Clin Invest. 2016 Jul;126(7): p. 2721-35* [1].

### 3.1.5 Mitochondrial membrane fluidity and swelling is reduced in *Atp7b*$^{-/-}$ rats with disease progression

Ultrastructural analyses of liver mitochondria from *Atp7b*$^{-/-}$ rats show alterations (especially at the mitochondrial membranes) that progress with disease state and copper load (Figure 3-2 – Figure 3-4). How are the membranes affected by this progressive copper burden? To address this issue, the mitochondrial membrane fluidity was measured by fluorescence polarisation in liver mitochondria freshly isolated from *Atp7b*$^{+/-}$ and *Atp7b*$^{-/-}$ rats using the fluorophores DPH and TMA-DPH [228-232]. Both compounds insert into biological membranes like the MIM: DPH in the membrane inner lipid phase and TMA-DPH in the lipid-water interface (Figure 3-5A) [230-232]. Excitation of the fluorophores with a defined wavelength leads to the emission of polarised light, whereby polarisation depends on the rotation of fluorophores within the membrane and thus on the membrane fluidity [233]. Less rotation leads to stronger polarised light, indicating less membrane fluidity, and strong motion ejects wider spread signals, indicating more fluid membranes [233].

For DPH, no alteration in polarisation is observed among the different disease states of *Atp7b*$^{-/-}$ rats relative to *Atp7b*$^{+/-}$ rats, indicating that the mitochondrial membrane fluidity is unaffected at the membrane inner lipid phase (Figure 3-5B, C) [1]. In contrast, polarisation of TMA-DPH increases in mitochondria from *Atp7b*$^{-/-}$ rats with disease progression compared to mitochondria from *Atp7b*$^{+/-}$ rats (Figure 3-5B, D) [1]. These results indicate a reduced membrane fluidity at the lipid-water interface (TMA-DPH) possibly induced by accumulated copper at the membrane surface [1].

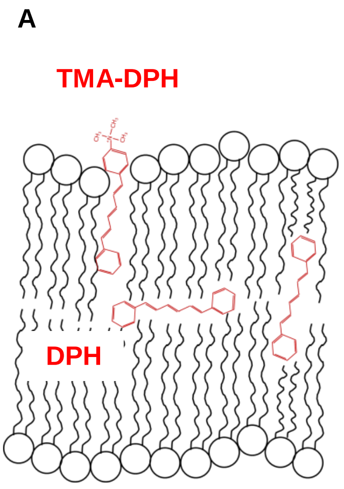

**B**

| Disease state | Control | Affected | Disease onset | Diseased |
|---|---|---|---|---|
| *Atp7b* genotype | +/- | -/- | -/- | -/- |
| Legend | ○ | ▬ | ▬ | ▬ |
| N (n) | 4 (8) | 3 (6) | 4 (8) | 3 (6) |
| DPH [mPol] | | | | |
| Control | 256 ± 7 | 258 ± 5 | 257 ± 7 | 259 ± 11 |
| Triton | 198 ± 1 | 197 ± 1[a] | 193 ± 4 | 199 ± 7 |
| TMA-DPH [mPol] | | | | |
| Control | 328 ± 6 | 338 ± 7* | 339 ± 5** | 344 ± 4*** |
| Triton | 389 ± 3 | 390 ± 6* | 392 ± 6** | 398 ± 6*** |

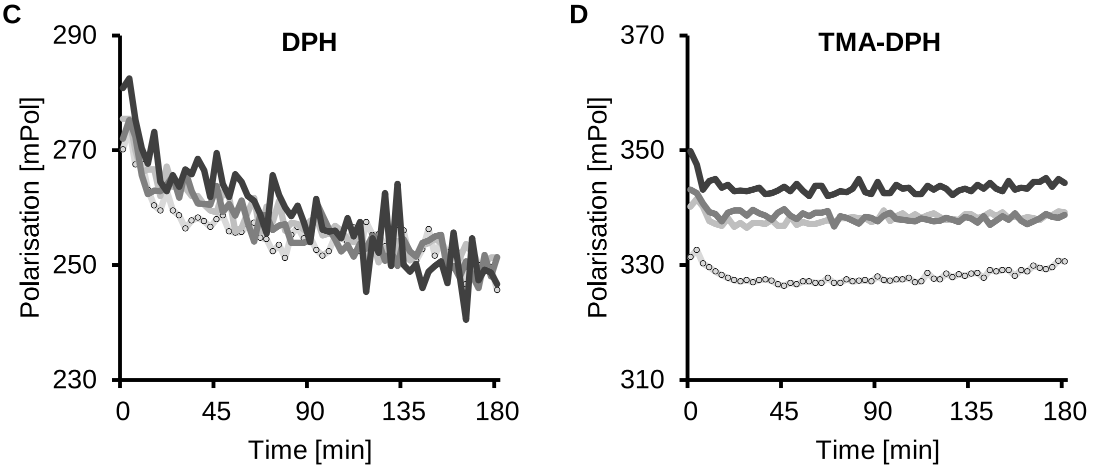

Figure 3-5 Mitochondrial membrane fluidity is reduced at the lipid-water interface in isolated *Atp7b*$^{-/-}$ rat liver mitochondria.

(A) *Localisation of the fluorophores DPH and TMA-DPH within membranes, adapted from Grebowski et al.* [230]*. DPH is localised at the membrane inner lipid phase, whereas TMA-DPH is localised at the lipid-water interphase.*

(B–D) *Fluorescence polarisation of isolated liver mitochondria in Atp7b*$^{+/-}$ *control and Atp7b*$^{-/-}$ *rats from different disease states is shown. Membrane fluidity of the inner lipid phase (DPH) shows no alterations among Atp7b*$^{+/-}$ *and Atp7b*$^{-/-}$ *mitochondria (B, C). In comparison, membrane fluidity of the lipid-water interface is reduced in Atp7b*$^{-/-}$ *rat liver mitochondria compared to Atp7b*$^{+/-}$ *control mitochondria and is increasingly harmed with disease progression of Atp7b*$^{-/-}$ *rats (B, D). N=number of rats, n=number of measurements.* [a]*N=3, n=5. Data are outlier corrected. One-way ANOVA with Tukey's multiple comparisons test. *Significant to control, *p<0.05, **p<0.01, ***p<0.001. Adapted from Josef Lichtmannegger et al. (2016) Methanobactin reverses acute liver failure in a rat model of Wilson disease. J Clin Invest. 2016 Jul;126(7): p. 2721-35* [1]*.*

Calcium ($Ca^{2+}$) or copper ($Cu^{2+}$) attacks mitochondrial membranes, leading to an increased water uptake and mitochondrial swelling (mitochondrial permeability transition, MPT) [152, 241, 242, 244]. This process describes the ability of mitochondria to unfold their inner membrane (MIM) [258]. As the mitochondrial membrane fluidity is progressively reduced in liver mitochondria isolated from *Atp7b*$^{-/-}$ rats (Figure 3-5B, D), it is hypothesised that the unfolding of the MIM is increasingly harmed with rising mitochondrial copper load and disease progression of *Atp7b*$^{-/-}$ rats. To experimentally verify this hypothesis, the extent of swelling was measured by the change of the optical density at 540 nm (Figure 3-6). Swelling extent of mitochondria isolated from *Atp7b*$^{+/-}$ control rats was set to 100% and used as reference point for mitochondria from *Atp7b*$^{-/-}$ rats. Upon challenge of mitochondria from *Atp7b*$^{-/-}$ rats with 100 µM $Ca^{2+}$ or 100 µM $Cu^{2+}$, swelling extent decreases with rising mitochondrial copper load and disease progression of *Atp7b*$^{-/-}$ rats [1]. Results are similar for $Ca^{2+}$ and $Cu^{2+}$ triggered MPT. These data show that mitochondria isolated from *Atp7b*$^{-/-}$ rats have a reduced ability to unfold their MIM with disease progression relative to mitochondria from *Atp7b*$^{+/-}$ rats. Possibly, copper deposition at the MIM induces these effects.

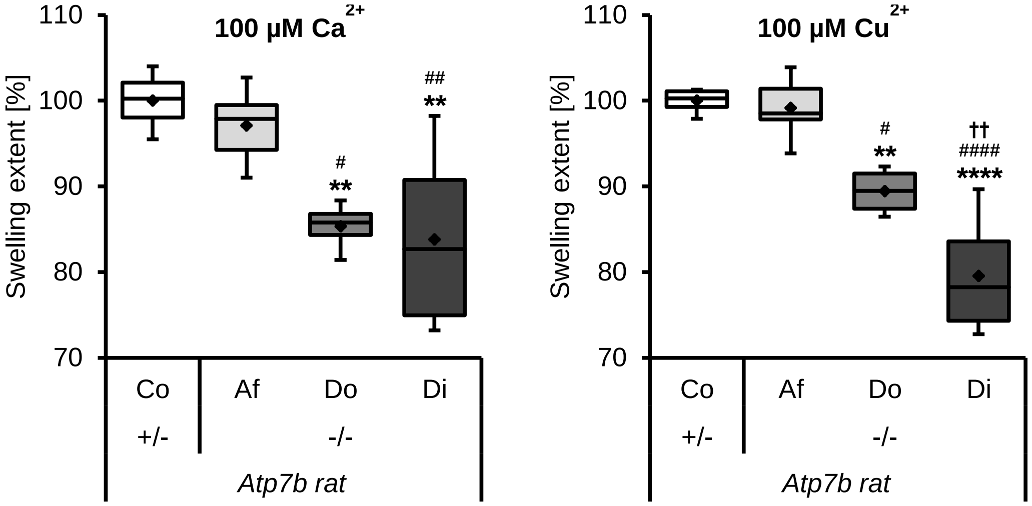

Figure 3-6 Mitochondrial swelling is reduced in *Atp7b*$^{-/-}$ rats with disease progression compared to *Atp7b*$^{+/-}$ rats.

*Isolated mitochondria from Atp7b*$^{+/-}$ *control (Co) and Atp7b*$^{-/-}$ *affected (Af) rats undergo large amplitude swelling if triggered with calcium (left) or copper (right). This process is significantly reduced in Atp7b*$^{-/-}$ *mitochondria from diseased (Di) and disease onset (Do) rats. (Co) control Atp7b*$^{+/-}$*: N=3, n=6; (Af) affected Atp7b*$^{-/-}$*: N=3, n=6; (Do) disease onset Atp7b*$^{-/-}$*: N=2, n=4; (Di) diseased Atp7b*$^{-/-}$*: N=3, n=6. Data are outlier corrected. One-way ANOVA with Tukey's multiple comparisons test. *Significant to control, *$^{\#}$*significant to affected, *$^{\dagger}$*significant to disease onset, *p<0.05, **p<0.01, ****p<0.0001.* **▬** *median, ♦ mean value, 25% and 75% quartile are indicated. Adapted from Josef Lichtmannegger et al. (2016) Methanobactin reverses acute liver failure in a rat model of Wilson disease. J Clin Invest. 2016 Jul;126(7): p. 2721-35* [1]*.*

MPT is mediated by cyclophilin D (CypD) as it binds to the MPT pore, mediating its opening [259, 260]. This process can be inhibited by the binding of cyclosporine A (CysA) to CypD [259-261]. As swelling is reduced in liver mitochondria from *Atp7b*$^{-/-}$ rats with disease progression, the question arises whether inhibition of this process is affected. Liver mitochondria isolated from *Atp7b*$^{+/-}$ and *Atp7b*$^{-/-}$ rats were triggered with 100 µM $Ca^{2+}$ and 5 µM CysA and duration of the swelling process was calculated. Swelling is decelerated in liver mitochondria from *Atp7b*$^{+/-}$ rats to approximately 70 minutes (Figure 3-7). Start as well as end of swelling is approximately 20–30 minutes earlier in progressed disease states from *Atp7b*$^{-/-}$ rats compared to affected *Atp7b*$^{-/-}$ rats. These data show that the ability of CysA to block calcium-induced swelling of the MIM is increasingly impaired in mitochondria from *Atp7b*$^{-/-}$ rats with disease progression of the animals. This indicates that copper attacks inner mitochondrial membrane processes.

| Disease state | Control | Affected | Disease onset | Diseased |
|---|---|---|---|---|
| *Atp7b* genotype | +/- | -/- | -/- | -/- |
| Legend | -○- | ▬ | ▬ | ▬ |
| N (n) | 3 (6) | 2 (4) | 2 (3) | 3 (5) |
| Start [min] | 71 ± 26 | 32 ± 3* | 23 ± 3** | 9 ± 4*** |
| End [min] | 113 ± 35 | 80 ± 4 | 66 ± 0 | 47 ± 11** |

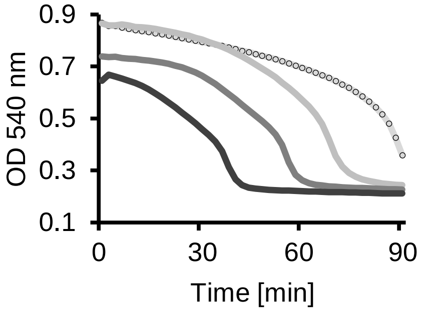

Figure 3-7 Inhibition of calcium-induced swelling with CysA is increasingly harmed in liver mitochondria isolated from *Atp7b*$^{-/-}$ rats with disease progression compared to *Atp7b*$^{+/-}$ rats.

*Calcium-induced (100 µM) swelling can be efficiently inhibited by CysA (5 µM) in Atp7b*$^{+/-}$ *rat liver mitochondria. This effect is massively impaired in mitochondria from diseased and disease onset Atp7b*$^{-/-}$ *rats. Table shows mean values and standard deviations, whereas curves depict one exemplary measurement. N=number of rats, n=number of measurements. Data are outlier corrected. One-way ANOVA with Tukey's multiple comparisons test. *Significant to control, *p<0.05, **p<0.01, ***p<0.001. Adapted from Josef Lichtmannegger et al. (2016) Methanobactin reverses acute liver failure in a rat model of Wilson disease. J Clin Invest. 2016 Jul;126(7): p. 2721-35* [1].

### 3.1.6 Mitochondrial function is increasingly harmed in *Atp7b*$^{-/-}$ rats with disease progression

An intact MIM is necessary for establishing a stable mitochondrial transmembrane potential (MMP) [92, 105, 106]. As shown in Figure 3-5 to Figure 3-7, mitochondrial membranes have altered characteristics in *Atp7b*$^{-/-}$ rats with disease progression. That is why the mitochondrial function was analysed by measuring the MMP of freshly isolated rat liver mitochondria using rhodamine 123, a fluorescence dye that is taken up by intact mitochondria, leading to self-quenching of the dyes fluorescence [234, 235]. If the MMP becomes impaired, the dye is released, leading to increasing fluorescence signals [235]. MMP is stable for approximately 120 minutes in liver mitochondria isolated from *Atp7b*$^{+/-}$ rats. With disease progression of *Atp7b*$^{-/-}$ rats, stability of MMP is increasingly harmed, as shown by an approximately 22–67 minutes earlier start of MMP loss in comparison to *Atp7b*$^{+/-}$ control rats (Figure 3-8) [1].

An intact MMP is the most important requirement to ensure mitochondrial ATP production [92, 105, 106]. The MMP stability is reduced in liver mitochondria isolated from *Atp7b*$^{-/-}$ rats with disease progression, promoting the hypothesis of an impaired mitochondrial energy production. ATP production was measured in liver mitochondria isolated from *Atp7b*$^{-/-}$ relative to mitochondria from *Atp7b*$^{+/-}$ rats using luciferin/luciferase assay. Figure 3-9 shows a significantly reduced ATP production in liver mitochondria from *Atp7b*$^{-/-}$ rats and decreases in parallel with disease progression of these rats [1].

| Disease state | Control | Affected | Disease onset | Diseased |
|---|---|---|---|---|
| *Atp7b* genotype | +/- | -/- | -/- | -/- |
| Legend | —○— | ▬ | ▬ | ▬ |
| N (n) | 3 (6) | 3 (6) | 2 (3) | 3 (6) |
| Start [min] | 116 ± 26 | 94 ± 9 | 77 ± 1 | 49 ± 19<br>**** ## |
| End [min] | 171 ± 9 | 163 ± 15 | 138 ± 1<br>** # | 124 ± 8<br>**** ### |

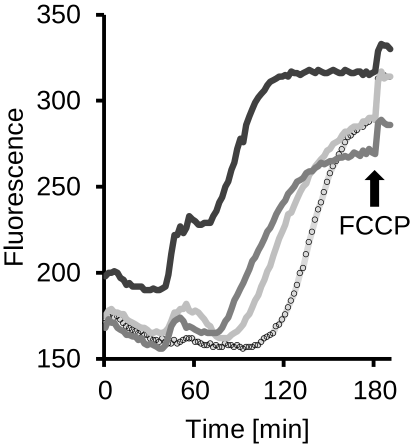

Figure 3-8 Mitochondrial transmembrane potential is less stable in liver mitochondria isolated from *Atp7b*$^{-/-}$ rats with disease progression compared to liver mitochondria from *Atp7b*$^{+/-}$ rats.

*MMP is stable in mitochondria from Atp7b*$^{+/-}$ *control rats for 120 minutes. MMP loss starts earlier in Atp7b*$^{-/-}$ *mitochondria with disease progression compared to control mitochondria. Table shows mean values and standard deviations, whereas curves depict one exemplary measurement. N=number of rats, n=number of measurements. Data are outlier corrected. One-way ANOVA with Tukey's multiple comparisons test. *Significant to control,* $^{\#}$*significant to affected, *p<0.05, **p<0.01, ***p<0.001, ****p<0.0001. Adapted from Josef Lichtmannegger et al. (2016) Methanobactin reverses acute liver failure in a rat model of Wilson disease. J Clin Invest. 2016 Jul;126(7): p. 2721-35* [1].

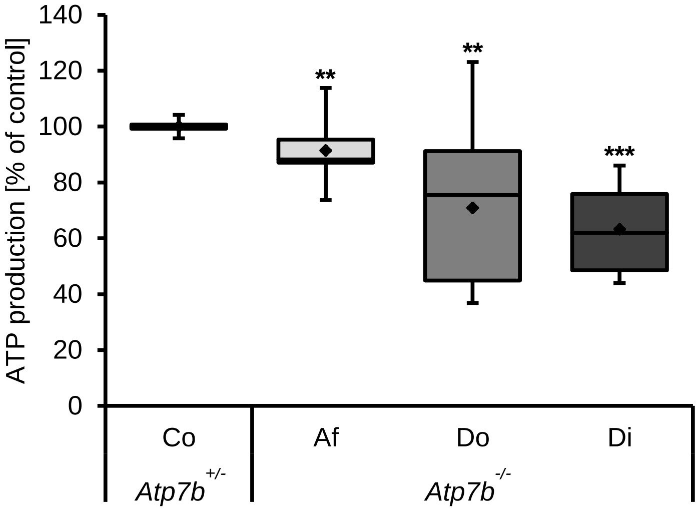

Figure 3-9 ATP production is increasingly harmed in liver mitochondria isolated from *Atp7b*$^{-/-}$ rats with disease progression compared to *Atp7b*$^{+/-}$ rats.

*ATP production progressively decreases in mitochondria isolated from Atp7b*$^{-/-}$ *rats at different disease states compared to mitochondria from Atp7b*$^{+/-}$ *control rats. (Co) control Atp7b*$^{+/-}$*: n=47, (Af) affected Atp7b*$^{-/-}$*: n=20, (Do) disease onset Atp7b*$^{-/-}$*: n=14, (Di) diseased Atp7b*$^{-/-}$*: n=6. n=number of measurements. Data are outlier corrected. One-way ANOVA with Tukey's multiple comparisons test. *Significant to control, **p<0.01, ***p<0.001. ▬ median, ♦ mean value, 25% and 75% quartile are indicated. Adapted from Josef Lichtmannegger et al. (2016) Methanobactin reverses acute liver failure in a rat model of Wilson disease. J Clin Invest. 2016 Jul;126(7): p. 2721-35* [1].

The data demonstrate that increasing mitochondrial copper burden in *Atp7b*$^{-/-}$ rats is paralleled by progressive impairments of the mitochondrial structure and function, such as the membrane fluidity and swelling of the MIM, causing instability of the MMP and a decreased ATP production. The progressing mitochondrial impairments are in parallel with disease progression of *Atp7b*$^{-/-}$ rats. Consequently, depletion of the mitochondrial copper overload may be a prerequisite for an efficient treatment in this WD animal model [1].

## 3.2 Methanobactin – a highly efficient agent to decopper liver mitochondria in a Wilson disease rat model

For treatment of WD, copper chelating agents such as D-PA or TETA are used [33, 158, 166-168, 172, 175, 176]. As both agents have an intermediate affinity for copper [198], they mobilise copper from the liver to the blood, which is maybe partially transported to the brain, leading to secondary neurologic effects [199-202]. Hence, other chelating agents with a higher affinity for copper and not inducing toxic side effects are necessary for successful treatment of WD [262]. One potential agent is the bacterial peptide methanobactin (MB) [206, 209].

### 3.2.1 Methanobactin efficiently decoppers HepG2 cells without severe toxic effects

Liver mitochondria from WD patients and *Atp7b*$^{-/-}$ rats show increasing copper burden with disease progression (Figure 3-1) [1]. In contrast to D-PA and TETA, ammonium tetrathiomolybdate (TTM) and MB were found to significantly reduce the copper load in liver mitochondria from *Atp7b*$^{-/-}$ rats [1]. Thus, the question arises whether these copper chelators can decopper HepG2 cells. Initially, cellular toxicity of increasing MB concentrations was analysed on HepG2 cells after 24 hours using neutral red assay and compared to D-PA, TETA and TTM (Figure 3-10). Millimolar concentrations of D-PA and TETA are not toxic to HepG2 cells (Figure 3-10B). MB induces cell death at millimolar concentrations, whereas 500 µM TTM reduces the amount of viable cells to approximately 50% (Figure 3-10A) [1]. As a positive control, HepG2 cells were treated with CCCP, as this agent is known to dissipate the MMP and to induce cell death.

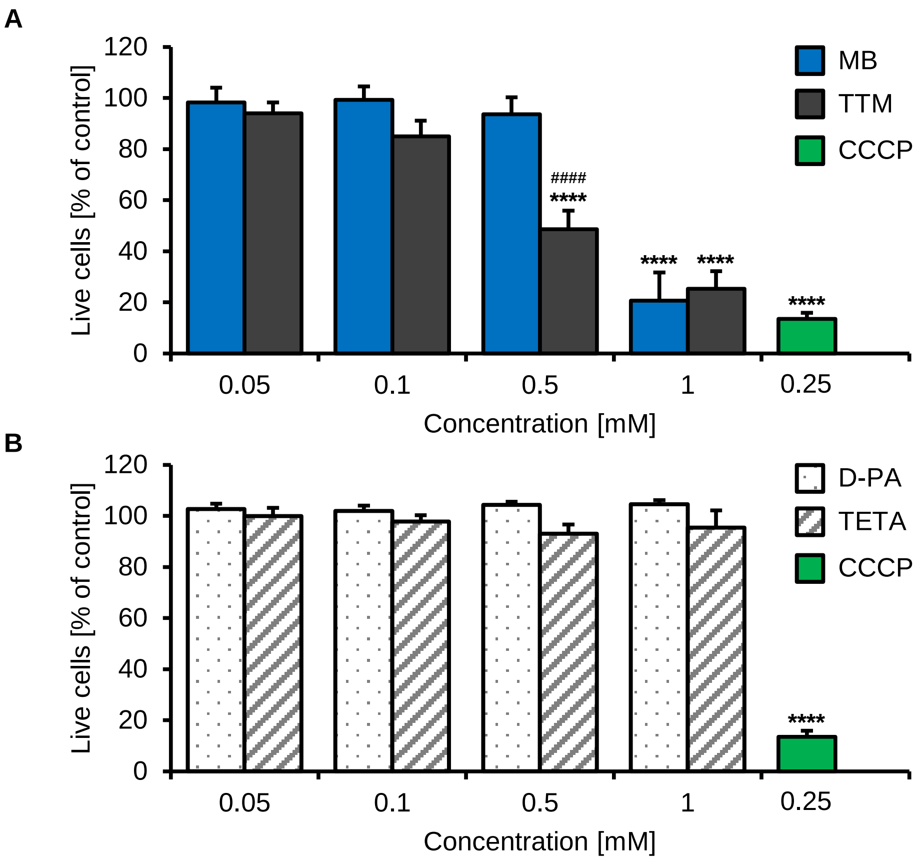

Figure 3-10 D-PA, TETA and MB are less toxic to HepG2 cells than TTM.

*Cellular toxicity of chelators with a high (A: MB, TTM) and an intermediate (B: D-PA, TETA) affinity for copper on HepG2 cells (N=3, n=9, neutral red assay) is shown. MB is toxic at millimolar concentrations, whereas even 0.5 mM TTM reduces the amount of viable cells for approximately 50%. Toxic concentrations of D-PA and TETA are above 1 mM. The MMP dissipating protonophor CCCP serves as toxic positive control. One-way ANOVA with Tukey's multiple comparisons test. *Significant to buffer control, $^{\#}$significant to respective concentration of MB. ****p<0.0001. Adapted from Josef Lichtmannegger et al. (2016) Methanobactin reverses acute liver failure in a rat model of Wilson disease. J Clin Invest. 2016 Jul;126(7): p. 2721-35 [1].*

As MB has a very high affinity for copper [206, 209], it could possibly induce mitochondrio-toxic effects by affecting the mitochondrial copper metabolism and copper-dependent mitochondrial enzymes, such as the cytochrome c oxidase (CcO). Therefore, it was analysed whether MB affects the mitochondrial transmembrane potential. Intact HepG2 cells were treated for two to six hours with either 0.5 mM MB or 0.01 mM TTM and MMP was analysed by immunofluorescence staining. Staining of HepG2 cells was done with Hoechst 33342 (nuclei, blue), MitoTracker® Deep Red (mitochondria with an intact MMP, orange-red) and NAO (mitochondria without an intact MMP, green) [1]. NAO stains mitochondria independent of their MMP [263], whereas uptake of MitoTracker® Deep Red depends on an intact MMP [264]. Non-toxic MB concentrations (0.5 mM) induce an intermediate loss of MMP after two hours which could be restored after six hours (Figure 3-11) [1]. In contrast to MB, 0.01 mM TTM dissipates MMP after two hours of treatment that cannot be recovered after six hours. Toxic concentrations of CCCP fully dissipate MMP.

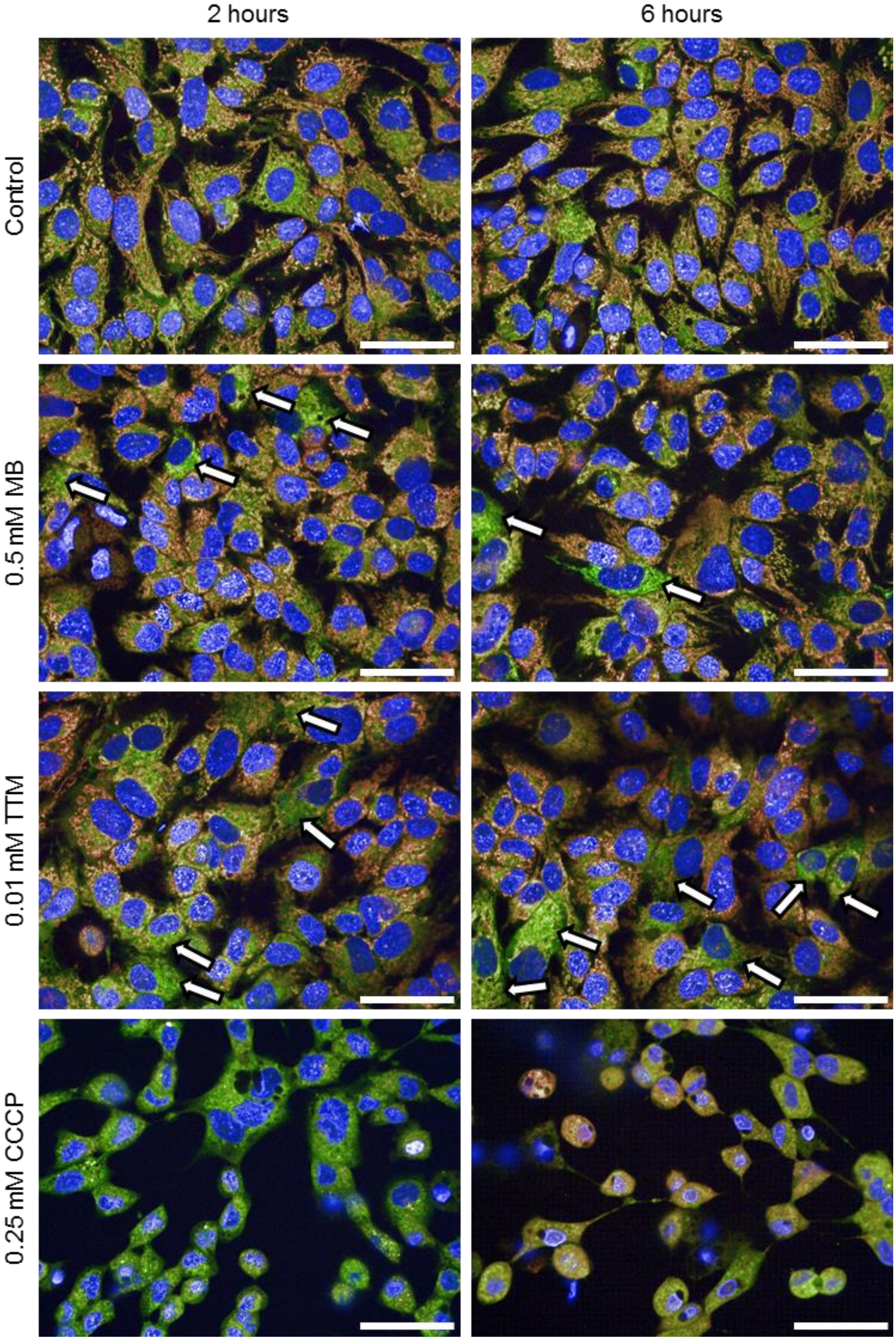

Figure 3-11 MB induces an intermediate loss of MMP after two hours of treatment which is recovered after six hours.

*Compared to control (N=2), HepG2 cells treated with 0.5 mM MB show intermediate phases of MMP loss (two hours) which is regenerated after six hours (N=2). MMP loss induced by 0.01 mM TTM after two hours cannot be restored after six hours (N=1). Treatment with toxic concentrations of CCCP (250 µM) fully dissipates MMP and reduces amount of cells (N=2). Staining indicates nuclei (blue), mitochondria with MMP (orange-red) and mitochondria without MMP (green) [1]. Scale bar: 50 µm. Adapted from Josef Lichtmannegger et al. (2016) Methanobactin reverses acute liver failure in a rat model of Wilson disease. J Clin Invest. 2016 Jul;126(7): p. 2721-35 [1].*

After excluding cellular toxicity of 1 mM D-PA and TETA, as well as 0.01 mM TTM and 0.5 mM MB, their decoppering efficiency on HepG2 cells was analysed. Therefore, HepG2 cells were treated for 24 hours with 0.5 mM MB and cellular copper concentration was measured in comparison to control cells (Supplementary Figure 1). MB significantly reduces cellular copper load to approximately 50%. Further, HepG2 cells were preloaded for 24 hours with 15 µM copper-histidine (Cu-His). This Cu-His concentration increases the cellular copper load approximately 50-fold compared to untreated control cells (Supplementary Figure 1, Figure 3-12). Treating copper-preloaded HepG2 cells for 24 hours with copper-chelators decreases the cellular copper concentration for 10–30% whereby MB has a significant decoppering efficiency (Figure 3-12).

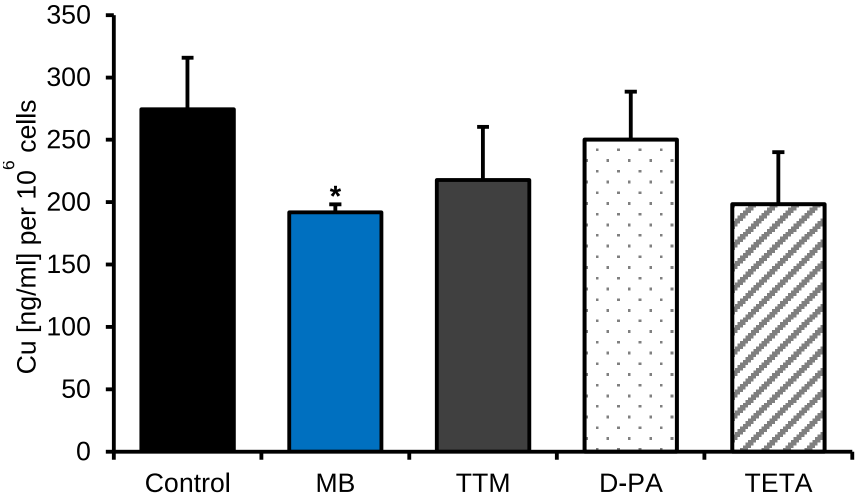

Figure 3-12 In contrast to TTM, D-PA and TETA, MB significantly reduces cellular copper concentration in copper-preloaded HepG2 cells.

*0.5 mM MB treated HepG2 cells, preloaded for 24 hours with 15 µM Cu-His, have a significantly reduced cellular copper load compared to control cells or HepG2 cells treated for 24 hours with 1 mM D-PA, 1 mM TETA or 10 µM TTM. N=4–6, one-way ANOVA with Tukey's multiple comparisons test, *significant to control, *p<0.05.*

### 3.2.2 Short-term methanobactin treatment of *Atp7b*$^{-/-}$ rats decoppers liver mitochondria *in vivo*

To test for *in vivo* toxicity of MB, *Atp7b*$^{+/-}$ rats were treated intraperitoneally once daily on two consecutive days with MB [1]. Body weight, the liver damage markers serum AST and bilirubin as well as copper concentrations in liver homogenate and liver mitochondria are not altered in comparison to untreated *Atp7b*$^{+/-}$ control rats (Supplementary Table 2) [1]. ATP production of liver mitochondria isolated from MB-treated and untreated *Atp7b*$^{+/-}$ rats is highly similar (Figure 3-17) [1]. These data show that MB has no apparent toxic effects on *Atp7b*$^{+/-}$ rats and rat liver mitochondria, leading to further experiments regarding its ability to prevent disease progression and to decopper liver mitochondria in *Atp7b*$^{-/-}$ rats [1].

To analyse whether MB can prevent liver damage and disease progression in rats, *Atp7b*$^{-/-}$ rats received a short-term treatment, consisting of single daily MB i.p. injections on three or five consecutive days at the age of disease onset (82–90 days) [1]. For comparison, rats were treated orally for four days using the copper chelators D-PA or TETA [1]. All MB treated animals regain body weight (Supplementary Table 2) [1]. Serum AST and bilirubin were analysed for the evaluation of the degree of liver damage (Figure 3-13, Supplementary Table 2). Upon treatment, all *Atp7b*$^{-/-}$ rats that received MB have normal serum AST and bilirubin levels, indicating that disease progression is successfully prevented [1]. Of note, three *Atp7b*$^{-/-}$ rats treated for five days with MB (two disease onset and one diseased animal at the start of treatment) are rescued from liver failure, as serum AST and bilirubin values are <200 U/L and <0.5 mg/dl, respectively [1]. In contrast, an increase of serum AST and bilirubin cannot be prevented using D-PA and TETA, indicating progressive liver damage (Figure 3-13) [1].

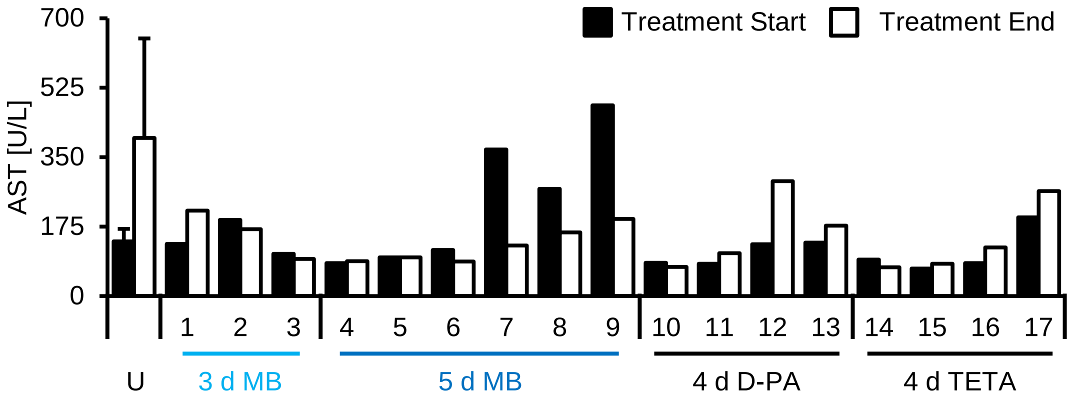

Figure 3-13 In contrast to D-PA and TETA, short-term MB treatment of *Atp7b*$^{-/-}$ rats reduces the liver damage marker AST.

*AST values decrease down to normal (<200 U/L) in two out of three and in four out of six Atp7b*$^{-/-}$ *rats treated for three or five days with MB, respectively, but not in untreated (U, N=6, 3 x affected, 3 x diseased) or short-term D-PA and TETA treated Atp7b*$^{-/-}$ *rats. Treatment start: 82–90 days. Numbers indicate the respective animal number. After Josef Lichtmannegger et al. (2016) Methanobactin reverses acute liver failure in a rat model of Wilson disease. J Clin Invest. 2016 Jul;126(7): p. 2721-35* [1].

The high efficiency of MB to decopper liver mitochondria was further evaluated *in vivo* and compared to D-PA and TETA treatment. From the above treated rats, liver mitochondria were isolated. Copper load was measured in liver homogenate and mitochondria. Compared to untreated *Atp7b*$^{-/-}$ rats, MB leads to a 31% reduction of whole liver copper which becomes significant in the mitochondria (65% reduction) (Figure 3-14) [1]. D-PA and TETA do not reduce the copper load in liver homogenate, but reduces it in liver mitochondria on average for approximately 46%. A broad distribution of the mitochondrial copper load is found due to different disease states of the animals in the D-PA and TETA treated groups. The mitochondrial decoppering is much more efficient in MB treated *Atp7b*$^{-/-}$ rats compared to D-PA or TETA treated ones.

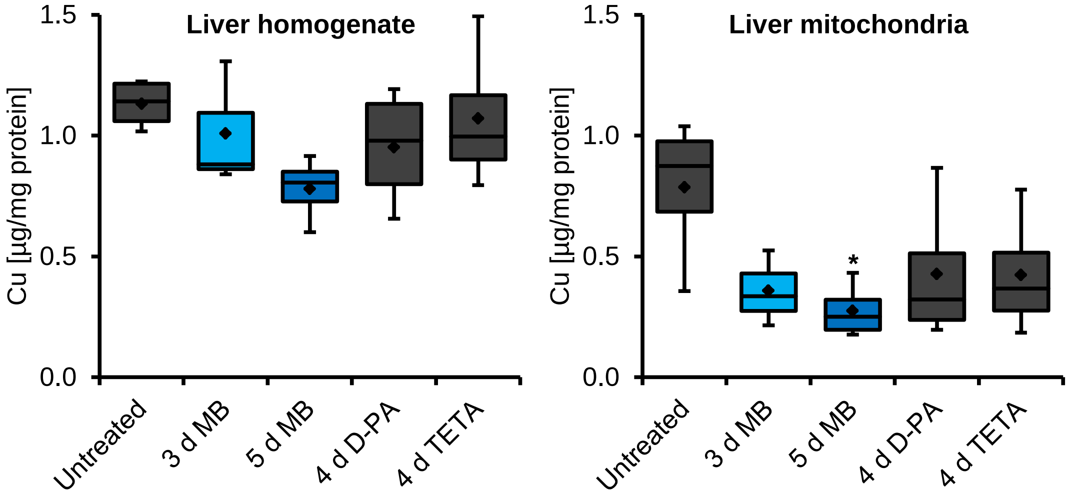

Figure 3-14 Short-term MB treatment of *Atp7b*$^{-/-}$ rats reduces copper burden in liver homogenate and isolated rat liver mitochondria.

*Slight reduction of the whole liver (left) and significant reduction of the mitochondrial copper level (right) is shown in short-term MB treated rats (3 days MB N=3, age 88–89 days, 2 x affected, 1 x disease onset, 5 days MB N=5, age 89–95 days, 5 x affected), but not in untreated (U, age 90–91 days, N=4, 2 x affected, 2 x diseased) or D-PA and TETA (N=4, age 86–89 days, 3 x affected, 1 x disease onset, each) treated Atp7b*$^{-/-}$ *rats. One-way ANOVA with Tukey's multiple comparisons test. *Significant to untreated controls. *$p<0.05$. ▬ median, ♦ mean value, 25% and 75% quartile are indicated. Adapted from Josef Lichtmannegger et al. (2016) Methanobactin reverses acute liver failure in a rat model of Wilson disease. J Clin Invest. 2016 Jul;126(7): p. 2721-35* [1].

The efficient copper depletion of MB treatment, as observed in *Atp7b*$^{-/-}$ rat liver mitochondria (Figure 3-14), was validated on ultrastructural and functional level [1]. The structure of liver mitochondria isolated from untreated and MB, D-PA or TETA treated *Atp7b*$^{-/-}$ rats was analysed using electron microscopy. As in Figure 3-4, four types of mitochondrial structural alterations were defined. Figure 3-15B includes only mitochondria with massive structural alterations (type 4; Figure 3-4) relative to all mitochondria seen in each figure. Mitochondria with massive structural alterations (type 4) are present for approximately 5% in isolates from MB treated *Atp7b*$^{-/-}$ rats and for approximately 10% in isolates from D-PA or TETA treated animals (Figure 3-15B) [1]. On functional level, mitochondrial ATP production was measured using luciferin/luciferase assay. Impaired ATP production of liver mitochondria isolated from untreated *Atp7b*$^{-/-}$ rats is fully restored by MB treatment (Figure 3-17) [1]. D-PA or TETA treatments are without therapeutic effect [1]. These results demonstrate that MB efficiently rescues mitochondria in *Atp7b*$^{-/-}$ rats.

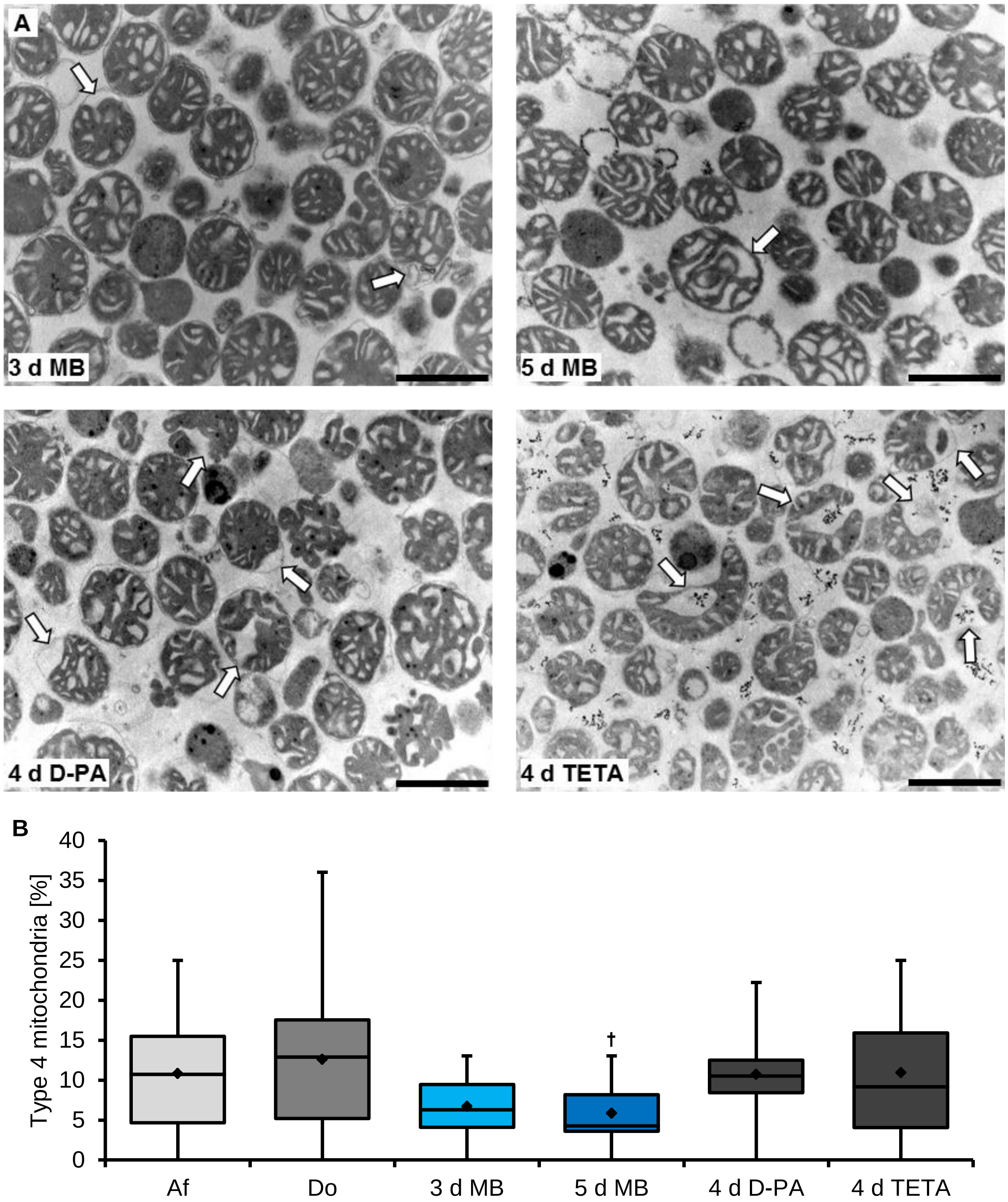
A
3 d MB
5 d MB
4 d D-PA
4 d TETA
B
Type 4 mitochondria [%]
0
5
10
15
20
25
30
35
40
†
Af
Do
3 d MB
5 d MB
4 d D-PA
4 d TETA

Figure 3-15 Short-term MB but not D-PA or TETA treatment of *Atp7b*$^{-/-}$ rats normalises mitochondrial structure.

(A) *Short-term MB treatment reverses massively impaired mitochondrial structure in contrast to mitochondria from untreated Atp7b*$^{-/-}$ *controls and D-PA or TETA treated Atp7b*$^{-/-}$ *rats. Scale bar: 1 µm.*

(B) *Quantification to Figure A. N=number of EM micrographs, n=number of mitochondria; (Af) affected Atp7b*$^{-/-}$*: N=31, n=807; (Do) disease onset Atp7b*$^{-/-}$*: N=24, n=734; 3 days MB: N=12, n=291; 5 days MB: N=18, n=460; D-PA: N=10, n=221; TETA: N=12, n=329. One-way ANOVA with Tukey's multiple comparisons test,* $^{\dagger}$*significant to disease onset,* $^{\dagger}p<0.05$*. ▬ median, ♦ mean value, 25% and 75% quartile are indicated. After Josef Lichtmannegger et al. (2016) Methanobactin reverses acute liver failure in a rat model of Wilson disease. J Clin Invest. 2016 Jul;126(7): p. 2721-35* [1].

### 3.2.3 Acute treatment with methanobactin rescues diseased *Atp7b*$^{-/-}$ rats from liver failure

D-PA or TETA treatment has to start before the onset of liver damage; otherwise treatment fails, leading to acute liver failure in WD patients [1, 155, 168, 169, 190, 191]. MB is shown to prevent disease progression in *Atp7b*$^{-/-}$ rats (Supplementary Table 2). However, the question has to be answered whether MB can rescue diseased *Atp7b*$^{-/-}$ rats from liver failure and death. Four *Atp7b*$^{-/-}$ rats with clear signs of liver damage, as shown by increased serum AST and partially bilirubin values, were treated by twice daily MB i.p. injections for eight days (Supplementary Table 2) [1]. Body weight, the liver damage markers serum AST and bilirubin, the mitochondrial function, structure as well as liver and mitochondrial copper load were analysed. All rats survive and gain body weight [1]. Elevated serum AST and bilirubin levels decrease to normal (AST <200 U/L, bilirubin <0.5 mg/dl) [1]. Mitochondrial ATP production recovered, reaching levels comparable to control rats (Figure 3-17). *Atp7b*$^{-/-}$ rats with massively increased serum AST and bilirubin values (termed as moribund) that receive no treatment, die within few days [1]. One such MB treated rat gains approximately 29% in body weight and shows a clearly improved structure of liver mitochondria *in situ* as well as isolated (Figure 3-16) [1]. Mitochondrial copper load decreases up to 85% (rat no. 3, Supplementary Table 2). Thus, in contrast to D-PA or TETA (Figure 3-13), MB treatment rescues diseased *Atp7b*$^{-/-}$ rats from acute liver failure and death with clear signs of liver regeneration [1].

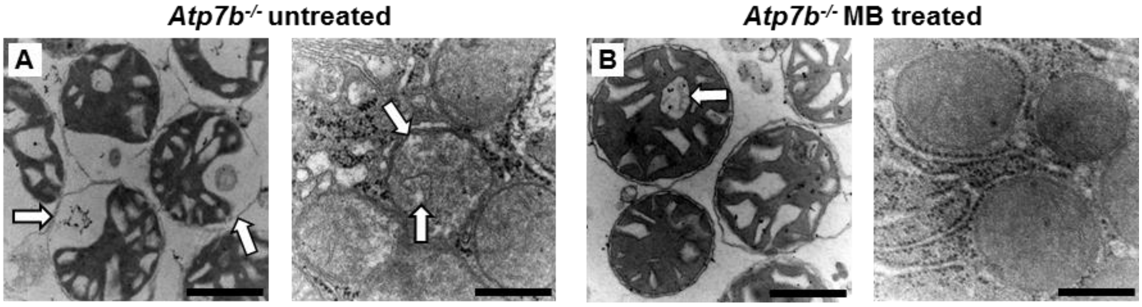

Figure 3-16 Acute MB treatment normalises the structure of liver mitochondria in *Atp7b*$^{-/-}$ rats.

*Mitochondria, either isolated (left) or in situ (right) from an untreated (A) and MB treated (B) moribund Atp7b*$^{-/-}$ *rat are shown. Only minor structural alterations are observed in MB treated Atp7b*$^{-/-}$ *rats in contrast to the untreated rat. Scale bar: 500 nm. After Josef Lichtmannegger et al. (2016) Methanobactin reverses acute liver failure in a rat model of Wilson disease. J Clin Invest. 2016 Jul;126(7): p. 2721-35* [1].

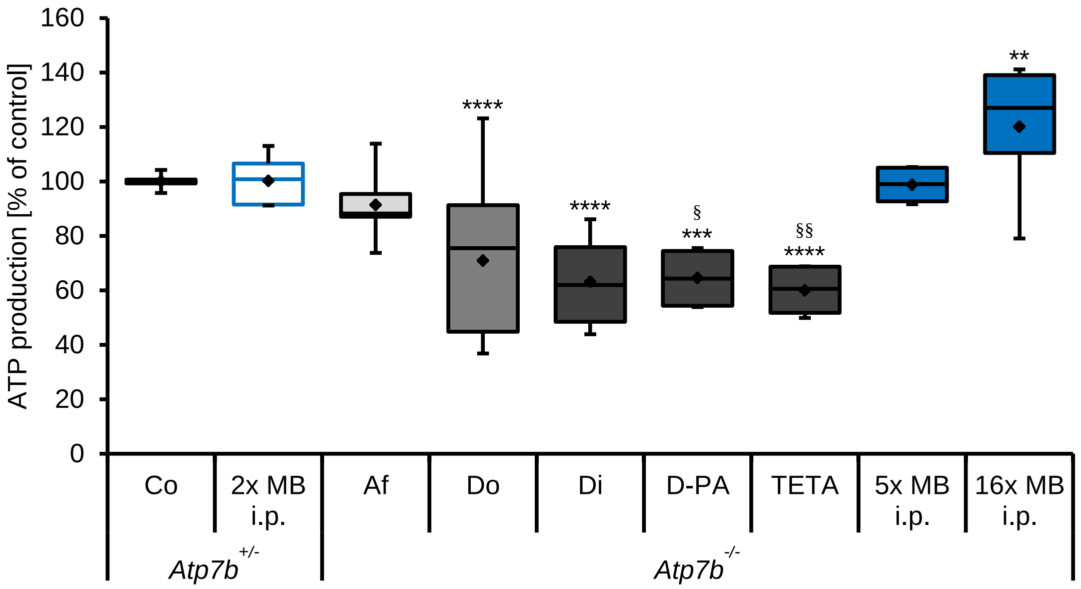

Figure 3-17 In contrast to D-PA and TETA, short-term MB treatment reverses ATP production in liver mitochondria isolated from *Atp7b*$^{-/-}$ rats.

*Short-term MB treatment reverses impaired mitochondrial ATP production, whereas D-PA and TETA do not. Data are outlier corrected, n=number of measurements, (Co) control Atp7b*$^{+/-}$*: n=47, 2x MB i.p.: n=7, (Af) affected Atp7b*$^{-/-}$*: n=20, (Do) disease onset Atp7b*$^{-/-}$*: n=14, (Di) diseased Atp7b*$^{-/-}$*: n=8, D-PA: n=4, TETA: n=4, 5x MB i.p.: n=4, 16x MB i.p.: n=8. One-way ANOVA with Tukey's multiple comparisons test. *Significant to control,* $^{\S}$*significant to 5x MB i.p. *p<0.05, **p<0.01, ***p<0.001, ****p<0.0001. Adapted from Josef Lichtmannegger et al. (2016) Methanobactin reverses acute liver failure in a rat model of Wilson disease. J Clin Invest. 2016 Jul;126(7): p. 2721-35* [1].

### 3.2.4 A new treatment strategy for Wilson disease using methanobactin

WD is currently treated by the daily and lifelong administration of D-PA or TETA [33, 66, 158, 166, 167, 172, 175, 265]. Termination of this treatment leads to acute liver failure in WD patients [33, 167, 174]. In section 3.2.2, it is shown that short-term MB treatment of *Atp7b*$^{-/-}$ rats prevents liver failure, reduces mitochondrial copper load and improves mitochondrial structure as well as ATP production. For how long does a single MB treatment cycle (five days) postpone the onset of liver failure in this WD rat model? This was analysed by a new treatment regimen in *Atp7b*$^{-/-}$ rats, consisting of short-term MB treatment (once daily on five consecutive days) followed by two to three weeks of observation [1]. In parallel to MB application, 1000 ppm zinc was given via the food [1], as this metal is clinically used for maintenance therapy in WD patients [33, 165, 177-180]. The disease progression was observed by measuring the liver damage markers serum AST and bilirubin. Upon MB treatment, serum AST and bilirubin values of all treated rats decrease to normal levels (AST <200 U/L, Figure 3-18A; bilirubin <0.5 mg/dl, data not shown) [1]. Both liver damage markers stay normal for at least two weeks [1], demonstrating a postponed disease onset in *Atp7b*$^{-/-}$ rats. Thereafter, AST levels and with a delay of one week bilirubin levels start to rise again [1]. At the time of analysis, one animal is still healthy (rat no. 1), whereas the other two rats manifest different stages of liver disease (no. 2 and 3) [1]. The reoccurrence of increased serum AST and bilirubin values is in parallel with rising mitochondrial but not total liver copper load (Figure 3-18B) and progressing structural alterations of liver mitochondria (Figure 3-18C) [1]. As a result, a five days MB treatment cycle postpones disease onset in *Atp7b*$^{-/-}$ rats for at least two weeks.

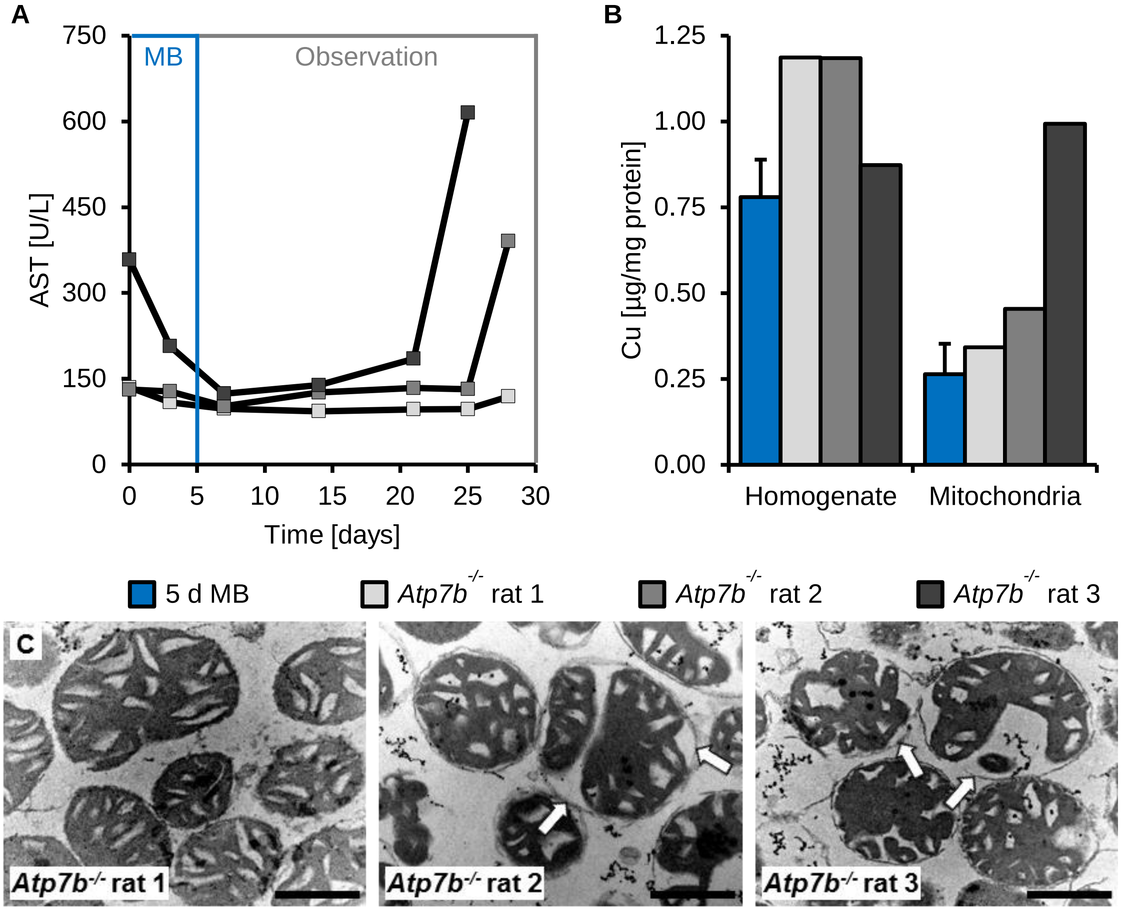

Figure 3-18 Short-term MB treatment postpones the onset of liver failure in *Atp7b*$^{-/-}$ rats for at least two weeks.

*(A) Short-term treatment of Atp7b*$^{-/-}$ *rats with MB (animal age at treatment start 84–85 days) reduces and stabilises serum AST and bilirubin values (not shown) for at least two weeks. At the time of analysis, one animal (rat no. 1) is still healthy, whereas rats no. 2 and 3 are diseased.*

*(B) Progression of liver and mitochondrial damage is paralleled by increasing mitochondrial copper load, whereas the copper concentration in liver homogenate is not affected. 5 days MB: N=5.*

*(C) Reoccurrence of elevated serum AST levels and mitochondrial copper load is paralleled by progressing structural alterations of liver mitochondria isolated from rat 1 to rat 3. Scale bar: 500 nm.*

*Adapted from Josef Lichtmannegger et al. (2016) Methanobactin reverses acute liver failure in a rat model of Wilson disease. J Clin Invest. 2016 Jul;126(7): p. 2721-35* [1]*.*

In *Atp7b*$^{+/-}$ control rats, MB is detectable in the serum for only 30 minutes [1]. This allows for repetitive MB applications per day. MB was applicated to *Atp7b*$^{-/-}$ rats intraperitoneally on five consecutive days three times daily and followed by several weeks of drug-free observation (Table 3-2). This initial experiment was done to analyse whether decoppering of *Atp7b*$^{-/-}$ rat liver mitochondria can be optimised and whether disease onset of *Atp7b*$^{-/-}$ rats can be further postponed. Five *Atp7b*$^{-/-}$ rats as well as five age and sex-matched *Atp7b*$^{+/-}$ untreated controls were analysed regarding the liver damage markers serum AST and bilirubin, liver and mitochondrial copper load and mitochondrial ATP production [1]. Pairs of rats were analysed at experimental days 1, 8, 29, 36 and 85, respectively (Table 3-2) [1]. At experimental day one, all animals are healthy as indicated by normal serum AST and bilirubin values (data not shown) [1]. The first *Atp7b*$^{-/-}$ rat shows a 10- to 70-fold increased copper load in liver mitochondria and homogenate, respectively, compared to the *Atp7b*$^{+/-}$ control rat (pair 1). This is paralleled by a 13% decreased ATP production compared to its *Atp7b*$^{+/-}$ control (data not shown) [1]. The remaining four *Atp7b*$^{-/-}$ rats received the first treatment cycle, consisting of three daily MB i.p. injections for five days [1]. After this week, all animals have normal serum AST values. A 40% reduction of copper load is measured at experimental day eight (pair 2) [1]. After three weeks of observation, copper increases back to the starting level (pair 3, experimental day 29) [1]. The second treatment cycle decreases copper loads to 25% of the starting level (pair 4, day 36) [1]. The last *Atp7b*$^{-/-}$ rat is observed for another seven weeks – during this time the rat stays healthy, as indicated by normal serum AST levels (pair 5, day 85) [1]. Liver and mitochondrial copper loads are similar to the *Atp7b*$^{-/-}$ rat at start of treatment [1]. Mitochondrial ATP production is decreased for 35% (data not shown). Using this treatment regimen, disease onset can be postponed in *Atp7b*$^{-/-}$ rats to more than 166 days of age, meaning a doubling of age when untreated *Atp7b*$^{-/-}$ rats become diseased [1].

This new treatment regimen, consisting of short intense decoppering treatment cycles and drug-free observation periods, indicates that the mitochondrial parameters copper concentration, structure and biochemical function can serve as early markers for disease progression in *Atp7b*$^{-/-}$ rats [1]. In *Atp7b*$^{-/-}$ rats, these parameters allow the evaluation of the treatment efficiency and reoccurrence of liver damage after treatment [1]. The repetitive MB injections show no toxic effects on *Atp7b*$^{-/-}$ rats. All rats gain body weight during treatment [1]. In contrast to the currently lifelong daily treatment regimen using D-PA or TETA in humans, MB treatment could be followed by drug-free observation periods without leading to the reoccurrence of immediate liver damage in *Atp7b*$^{-/-}$ rats [1].

Table 3-2 A new treatment regimen, consisting of intense MB treatment (3x/d i.p.) cycles interrupted by drug-free observation periods, postpones the disease onset in *Atp7b*$^{-/-}$ rats to more than 166 days of age.

*A 77% reduced mitochondrial copper load is found in Atp7b*$^{-/-}$ *rats after the second treatment cycle, paralleled by a disease-free state until experimental day 85 – corresponding to a doubling of age when untreated Atp7b*$^{-/-}$ *rats become diseased* [1]*. Adapted from Josef Lichtmannegger et al. (2016) Methanobactin reverses acute liver failure in a rat model of Wilson disease. J Clin Invest. 2016 Jul;126(7): p. 2721-35* [1]*.*

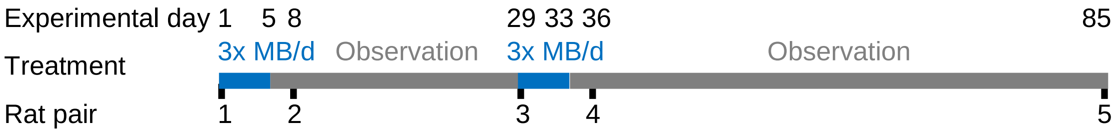

| **Rat pair** | **1** | | **2** | | **3** | | **4** | | **5** | |
|---|---|---|---|---|---|---|---|---|---|---|
| ***Atp7b* genotype** | **+/-** | **-/-** | **+/-** | **-/-** | **+/-** | **-/-** | **+/-** | **-/-** | **+/-** | **-/-** |
| Age [d] | 82 | 82 | 89 | 89 | 109 | 109 | 117 | 116 | 166 | 166 |
| Sex | f | f | f | f | f | f | m | m | m | m |
| Ceruloplasmin [U/L] | 234 | 8 | 227 | 1 | 194 | 1 | 163 | 0 | 188 | 0 |
| AST [U/L] Start | - | - | - | 88 | - | 110 | - | 94 | - | 88 |
| AST [U/L] End | 118 | 113 | 93 | 88 | 78 | 86 | 90 | 83 | 137 | 109 |
| Body weight [g] Start | - | - | - | 156 | - | 151 | - | 258 | - | 278 |
| Body weight [g] End | 170 | 179 | 163 | 155 | 186 | 177 | 349 | 291 | 413 | 357 |
| Cu [µg/mg protein] | | | | | | | | | | |
| Homogenate | 0.013 | 0.917 | 0.014 | 0.593 | 0.012 | 1.001 | 0.013 | 0.226 | 0.014 | 1.019 |
| Mitochondria | 0.028 | 0.296 | 0.027 | 0.167 | 0.027 | 0.267 | 0.028 | 0.067 | 0.023 | 0.266 |

## 3.3 Increasing mitochondrial copper load is paralleled by COX17 upregulation

In section 3.1.2, it is shown that the mitochondrial copper load increases with disease progression of *Atp7b*$^{-/-}$ rats. In *Atp7b*$^{-/-}$ rats, the mitochondrial function can be maintained up to a mitochondrial copper load of approximately 7 nmol copper per mg mitochondrial protein [58, 152]. If *Atp7b*$^{-/-}$ rats become diseased, the mitochondrial copper load exceeds this point to be regulated, leading to the break down and massive functional impairments of liver mitochondria [58, 152]. This raises the question how mitochondria buffer progressing copper accumulation in WD. It is known that in *Atp7b*$^{-/-}$ rats mitochondrial copper reacts with thiol-containing proteins [152]. A detailed analysis, which mitochondrial proteins are involved in copper binding in WD, is absent. To address this issue, mitochondria from each two heterozygous control (Rats 1 and 2) and *Atp7b*$^{-/-}$ rat livers (Rats 3 and 4) were isolated. Protein subfractionation was done by sonication, gel filtration and anion exchange chromatography using a similar protocol described by Cobine *et al.* [139, 140]. Copper-rich fractions (Figure 3-19A) finally underwent proteomic analysis.

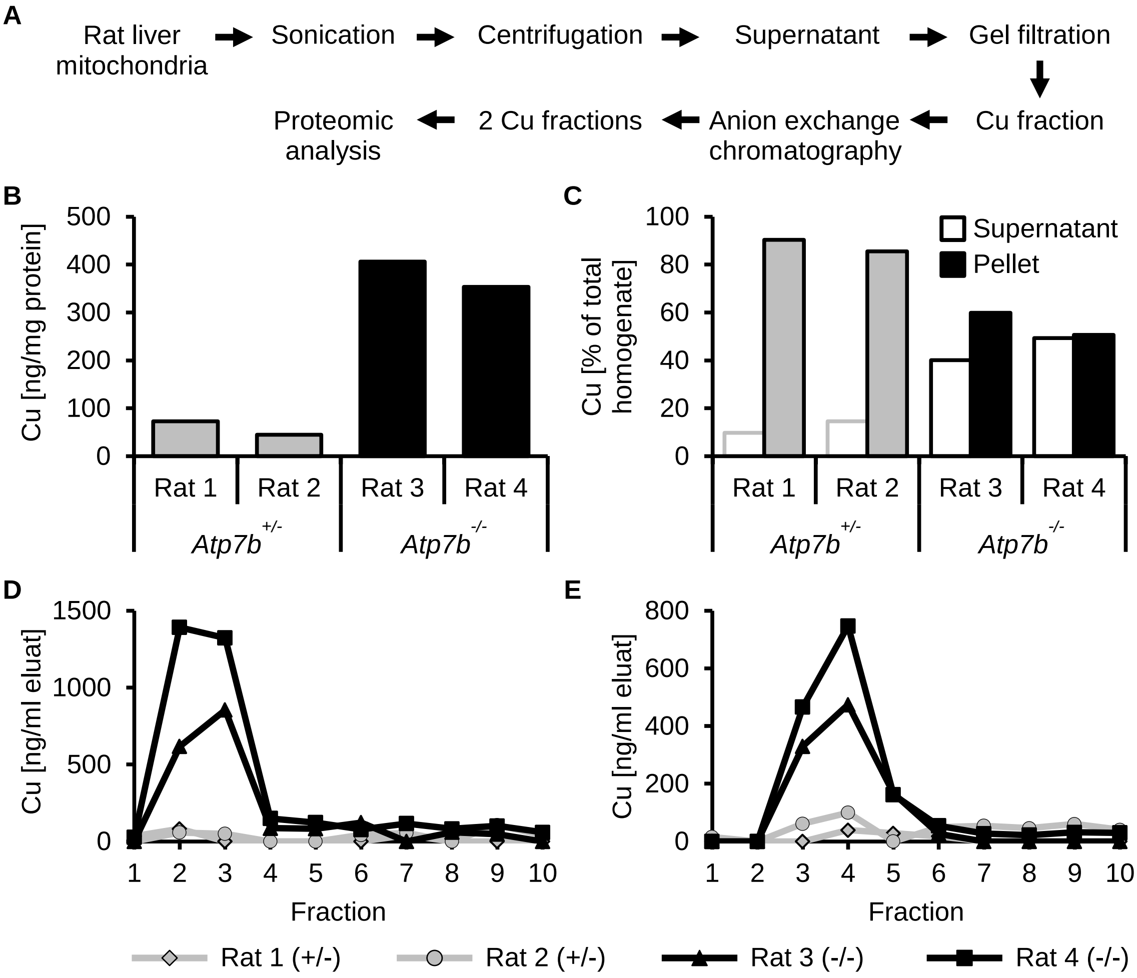

Figure 3-19 Subfractionated *Atp7b*$^{-/-}$ rat liver mitochondria have an increased copper load compared to *Atp7b*$^{+/-}$ rats.

*(A) Scheme for subfractionation of isolated rat liver mitochondria.*

*(B) Liver mitochondria isolated from copper-burdened Atp7b*$^{-/-}$ *rats (rat 3 and 4) have an up to sevenfold increased mitochondrial copper load compared to Atp7b*$^{+/-}$ *controls (rats 1 and 2).*

*(C) Isolated rat liver mitochondria from (B) were sonicated and centrifuged over night. Determination of copper concentrations indicates a shift of copper from the pellet fraction to the supernatant.*

*(D) Supernatant from (C) was used for gel filtration. Fractions two and three contain the highest amount of copper, indicating copper-binding proteins with a molecular weight greater than 6 kDa.*

*(E) Fractions two and three from (D) were pooled and purified via an anion exchange column. Fractions three and four contain the highest amount of copper and are used for proteomic analysis.*

Liver mitochondria isolated from *Atp7b*$^{-/-}$ rats contain an approximately sevenfold increased copper load compared to mitochondria from *Atp7b*$^{+/-}$ rats (Figure 3-19B). After sonication of the mitochondria and centrifugation over night, increasing copper concentrations are detected in the supernatant with a concomitant decrease of the copper load in the pellet fraction of *Atp7b*$^{-/-}$ rat liver mitochondria (Figure 3-19C). In this analysis, the supernatant is of interest, as copper-binding proteins, such as SOD1 or CCS1, are soluble proteins [266]. The supernatants were used for gel filtration, whereby fractions two and three contain the highest copper amount (Figure 3-19D). These data indicate, as specified by the manufacturer of the size exclusion column, copper-containing proteins with a molecular weight of more than 6 kDa. Fractions two and three were pooled and subjected to anion exchange chromatography, upon which the highest copper concentrations are measured in fractions three and four (Figure 3-19E).

Protein abundances from proteomic analysis were used for the identification of proteins that are related to the copper overload in WD. Therefore, it was analysed which proteins are enriched in fractions three and four from anion exchange chromatography relative to native mitochondria (IEX_F3/mitochondria and IEX_F4/mitochondria; proteomic analysis was done in close collaboration with Dr. Christine von Törne). The ratio for each fraction was compared among the two rat genotypes to identify proteins that are upregulated in copper-loaded *Atp7b*$^{-/-}$ rats compared to *Atp7b*$^{+/-}$ rats (Table 3-3). This calculation identifies 14 proteins to be upregulated in IEX_F3 and IEX_F4 in *Atp7b*$^{-/-}$ rats compared to *Atp7b*$^{+/-}$ rats. Out of these, COX17 is the only protein with known copper ion binding. It is about eightfold upregulated in *Atp7b*$^{-/-}$ rats compared to *Atp7b*$^{+/-}$ rats. Other mitochondrial proteins with a function in copper metabolism, such as SCO1, SOD1 and COX11 are either up- or downregulated in one of the two fractions or unregulated (Supplementary Table 3). Another point to consider is the appearance of electron-dense deposits within the IMS of liver mitochondria from diseased *Atp7b*$^{-/-}$ rats (Figure 3-4, Figure 3-16, Figure 3-18). As COX17 is localised within the IMS [11, 133, 139], this supports the hypothesis that these deposits may be copper-COX17 complexes. Due to these results, further analyses focus on the copper-binding protein COX17.

Table 3-3 Proteomic analysis of subfractionated rat liver mitochondria presents COX17 as an important protein for balancing the mitochondrial copper overload in *Atp7b*$^{-/-}$ rat liver mitochondria.

*Proteins that are upregulated in IEX_F3 and IEX_F4 from Atp7b*$^{-/-}$ *rats compared to Atp7b*$^{+/-}$ *rats are listed. Additionally, the appropriate accession number, regulation, localisation and function of the proteins are denoted. Information about localisation and function are obtained from UniProt.*

| **Protein** | **Accession No.** | **Ratio -/- vs. +/-** | | **Localisation** | **Function** |
|---|---|---|---|---|---|
| | | **IEX_F3** | **IEX_F4** | | |
| CHCHD4 (MIA40)<br>(Mitochondrial intermembrane space import and assembly protein 40) | Q5BJN5 | 577.44 | 10.28 | IMS | Protein import into IMS |

Table 3-3 Proteomic analysis of subfractionated rat liver mitochondria presents COX17 as an important protein for balancing the mitochondrial copper overload in *Atp7b*$^{-/-}$ rat liver mitochondria.

| **Protein** | **Accession No.** | **Ratio -/- vs. +/-** | | **Localisation** | **Function** |
|---|---|---|---|---|---|
| | | **IEX_F3** | **IEX_F4** | | |
| LOC691083<br>(Uncharacterised protein) | D4AEL0 | 81.15 | 6.14 | Mitochondrion | Unknown |
| ATPAF1<br>(ATP synthase mitochondrial F1 complex assembly factor 1) | NP_001101429 | 23.19 | 3.18 | Mitochondrion | Protein complex assembly |
| RHOC<br>(Transforming protein RhoA) | P61589 | 21.84 | 3.66 | Mitochondrion | GTPase activity |
| TTC19<br>(Tetratricopeptide repeat protein 19) | D4A6D7 | 14.52 | 4.19 | MIM | Component of the PAM complex (translocation of transit peptide-containing proteins from the MIM into the mitochondrial matrix in an ATP-dependent manner) |
| PRDX3<br>(Thioredoxin-dependent peroxide reductase) | Q9Z0V6 | 7.36 | 2.34 | Mitochondrion<br>(human homologue: matrix) | Redox regulation of the cell |
| **COX17**<br>(Cytochrome c oxidase assembly protein) | NP_445992 | 6.97 | 8.90 | IMS | Copper chaperone activity, copper ion transport |
| CAR5B<br>(Carbonic anhydrase 5B) | Q66HG6 | 5.89 | 2.53 | Mitochondrion | Reversible hydration of carbon dioxide |
| FDX1<br>(Adrenodoxin-like protein) | P24483 | 5.80 | 4.96 | Matrix | Synthesis of various steroid hormones, iron ion binding |
| COASY<br>(Bifunctional coenzyme A synthase) | NP_001006955 | 5.65 | 2.40 | Matrix | Coenzyme A biosynthetic process |
| NUDT9<br>(Nucleoside diphosphate-linked moiety X motif 19) | Q5XIG0 | 5.59 | 4.50 | Mitochondrion<br>(human homologue: matrix) | Hydrolyses ADP-ribose (ADPR) to AMP and ribose 5'-phosphate |
| HDHD3<br>(Haloacid dehalogenase-like hydrolase domain-containing protein 3) | NP_001102981 | 4.89 | 3.79 | Mitochondrion | Hydrolase activity |
| FAM82A2<br>(Regulator of microtubule dynamics protein 3) | Q66H15 | 3.57 | 2.81 | MOM | Cellular calcium homeostasis regulation |
| ISCA2<br>(Similar to HESB like domain containing 1 (RGD1563216)) | NM_001109278 | 3.21 | 2.44 | Mitochondrion | Iron-sulfur cluster assembly |

The increased COX17 abundance in *Atp7b*$^{-/-}$ rats raises the question of whether COX17 levels depend on the disease state of these rats and whether it is increased in WD patients as well. COX17 abundances were analysed in liver mitochondria isolated from *Atp7b*$^{+/-}$ controls, *Atp7b*$^{-/-}$ rats of progressing disease states and WD patients using immunoblot analysis (Figure 3-20). COX17 level is low in mitochondria isolated from *Atp7b*$^{+/-}$ control rats, increases approximately threefold in affected and approximately sixfold in diseased *Atp7b*$^{-/-}$ rats. COX17 abundances in liver mitochondria isolated from untreated WD patients are comparable to those of diseased *Atp7b*$^{-/-}$ rats. Liver mitochondria isolated from D-PA pretreated WD patients have a reduced COX17 amount compared to untreated WD patients (Figure 3-20B) which is in parallel with the reduced mitochondrial copper load (Figure 3-1).

**A**

| Rat ID | 1 | 2 | 3 | 4 | 5 | 6 | 7 | 8 |
|---|---|---|---|---|---|---|---|---|
| *Atp7b* genotype | +/- | +/- | +/- | -/- | -/- | -/- | -/- | -/- |
| AST [U/L] | 111 | 95 | 127 | 89 | 173 | 437 | 351 | 540 |
| Bilirubin [mg/dl] | <0.5 | <0.5 | <0.5 | <0.5 | <0.5 | 3.0 | 7.9 | 17.2 |
| Mitochondrial Cu [µg/mg protein] | 0.052 | 0.028 | 0.029 | 0.363 | 0.463 | 1.338 | 1.097 | 1.699 |
| Disease state | healthy | | | affected | | diseased | | |

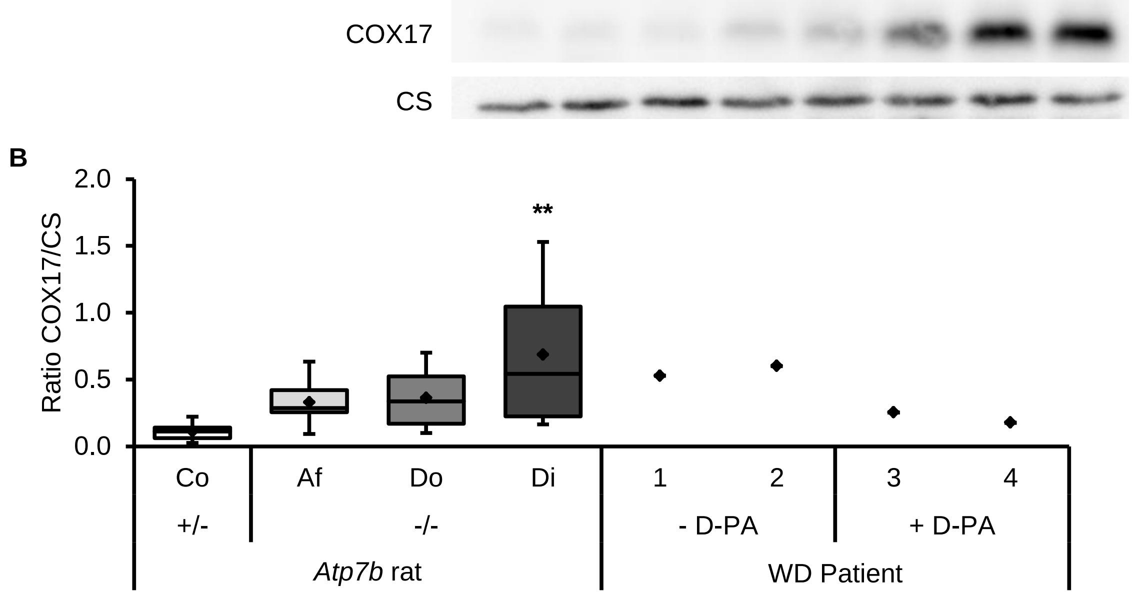

Figure 3-20 Protein amount of mitochondrial COX17 increases with disease progression of *Atp7b*$^{-/-}$ rats and is comparable to that from WD patients.

(A) *Immunoblot analysis for* COX17 *in liver mitochondria isolated from Atp7b*$^{+/-}$ *controls and different disease states of Atp7b*$^{-/-}$ *rats.* COX17 *abundance increases with disease progression.*

(B) *Quantification of* COX17 *amount normalised to the mitochondrial citrate synthase (CS, immunoblot) in liver mitochondria isolated from Atp7b*$^{+/-}$ *controls and different disease states of Atp7b*$^{-/-}$ *rats. As shown in (A),* COX17 *amount increases with disease progression. Similar* COX17 *amounts are detected for untreated WD patients (1 and 2). D-PA pretreated WD patients (3 and 4) show reduced* COX17 *levels. (Co) control Atp7b*$^{+/-}$*: N=8, (Af) affected Atp7b*$^{-/-}$*: N=9, (Do) disease onset Atp7b*$^{-/-}$*: N=9, (Di) diseased Atp7b*$^{-/-}$*: N=5. One-way ANOVA with Tukey's multiple comparisons test. *Significant to Atp7b*$^{+/-}$ *control, **p<0.01.* ▬ *median,* ♦ *mean value, 25% and 75% quartile are indicated.*

Immunohistochemistry staining of rat liver tissue with COX17 (done in close collaboration with Dr. Michaela Aichler, Claudia-Mareike Pflüger and Dr. Annette Feuchtinger) confirms the results obtained by immunoblot analyses (Figure 3-21). Scanned tissue sections were quantified using Definiens Developer. Cells were characterised due to their staining intensity into (1) unstained, (2) low staining, (3) middle intensity and (4) strong staining. State 3 and 4 are quantified for Figure 3-21B. Liver tissues from *Atp7b*$^{+/-}$ rats show very low detection of COX17 positive cells, whereas the amount of COX17 stained cells increases with disease progression of *Atp7b*$^{-/-}$ rats. These data show that COX17 upregulation is in parallel with the mitochondrial copper load and disease progression of *Atp7b*$^{-/-}$ rats, in agreement with a potential copper-buffering role for COX17 in mitochondria from *Atp7b*$^{-/-}$ rats (see section 3.4).

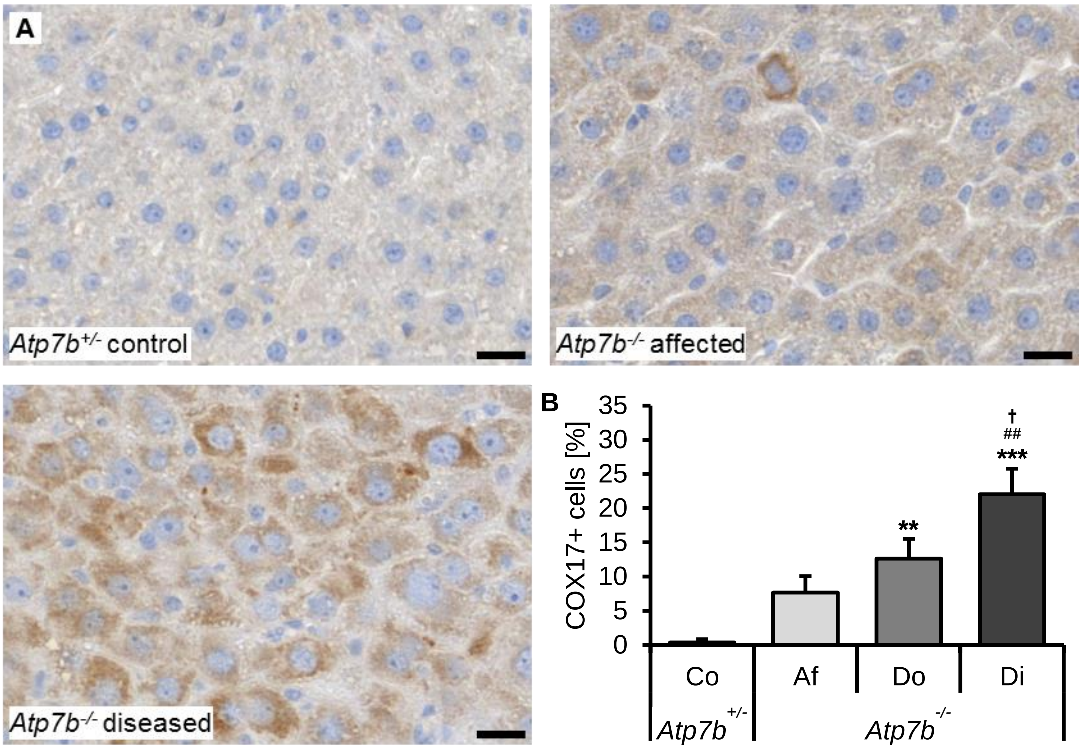

Figure 3-21 Amount of COX17 positive liver cells increases in liver tissue with disease progression of *Atp7b*$^{-/-}$ rats.

(A) *Immunohistochemical staining for* COX17 *of rat liver tissue. Heterozygous control tissues show a few* COX17 *positive cells, whereas in liver tissues from Atp7b*$^{-/-}$ *rats amount of* COX17 *positive cells increases with rising mitochondrial copper load and disease progression. Each one out of three experiments is shown. Scale bar: 20 µm.*

(B) *Quantification of* COX17 *immunohistochemical staining from (A). Medium and strongly stained cells are summed up. N=3, each. (Co) control Atp7b*$^{+/-}$*, (Af) affected Atp7b*$^{-/-}$*, (Do) disease onset Atp7b*$^{-/-}$*, (Di) diseased Atp7b*$^{-/-}$*. One-way ANOVA with Tukey's multiple comparisons test. *Significant to Atp7b*$^{+/-}$ *control,* $^{\#}$*significant to Atp7b*$^{-/-}$ *affected,* $^{\dagger}$*significant to Atp7b*$^{-/-}$ *disease onset. *p<0.05, **p<0.01, ***p<0.001.*

In liver mitochondria from copper-loaded *Atp7b*$^{-/-}$ rats, copper possibly alters interactions among proteins. To identify interaction partners of COX17 in situations with elevated copper such as WD, immunoprecipitation for endogenous COX17 was performed using liver mitochondria isolated from *Atp7b*$^{+/-}$ and diseased *Atp7b*$^{-/-}$ rats followed by proteomic analysis of the bead fraction (containing COX17 protein, antibody against COX17 and beads; Figure 3-22). COX17 is enriched in liver mitochondria from both genotypes, whereby COX17 amount is higher in liver mitochondria from *Atp7b*$^{-/-}$ rats compared to *Atp7b*$^{+/-}$ controls (Figure 3-22A). The bead fraction from *Atp7b*$^{-/-}$ rat liver mitochondria contains an approximately fourfold higher copper amount (Figure 3-22B left) paralleled by an approximately threefold increased COX17 abundance (Figure 3-22B right) compared to the bead fraction from *Atp7b*$^{+/-}$ rat liver mitochondria. Possible interaction partners of COX17 are identified according to the following evaluation and are summarised in Figure 3-22C:

1) proteins were detected in all three replicates of the bead fraction of the two groups (*Atp7b*$^{+/-}$ and *Atp7b*$^{-/-}$ rat liver mitochondria, respectively),
2) abundances of the proteins in the two groups were referred to the COX17 abundance of the respective group (defined as relative protein abundance),
3) relative protein abundances from the *Atp7b*$^{-/-}$ group were referred to the relative protein abundance of the *Atp7b*$^{+/-}$ group to identify proteins that are enriched in mitochondria with copper overload (proteins with a threshold >1.5), and
4) possible interaction partners were localised within the mitochondrial intermembrane space or the mitochondrial inner membrane to interact with COX17.

Two of the four listed proteins, the acyl-CoA dehydrogenase family member 11 (ACAD11) and the MICOS subunit Mic25 (CHCHD6, marked in **bold**), are located at mitochondrial membranes (Figure 3-22C). ACAD11 is involved in β-oxidation and CHCHD6 is involved in maintaining the mitochondrial ATP production and cristae structure. In *Atp7b*$^{-/-}$ rats, liver mitochondria present with progressing structural (Figure 3-3) and functional impairments, including reduced stability of the MMP (Figure 3-8) and a reduced capacity for ATP production (Figure 3-9). Not only CHCHD6 [267, 268], but also COX17 [142] is involved in the mitochondrial contact site and cristae organisation system (MICOS). Thus, CHCHD6 would be of particular interest as an interaction partner for COX17.

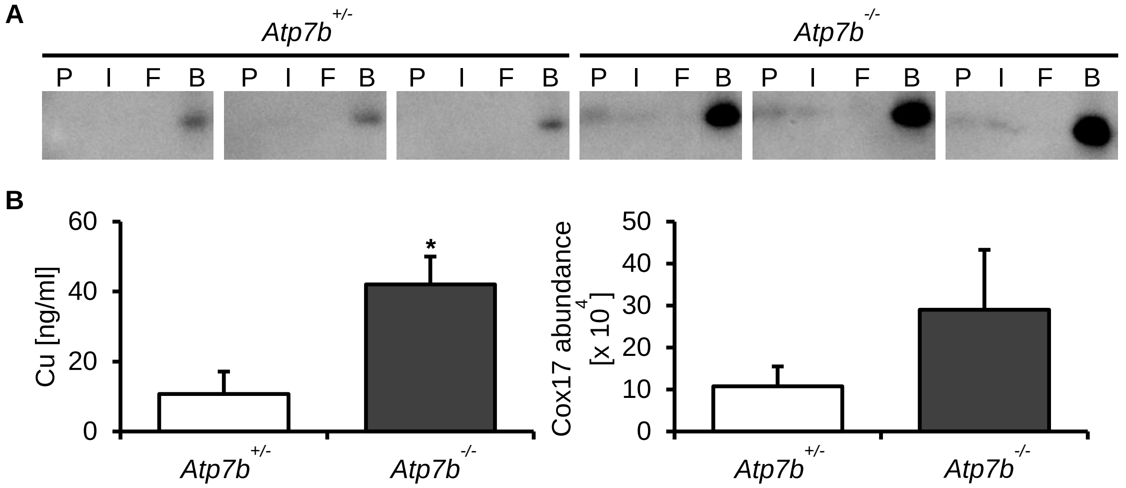

C

| Protein | Accession No. | Ratio -/- vs. +/- normalised to COX17 | Localisation | Function |
|---|---|---|---|---|
| ACAD11<br>(Acyl-CoA dehydrogenase family, member 11) | 1306270 | 3.51 | Mitochondrial inner membrane | Fatty acid β-oxidation using acyl-CoA dehydrogenase (maximal activity towards saturated C22-Co) |
| ACO2<br>(Aconitase 2) | 621360 | 3.06 | Mitochondrion<br>(human homologue: matrix) | Tricarboxylic acid cycle |
| GLDC<br>(glycine dehydrogenase (decarboxylating)) | 1308660 | 2.06 | Mitochondrion<br>(human homologue: matrix) | Pyridoxal phosphate binding |
| **CHCHD6**<br>(MICOS complex subunit Mic25) | D4A7N1 | 1.92 | Mitochondrial inner membrane | Maintaining mitochondrial cristae morphology, ATP production and oxygen consumption |

Figure 3-22 ACAD11 and CHCHD6 are possible interaction partners of COX17 in situations with elevated copper, such as Wilson disease.

*(A)* *Immunoblot analysis of* COX17 *confirms its enrichment in the bead fraction from diseased Atp7b*$^{-/-}$ *rats and heterozygous controls.* COX17 *level is much higher in Atp7b*$^{-/-}$ *rats compared to Atp7b*$^{+/-}$ *rats. N=3. P: pellet, I: input, F: flow, B: beads.*

*(B)* *Bead fraction from (A) is analysed for copper load (left) and* COX17 *abundance using proteomic analysis (right). Due to* COX17 *immunoprecipitation,* COX17 *is confirmed to be upregulated in Atp7b*$^{-/-}$ *rats paralleled by an increased copper load. Unpaired two-tailed Student's t-test with Welch's correction. *Significant to Atp7b*$^{+/-}$*, *p<0.05.*

*(C)* *Possible interaction partners of* COX17 *in WD. CHCHD6 (marked in* **bold***) would be of particular interest, as it is involved in maintaining the mitochondrial structure and ATP production. Abundances of the proteins were normalised to the abundance of* COX17 *of the respective genotype (Atp7b*$^{+/-}$ *or Atp7b*$^{-/-}$*, respectively). The ratio from the consequential values from Atp7b*$^{-/-}$ *versus Atp7b*$^{+/-}$ *was used to analyse which proteins are in relation to WD. Information about localisation and function of the proteins are obtained from UniProt.*

## 3.4 COX17 upregulation is simulated in Cu-His treated HepG2 WT cells

In section 3.3, COX17 is found to be upregulated in liver mitochondria isolated from *Atp7b*$^{-/-}$ rats with disease progression. Here, the question is addressed whether COX17 upregulation due to increasing mitochondrial copper load is protective or damaging for these organelles. Simulating an increasing mitochondrial copper load was done by treating human hepatocytes (HepG2 cells) with a copper-histidine solution (Cu-His).

### 3.4.1 Millimolar Cu-His concentrations are toxic to HepG2 WT cells

First, the susceptibility of HepG2 wild type (WT) cells towards Cu-His was analysed using neutral red and CellTiterGlo assay to determine a non-toxic copper concentration after 24 hours of treatment. Viable cells take up neutral red, whereas non-viable cells do not [220]. CellTiterGlo assay uses luciferase to measure cellular ATP content [221]. In contrast to dead cells, living cells produce ATP [221]. Figure 3-23 demonstrates that 10 µM Cu-His (0.2 nmol copper per $10^5$ cells) is not toxic to HepG2 WT cells after 24 hours of treatment, as shown by an unaffected vitality (Figure 3-23A) and ATP content (Figure 3-23B) of these cells. HepG2 WT cells are sensitive towards increasing Cu-His concentrations after 24 hours of treatment. Millimolar concentrations of Cu-His reduce cellular vitality for 38% and ATP content for 30%. No toxic effects on WT cells are observed with histidine alone (data not shown).

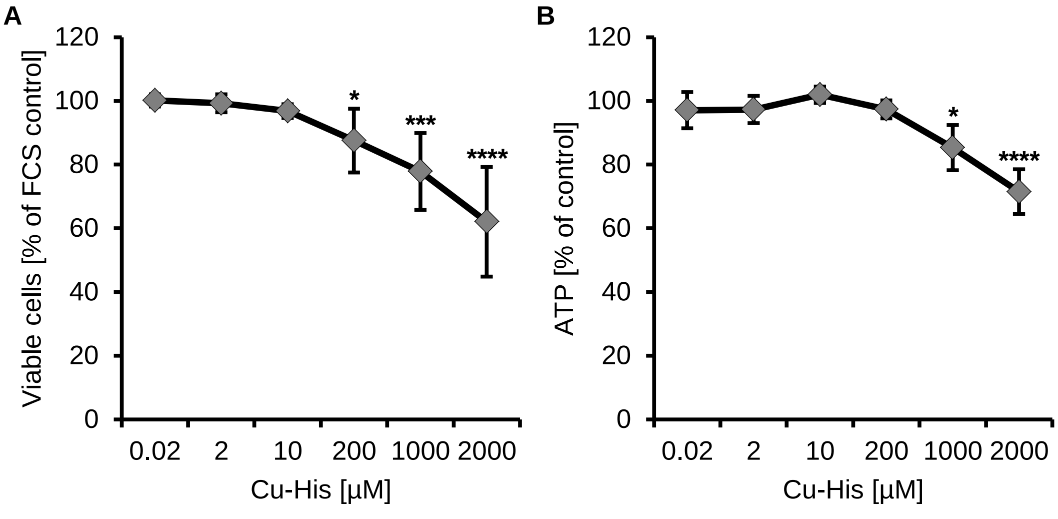

Figure 3-23 Millimolar Cu-His concentrations are toxic to HepG2 WT cells.

*Neutral red assay (A) and ATP content (B) for HepG2 WT cells treated for 24 hours with increasing Cu-His concentrations. Millimolar concentrations of Cu-His reduce cellular viability for 22–38% and ATP content for 15–29%. Neutral red assay: N=5, n=15. CellTiterGlo assay: N=3, n=9. One-way ANOVA with Tukey's multiple comparisons test. *Significant to control, *p<0.05, ***p<0.001, ****p<0.0001.*

The concentration of 0.2 nmol copper per $10^5$ cells (Table 2-13, here meaning 15 µM Cu-His) was used to assess the cellular vitality and proliferation for up to 48 hours of treatment (Table 3-4). The number of control cells increases threefold, whereas the number of Cu-His treated cells increases approximately twofold within 48 hours of treatment, meaning a 34% reduced cellular proliferation compared to control cells. Treating HepG2 cells for 48 hours with Cu-His reduces vitality for 25%. These data show that Cu-His (in concentrations that are not acutely toxic to HepG2 cells) reduces cellular vitality and proliferation, leading to the question of whether this is due to copper accumulation within cells and mitochondria.

Table 3-4 15 µM Cu-His reduces cellular proliferation and vitality of HepG2 WT cells for approximately 30%.

| **Parameter** | **Treatment [hours]** | **Condition** | ***** | **Change [%] relative to control** |
|---|---|---|---|---|
| Cellular proliferation | 24 | Control | 0.21 | |
| *[Cell number x $10^5$ cells/well] | 48 | Control | 0.32 | |
| N=3 | 24 | 15 µM Cu-His | 0.16 | -25.9 |
| | 48 | 15 µM Cu-His | 0.21 | -33.8 |
| Vitality | 24 | Control | 82 | |
| *[%] | 48 | Control | 86 | |
| N=3 | 24 | 15 µM Cu-His | 82 | 0.0 |
| | 48 | 15 µM Cu-His | 65 | -24.4 |

### 3.4.2 Treatment of HepG2 WT cells with rising Cu-His concentrations raises cellular and mitochondrial copper load

Millimolar concentrations or prolonged treatments with Cu-His are toxic to HepG2 WT cells. For comparison, in *Atp7b*$^{-/-}$ rats, progressive copper accumulation in liver and mitochondria lead to mitochondrial structural alterations and functional impairments. Toxic effects of Cu-His on HepG2 WT cells are possibly due to increased copper accumulation within cells or mitochondria. To address this issue, HepG2 WT cells were treated for 24 hours with non-toxic Cu-His concentrations and cellular and mitochondrial copper concentrations were measured using ICP-OES. With increasing Cu-His concentration, cellular copper load raises in HepG2 WT cells (Figure 3-24A). At least, 15 µM Cu-His (0.2 nmol copper per $10^5$ cells) is necessary to induce a significant, 38-fold increase in cellular copper load (0.3627 µg copper per 1 x $10^6$ cells) compared to control cells (0.0096 µg copper per 1 x $10^6$ cells). Due to this significant increase in cellular copper load but non-toxic effects on HepG2 WT cells after 24 hours of treatment, this concentration is used for the following analyses. The mitochondrial copper load was measured in mitochondria isolated from control cells and 24 hours 15 µM Cu-His treated cells. Cu-His treatment of the cells raises the mitochondrial copper concentration twelvefold to approximately 1.4 µg copper per mg protein (Figure 3-24B). This mitochondrial copper load is comparable to liver mitochondria isolated from diseased *Atp7b*$^{-/-}$ rats.

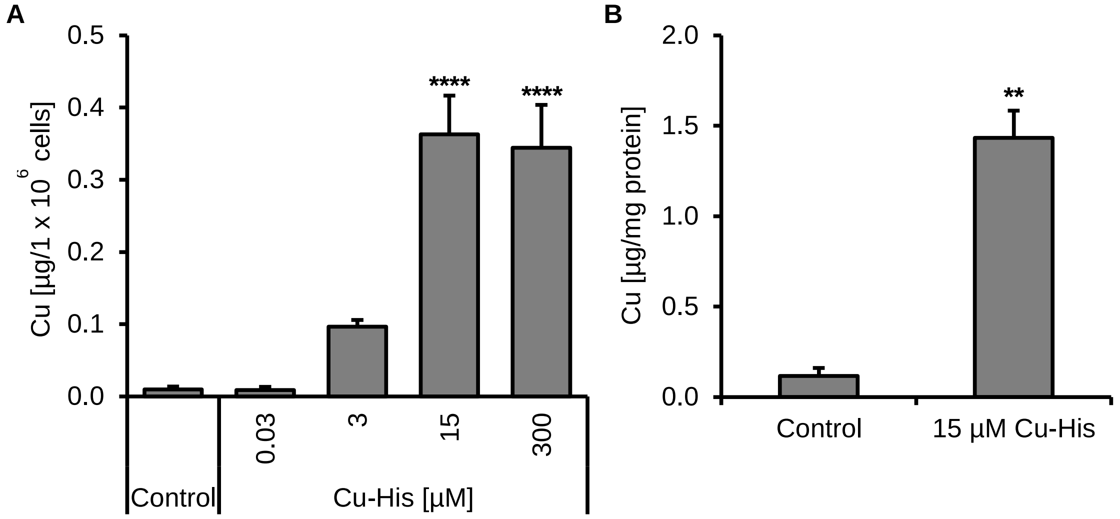

Figure 3-24 Treatment of HepG2 WT cells with increasing Cu-His concentrations induces a raise in cellular and mitochondrial copper load.

(A) *Treating HepG2 WT cells with increasing Cu-His concentrations progressively raises cellular copper concentrations. At least, a concentration of 15 µM Cu-His is necessary to reach cellular copper concentrations comparable to liver homogenate from Atp7b*$^{-/-}$ *rats. N=4. One-way ANOVA with Tukey's multiple comparisons test. *Significant to control, ****p<0.0001.*

(B) *Treating HepG2 WT cells with 15 µM Cu-His significantly raises the mitochondrial copper load up to twelvefold. The mitochondrial copper load of approximately 1.4 µg Cu per mg protein is comparable to liver mitochondria isolated from diseased Atp7b*$^{-/-}$ *rats. N=3. Unpaired two-tailed Student's t-test with Welch's correction. *Significant to control, **p<0.01.*

### 3.4.3 Cu-His treatment of HepG2 WT cells increases cellular and mitochondrial COX17 abundance

In *Atp7b*$^{-/-}$ rats, a rising copper load of the liver mitochondria is paralleled by an increasing abundance of COX17 (Figure 3-1, Figure 3-20). Thus, the question is of whether the increasing cellular and mitochondrial copper load in Cu-His treated HepG2 WT cells is paralleled by an upregulation of COX17. HepG2 WT cells were treated with increasing Cu-His concentrations (see section 3.4.2) and lysed for immunoblot analysis. Figure 3-25A shows an approximately two- to threefold increasing COX17 abundance with rising Cu-His concentrations in HepG2 WT cells. In mitochondria isolated from 24 hours 15 µM Cu-His treated HepG2 WT cells, COX17 abundance increases approximately twofold relative to mitochondria isolated from control cells (Figure 3-25B). These data demonstrate that increasing mitochondrial copper load is paralleled by an upregulation of COX17 in mitochondria isolated from Cu-His treated HepG2 WT cells as observed in *Atp7b*$^{-/-}$ rat liver mitochondria.

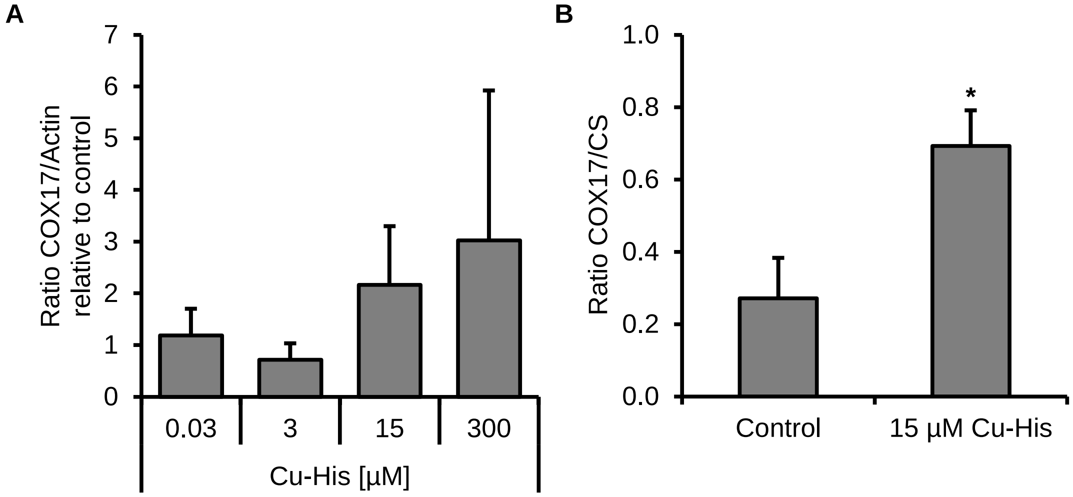

Figure 3-25 Treating HepG2 WT cells with increasing Cu-His concentrations raises cellular and mitochondrial abundance of COX17.

*(A)* *Treating HepG2 WT cells with increasing Cu-His concentrations progressively raises cellular* COX17 *level compared to control cells. N=4. Normalised to actin.*

*(B)* *Mitochondria isolated from 15 µM Cu-His treated HepG2 WT cells have an approximately 2.5-fold increased level of* COX17. *Normalised to the mitochondrial citrate synthase (*CS*). N=3. Unpaired two-tailed Student's t-test with Welch's correction. *Significant to control, *p<0.05.*

### 3.4.4 COX17+ cells are less susceptible towards Cu-His than COX17- cells

As shown in section 3.3, upon progressive copper accumulation in liver tissue and liver mitochondria from *Atp7b*$^{-/-}$ rats, COX17 is upregulated. A similar result is found in Cu-His treated HepG2 WT cells (section 3.4.3). These data indicate a potentially protective role of COX17 towards excess copper in mitochondria. To corroborate this hypothesis, HepG2 cells were modified as follows:

1) HepG2 WT cells were treated with siRNA against *COX17* (COX17-) to downregulate the protein abundance and
2) HepG2 WT cells were transfected with pcDNA3.1(+) with human *COX17* (COX17+) to upregulate the abundance of this protein.

### 3.4.4.1 Establishing *COX17* knockdown and overexpression

Establishing *COX17* knockdown and overexpression was done under the supervision of Dr. Michelle Vincendeau. HepG2 cells were reverse transfected with siRNA (nonsilencing RNA or siCOX17) or vector (containing or not containing COX17). 24 hours post-transfection cells received fresh medium and were incubated up to 48 and 72 hours post-transfection. *COX17* expression level was analysed by quantitative real-time PCR (qRT-PCR) from RNA isolated from transfected cells 48 and 72 hours post-transfection as these time points are relevant to the performed experiments. Expression level of *COX17* was normalised to the RNA of the house-keeping enzyme *RNA polymerase II* (*RPII*) [252]. Normalised expression level was further calculated relative to the controls not influencing *COX17* expression – nonsilencing RNA or empty vector, respectively. Another aliquot of cells was lysed for immunoblot analysis and protein abundance was normalised to GAPDH as loading control [269].

For *COX17* knockdown, HepG2 cells were reverse transfected with three different siRNAs against *COX17* using Lipofectamin RNAiMAX on day one. Out of the three tested siRNAs, the first induces massive cell death and the second cannot reduce expression of *COX17* (data not shown). Only siRNA3 shows no toxic effects while inducing knockdown of *COX17* for 90–95% 48 to 72 hours post-transfection (Figure 3-26). Similar results are obtained on immunoblot analysis (Figure 3-26B). Due to these results, siRNA3 is used for all other *COX17* knockdown experiments.

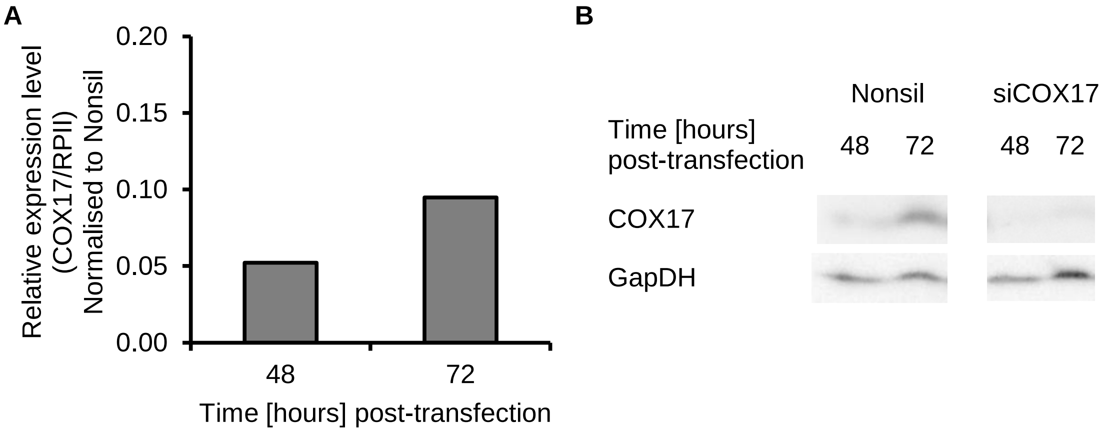

Figure 3-26 Knockdown of *COX17* in HepG2 cells reduces *COX17* level for up to 95% relative to the nonsilencing control.

(A) *Transfecting HepG2 cells with siCOX17 induces an approximately 90–95% reduction of COX17 48–72 hours post-transfection. Expression level of COX17 is normalised to RNA polymerase II (RPII). Values are further related to the respective expression level of the nonsilencing control RNA (Nonsil) at 48 and 72 hours post-transfection. N=2.*

(B) *Immunoblot analyses of siCOX17 transfected HepG2 cells 48 and 72 hours post-transfection.* COX17 *(~7 kDa) is efficiently downregulated using siCOX17 compared to cells transfected with nonsilencing control RNA (Nonsil). One out of two experiments is shown.*

For overexpression, *COX17* was specifically amplified and cloned into pcDNA3.1(+) vector without any tags as this construct is the least modified. Vector with *COX17* insert was reverse transfected into HepG2 cells on day one using Fugene [270]. 48 to 72 hours post-transfection *COX17* mRNA is increased about 200-fold (Figure 3-27A) and protein is increased about twofold relative to the empty vector control (Figure 3-27B).

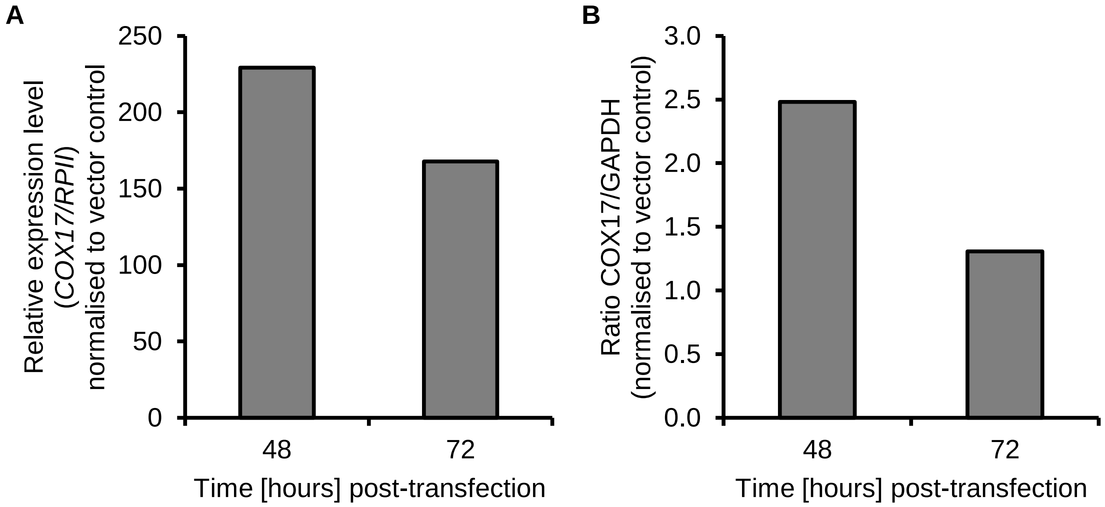

Figure 3-27 Overexpression of *COX17* in HepG2 cells increases cellular COX17 level up to 2.5-fold relative to the vector control.

*(A) Transfecting HepG2 cells with pcDNA3.1(+) vector containing human COX17 insert increases COX17 expression approximately 200-fold 48–72 hours post-transfection. Expression level of COX17 is normalised to RNA polymerase II (RPII). Values are further related to the respective expression level of the empty vector control at 48 and 72 hours post-transfection. N=2.*

*(B) Immunoblot analyses of* COX17 *overexpressed HepG2 cells 48 and 72 hours post-transfection.* COX17 *is upregulated using pcDNA3.1(+)*-COX17 *compared to cells transfected with empty vector control. One out of two experiments is shown.*

#### 3.4.4.2 *COX17* protects HepG2 cells against toxic Cu-His

The effects of *COX17* knockdown and overexpression on HepG2 cells were analysed to address the question of whether *COX17* upregulation is a buffering system for balancing elevated cellular copper concentrations. Cellular proliferation and vitality of untreated and Cu-His treated COX17- and COX17+ cells were analysed time- and dose-dependently and compared to the respective control cells (HepG2 cells transfected with nonsilencing RNA for COX17- cells, HepG2 cells transfected with empty pcDNA3.1(+) vector for COX17+ cells; Table 3-5, Supplementary Figure 3). Cells were treated for 24 to 48 hours with medium containing or not containing Cu-His.

At standard subcultivation conditions, 48 hours after treatment cellular proliferation of COX17- cells is reduced for 21% and vitality is reduced for 10% compared to control cells (Table 3-5). 48 hours post-treatment, proliferation of COX17+ cells is increased for about 26% compared to the control cells, whereas vitality is reduced for 7.5% in COX17+ cells compared to control cells.

Treating COX17- cells with 15 µM Cu-His reduces cellular proliferation for 37% and cellular vitality for 11% 48 hours post-treatment compared to HepG2 cells transfected with the nonsilencing control RNA. 15 µM Cu-His treated COX17+ cells show an 9% increased cellular proliferation and a 15% increased cellular vitality 48 hours post-treatment compared to control cells.

The treatment of COX17- cells with increasing Cu-His concentrations progressively reduces cellular vitality. Millimolar Cu-His concentrations reduce the amount of viable cells for 25% compared to control cells. For COX17+ cells, high Cu-His concentrations have no effect on cellular vitality compared to control cells.

These data show that COX17+ cells are less susceptible towards 48 hour treatment with 15 µM Cu-His or higher concentrations of Cu-His for 24 hours than COX17- cells. Therefore, COX17 protects HepG2 cells against toxic effects of elevated copper concentrations.

Table 3-5 COX17- cells are more susceptible towards Cu-His treatment than COX17+ cells.

*COX17 knockdown inhibits cellular proliferation under standard subcultivation conditions and 15 µM Cu-His, and reduces vitality towards rising Cu-His concentrations in HepG2 cells compared to HepG2 cells transfected with the nonsilencing control RNA (marked in italic). COX17 overexpression promotes cellular proliferation under standard subcultivation conditions and improves tolerance of 15 µM Cu-His 48 hours post-treatment compared to cells transfected with the empty vector control. Regarding increasing Cu-His concentrations, 24 hours post-treatment no alterations are measured for cellular vitality of COX17+ cells compared to the empty vector control. Negative values indicate a reduction, whereas positive values indicate an improvement relative to the respective control. N=3–4, n=6–8.*

| **Assay** | **Treatment [hours]** | **Condition** | **Change [%] relative to control** | |
|---|---|---|---|---|
| | | | **COX17-** | **COX17+** |
| Cellular proliferation | 24 | Standard subcultivation condition | -17.7 | -3.0 |
| | *48* | *Standard subcultivation condition* | *-20.9* | *+25.6* |
| Vitality | 24 | Standard subcultivation condition | -1.5 | -2.4 |
| | *48* | *Standard subcultivation condition* | *-9.8* | *-7.5* |
| Cellular proliferation | 24 | 15 µM Cu-His | -2.7 | +4.7 |
| | *48* | *15 µM Cu-His* | *-37.0* | *+8.7* |
| Vitality | 24 | 15 µM Cu-His | -2.3 | +4.2 |
| | *48* | *15 µM Cu-His* | *-11.1* | *+14.7* |
| Vitality | 24 | 0.02 µM Cu-His | +3.7 | +4.6 |
| | 24 | 2 µM Cu-His | ±0.0 | +1.3 |
| | 24 | 10 µM Cu-His | +1.8 | +0.2 |
| | 24 | 200 µM Cu-His | -7.7 | +0.1 |
| | *24* | *1000 µM Cu-His* | *-15.5* | *-2.6* |
| | *24* | *2000 µM Cu-His* | *-24.6* | *-2.1* |

# 4 Discussion

## 4.1 The LPP rat as an animal model for studying alterations of liver mitochondria in Wilson disease

The first part of this thesis aimed to further understand liver mitochondrial alterations in Wilson disease (WD) by using the LPP rat as an animal model. The LPP rat used in this study carries a loss-of-function mutation in the *Atp7b* gene [2], resulting in impaired copper excretion via the bile [49, 53] and copper accumulation within the liver, leading to acute liver failure and death of these animals [152]. As this animal model bears the same genetic dysfunction as human WD patients [2], it is a valid model to analyse alterations of liver mitochondria in WD.

### 4.1.1 Liver mitochondrial damage in diseased *Atp7b*$^{-/-}$ rats is highly comparable to that observed in Wilson disease

The liver damage markers serum aspartate aminotransferase (AST) and bilirubin were used to classify *Atp7b*$^{-/-}$ rats into progressing disease states: affected (AST <200 U/L, bilirubin <0.5 mg/dl), disease onset (AST >200 U/L, bilirubin <0.5 mg/dl) and diseased (AST >200 U/L, bilirubin >0.5 mg/dl; Table 3-1) [1]. In a previous study, immunohistochemical analysis of the liver tissue from *Atp7b*$^{-/-}$ rats showed increasing liver tissue damage with disease progression [1]. The increased level of liver damage markers observed in *Atp7b*$^{-/-}$ rats was paralleled by an approximately 40- to 100-fold higher copper accumulation in liver mitochondria and liver homogenate compared to *Atp7b*$^{+/-}$ control rats (Figure 3-1). Liver copper values are comparable to a previous study, in which this parameter was not related to defined disease states but to the increasing age of rats [152]. In this thesis, it was demonstrated that copper concentrations in liver homogenate and liver mitochondria isolated from untreated WD patients are similar to those from diseased *Atp7b*$^{-/-}$ rats (Figure 3-1) [1]. Electron micrographs of liver mitochondria isolated from WD patients and diseased *Atp7b*$^{-/-}$ rats showed identical structural alterations (Figure 3-2), such as separation of the inner and outer mitochondrial membrane, cristae dilations, brightening of the normally electron-dense matrix and several vacuoles [1]. Such mitochondrial structural alterations were described from WD patient samples by Sternlieb *et al.* [33, 58, 70-72, 143-145]. Thus, the *Atp7b*$^{-/-}$ rat demonstrates mitochondrial features characteristic for WD.

In the present study, liver samples from four WD patients were included [1]. Two of the WD patients received no treatment prior to liver transplantation. The other two patients received D-penicillamine (D-PA) treatment but, as this treatment could not prevent the development of acute liver failure, both patients underwent liver transplantation [1]. Liver homogenate and liver mitochondria from D-PA pretreated WD patients show a three- to fourfold reduction in copper load compared to untreated WD patients (Figure 3-1). The clinically used copper chelating agent D-PA slowly reduces body copper stores (it is six to twelve months until urinary copper excretion is within the normal range) [56], but D-PA is often ineffective in patients with chronic WD and fails to rescue WD patients with acute fulminant hepatitis and liver failure, as exemplified by the two included D-PA pretreated WD patients [1, 33, 34, 65, 66, 271]. The majority of mitochondria from D-PA pretreated WD patients showed massive structural impairments (Figure 3-2) [1]. Even so, some regions still contain mitochondria without these structural alterations, demonstrating an at least partial improvement of the mitochondrial structure (Figure 3-2) [1]. D-PA is described to be successful in reversing WD symptoms and mitochondrial structure back to normal, but only if treatment starts before the onset of clinical symptoms [72, 152, 168, 169]. The heterogeneity of the mitochondrial structure in D-PA pretreated WD patients possibly results from the lack of homogeneity and the highly fibrotic nature of liver tissue [1]. If D-PA treatment fails, not only structural [33, 58, 70-72, 143-145], but also biochemical impairments can be observed in liver mitochondria from WD patients [59]. As Gu *et al.* excluded toxic effects of D-PA on liver mitochondria [59], the mitochondrial impairments might be due to the still increased mitochondrial copper load [59, 70-73]. This is in line with results obtained from liver mitochondria isolated from D-PA treated *Atp7b*$^{-/-}$ rats (Figure 3-15). The ineffectiveness of D-PA in short-term treatments to decopper liver mitochondria and to prevent disease progression in severe cases of WD defines a medical need for new therapies in WD.

### 4.1.2 The detrimental effect of mitochondrial copper overload in *Atp7b*$^{-/-}$ rats

With increasing mitochondrial copper load, mitochondrial membrane fluidity was progressively reduced at the lipid-water interface (TMA-DPH [230-232]), but not at the membrane inner-lipid-phase (DPH [230-232], Figure 3-5), thus specifically impairing the mitochondrial membrane surface [1]. This can be explained by increasing copper deposition to mitochondrial membrane proteins [1, 152]. Copper mediates the oxidation of cysteine residues, leading to the formation of stable disulfide bonds within [272] and crosslinks among proteins [152], thereby possibly reducing mitochondrial membrane fluidity.

The increasing mitochondrial copper load together with the reduced mitochondrial membrane fluidity impair the organelles ability to unfold their inner membrane upon elicitation of the cation-induced mitochondrial permeability transition (MPT; Figure 3-6, Figure 3-7) [1, 258]. Exposing mitochondria to cations, such as calcium or copper, leads to an increase of the mitochondrial inner membrane (MIM) permeability [236, 237, 240], allowing molecules and ions smaller than 1.5 kDa to enter the matrix [236, 238, 240]. The increasing ion concentration within the matrix, and the concomitant increased water influx, lead to matrix swelling [237, 241], MIM unfolding and finally to mitochondrial outer membrane permeabilisation (MOMP) and rupture [239, 241, 242]. The extent of swelling of mitochondria from *Atp7b*$^{-/-}$ rats was increasingly impaired with disease progression of these rats relative to mitochondria from heterozygous controls (Figure 3-6) [1]. Triggering copper-loaded liver mitochondria isolated from *Atp7b*$^{-/-}$ rats with 100 µM $Ca^{2+}$ has already been shown to reduce the extent of swelling [273]. Perhaps the massive copper deposition at the mitochondrial membrane surface inhibits mitochondria from undergoing the full extent of swelling upon the permeability transition [273]. Typically, a calcium-induced MPT can be efficiently blocked by cyclosporine A (CysA) [274], as this agent binds to cyclophilin D (CypD) [1, 260, 261, 275-277], preventing the opening of the mitochondrial permeability transition pore (MPTP, consisting of $F_O$ dimers of the ATP synthase and requiring inorganic phosphate; cyclophilin D binds to the $F_O$ subunit of the ATP synthase [278-280]) localised within the mitochondrial membranes [259, 260]. In *Atp7b*$^{-/-}$ rats, the ability of CysA to prevent MPT was reduced with disease progression of the rats [1]. Two explanations for this are that copper could crosslink CypD to the MPT pore or, it may instead bind to the CysA binding site of CypD [273]. Both possibilities would inhibit the binding of CysA to CypD and thus, MPT induction cannot be prevented [273]. In order to further explore the role of copper in MPT, future studies could distinguish between these possibilities.

Increasing copper deposition at mitochondrial membranes has biochemical consequences [1]. Liver mitochondria isolated from *Atp7b*$^{-/-}$ rats lost their MMP much earlier compared to mitochondria from *Atp7b*$^{+/-}$ control rats (Figure 3-8) [1]. A permeable MIM would impair electron transport via the mitochondrial electron transport chain [281]. Moreover, the formation of pores (MPTP) within the MIM would dissipate the proton gradient across the membrane [281, 282]. Both possibilities would reduce the mitochondrial transmembrane potential, leading to reduction of mitochondrial ATP production [281]. Hosseini *et al.* discussed that the oxidation of mitochondrial membranes leads to the disruption of the mitochondrial energy transfer chain, dissipation of the MMP and a reduction in mitochondrial ATP production [281]. Measurement of the mitochondrial respiration would answer the question of whether MIM becomes increasingly permeable due to copper overload [211]. However, Sokol *et al.* found that coupling of electron transport and ATP production is not affected in copper-loaded rat liver mitochondria, indicating that increasing mitochondrial copper load does not affect the permeability of the mitochondrial inner membrane [211]. Rather, it is more likely that the electron transport chain itself is impaired, possibly due to an altered structure or composition of the MIM [211]. The reduced MMP stability indicates impaired mitochondrial membrane integrity. The less stable MMP was paralleled by a decreased capacity of liver mitochondria isolated from *Atp7b*$^{-/-}$ rats to produce ATP (Figure 3-9) [1]. This relation increases with disease progression of *Atp7b*$^{-/-}$ rats [1]. This might be explained by an enforced interaction of copper with the adenine nucleotide transporter (ANT) located at the MIM [283, 284]. ANT has pairs of cysteine residues that have been shown to be attacked by copper [152, 283, 284]. Consequently, the exchange of ATP and ADP across the MIM would be impaired [109, 283, 285], leading to an imbalance of cytosolic energy consumption and mitochondrial energy formation [111, 112].

The presented results show that the structural and functional mitochondrial impairments progress with rising mitochondrial copper load and disease progression in LPP *Atp7b*$^{-/-}$ rats [1]. Consequently, a reduction of the mitochondrial copper load may recover the mitochondrial structure and function [1]. This might be achieved by compounds with a high affinity for copper, such as those discussed in detail in the next section.

## 4.2 Methanobactin – a highly efficient treatment prevents disease progression in a Wilson disease rat model

The second part of this thesis focused on the treatment of LPP *Atp7b*$^{-/-}$ rats with the bacterial peptide methanobactin (MB). This copper chelator has a much higher affinity for copper (>$10^{-21}$ M [209]) than mitochondrial copper-binding proteins in eukaryotic cells ($10^{-12}$–$10^{-15}$ M [138]), making this compound a strong candidate for treating WD [1].

### 4.2.1 Methanobactin efficiently decoppers HepG2 cells

The cellular toxicity of MB was compared to D-PA, TETA and TTM (Figure 3-10, Figure 3-11). 1 mM D-PA and TETA as well as 0.5 mM MB did not affect viability of HepG2 cells, whereas 0.5 mM TTM reduced cellular viability for approximately 50%, demonstrating that TTM is more toxic than the other tested copper chelators [1]. MB induced an intermediate reduction of the mitochondrial transmembrane potential after two hours of treatment, but this is reversed after six hours of treatment [1]. On the contrary, 50 µM TTM was not toxic in neutral red assay (Figure 3-10) but significantly impaired cytochrome c oxidase activity in isolated rat liver mitochondria [1] and several cell lines [286], and 10 µM TTM irreversibly impaired the MMP (Figure 3-11), confirming the higher toxicity of TTM compared to MB [1]. This could be explained by a higher affinity of TTM for copper, leading to the decoppering of the cytochrome c oxidase [287, 288] – the mitochondrial copper-dependent complex that maintains MMP [91, 95, 101, 114-126]. Moreover, TTM forms insoluble complexes with copper that could possibly be toxic [33, 188, 189]. In animals, due to its high copper affinity, TTM may even induce copper deficiency [287, 288].

For the evaluation of decoppering efficiency of the above mentioned copper chelators on copper preloaded HepG2 cells, the following non-toxic concentrations were used: 1 mM D-PA and TETA, 0.5 mM MB and 10 µM TTM. 0.5 mM MB significantly reduced cellular copper load for approximately 30% after 24 hours of treatment (Figure 3-12), whereas the other copper chelators did not significantly reduce the cellular copper load. These data are in agreement with the approximately 50% reduction in copper load in isolated *Atp7b*$^{-/-}$ or copper-preloaded control rat liver mitochondria using MB or TTM, whereas D-PA and TETA do not reduce the mitochondrial copper load [1]. In contrast to D-PA, TETA and TTM, MB reduced liver copper concentration on the whole organ level by about 25% [1]. During liver perfusion experiments in *Atp7b*$^{-/-}$ rats, MB-bound copper was excreted largely via the bile – the major physiological excretion route for copper [1]. D-PA and TETA direct copper to the urine [158, 175] and TTM leads to the formation of precipitates within the liver [33, 188, 189]. Thus, these results point to a superior therapeutic effect of MB versus other copper chelators towards an efficient decoppering associated with low toxicity and physiological copper excretion.

### 4.2.2 Short-term methanobactin treatment prevents acute liver failure in *Atp7b*$^{-/-}$ rats

To test for efficient decoppering of liver mitochondria via MB *in vivo*, the effects of short-term treatment were investigated in *Atp7b*$^{-/-}$ rats. Instead of the typical WD treatment regimen comprising long-term oral application of D-PA or TETA, a short-term treatment by repetitive MB i.p. injections was compared to the short oral treatment with D-PA and TETA (Figure 3-13 – Figure 3-15, Figure 3-17, Supplementary Table 2) [1]. Using this treatment procedure, MB reduced elevated liver damage markers (Figure 3-13, [1]), whereas short-term oral treatment with D-PA or TETA did not. This was paralleled by decreasing liver and mitochondrial copper loads in MB treated *Atp7b*$^{-/-}$ rats (Figure 3-14). For D-PA and TETA, no reduction of copper load was observed in liver homogenate, and in the respective mitochondria decoppering was 20% less compared to MB. In contrast to D-PA and TETA, decoppering of liver mitochondria isolated from MB treated *Atp7b*$^{-/-}$ rats was paralleled by an improvement in mitochondrial structure (Figure 3-15) and a recovery of mitochondrial ATP production

(Figure 3-17). These data show that the superior treatment effect of MB in *Atp7b*$^{-/-}$ rats aims to mitochondria.

In contrast to MB, D-PA or TETA treatment has to start prior to the onset of liver damage. But, is MB able to reduce liver damage in already diseased *Atp7b*$^{-/-}$ rats by improving decoppering efficiency? In a recent study, a very short systemic residence time of approximately 30 minutes of MB in the blood was found [1], allowing repeated daily i.p. injections of MB (twice daily for eight consecutive days; Figure 3-16). This enforced MB therapy caused a massive reduction of mitochondrial copper load for up to 85% (Supplementary Table 2). This was in parallel with an increase in body weight, a decrease in the liver damage markers serum AST and bilirubin as well as an improvement of the mitochondrial structure and biochemical function (ATP production; Figure 3-17).

This treatment approach is extremely promising for rescuing diseased *Atp7b*$^{-/-}$ rats with strongly elevated serum AST and bilirubin levels from acute liver failure by a rapid and efficient decoppering of liver mitochondria [1]. Short-term D-PA [152] and TETA treatments are not suitable for *Atp7b*$^{-/-}$ rats with increased liver damage markers (serum AST and bilirubin), as mitochondrial decoppering is ineffective. If diseased *Atp7b*$^{-/-}$ rats receive no treatment, they normally die within few days [1].

### 4.2.3 Methanobactin – a new treatment strategy to decopper liver mitochondria in Wilson disease

As short-term MB treatment efficiently decoppers liver mitochondria and prevents acute liver failure in *Atp7b*$^{-/-}$ rats, a new treatment strategy was analysed to answer the question of whether, and how long, MB can postpone the onset of liver failure in these rats [1]. *Atp7b*$^{-/-}$ rats were treated i.p. for five days with MB and subsequently observed for two to three weeks (Figure 3-18) [1]. MB reduced elevated serum AST levels. All rats remained healthy for at least two weeks, indicating delayed disease onset (Figure 3-18A) [1]. At the time of analysis, the disease state of these rats is reflected by serum AST, mitochondrial structure and copper load, but not at the whole liver copper load (Figure 3-18) [1]. The mitochondrial parameters copper concentration, structure and biochemical function cannot only serve as early markers for disease progression in *Atp7b*$^{-/-}$ rats, but also be used to monitore treatment efficiency and reoccurrence of liver damage after treatment of these rats (Figure 3-18) [1].

In an additional experiment, *Atp7b*$^{-/-}$ rats were treated with MB i.p. three times daily for five consecutive days and observed for three to seven weeks (Table 3-2) [1]. This treatment intermediately reduced the liver and mitochondrial copper load approximately fourfold (*Atp7b*$^{-/-}$ rat from pair 4) compared to the untreated *Atp7b*$^{-/-}$ rat (pair 1). Liver damage markers remained within the normal range (serum AST <200 U/L, serum bilirubin <0.5 mg/dl, all rats) [1]. Disease onset was postponed to an age greater than 166 days, meaning a doubling of the disease-free state in the *Atp7b*$^{-/-}$ rat [1].

Using bacterial siderophores for treatment of humans is not unknown, as shown by the use of desferrioxamine from *Streptomyces pilosus* [1, 289]. This agent is used for the treatment of iron intoxication [1, 289]. Methanobactin – produced by *Methylosinus trichosporium* OB3b – is another siderophore-like peptide [206, 208]. Its very high copper affinity of >$10^{-21}$ M [209] is much higher than that of copper-binding proteins in eukaryotic cells ($10^{-12}$–$10^{-15}$ M) [138]. Consequently, a short but intense decoppering treatment using MB might be a very promising therapeutic strategy against disease progression in WD [1].

## 4.3 COX17 – balancing the mitochondrial copper overload in Wilson disease

In the first part of this study, it was shown that the liver mitochondrial structure and function is increasingly impaired with disease progression of untreated LPP *Atp7b*$^{-/-}$ rats. The mitochondria can regulate their copper load up to approximately 7 nmol copper per mg mitochondrial protein [58]. At a late stage of liver damage (diseased *Atp7b*$^{-/-}$ rats), the mitochondrial copper load exceeds this concentration, leading to the break down of the mitochondrial structure and function. This raises the question how mitochondria balance elevated copper concentrations up to this threshold.

### 4.3.1 COX17 upregulation for the export of excess mitochondrial copper

In a previous study, copper has been shown to interact with thiol-containing membrane proteins, such as VDAC or ANT [152]. This may explain structural and functional alterations of rat liver mitochondria [152]. However, it remains unknown which proteins are involved in balancing elevated mitochondrial copper loads in WD. To address this question, liver mitochondria and copper-rich mitochondrial subfractions from *Atp7b*$^{+/-}$ and *Atp7b*$^{-/-}$ rats were proteomically analysed (Figure 3-19, Table 3-3). Around 400 mitochondrial proteins have been identified in the present analysis for quantitative comparison. For the identification of proteins involved in balancing elevated copper in WD, the following parameters were defined:

1) Proteins of interest were enriched during subfractionation and upregulated in fractions from *Atp7b*$^{-/-}$ rats compared to *Atp7b*$^{+/-}$ rats.

2) The proteins should have a function in copper metabolism to bind and detoxify excess copper in liver mitochondria from *Atp7b*$^{-/-}$ rats.

According to the first parameter, 14 mitochondrial proteins were enriched in all fractions with high copper load and in *Atp7b*$^{-/-}$ rats compared to *Atp7b*$^{+/-}$ rats (Table 3-3). For 13 of these proteins identified in the proteomic analysis, nothing is known to date regarding their involvement in copper ion binding. In WD, these proteins could have an additional function in copper metabolism, such as copper binding or crosslinking of proteins, containing sulfide residues.

Other mitochondrial proteins with a known function in copper ion binding are COX11, SCO1 and SOD1 [118, 120, 128, 131]. These proteins either presented with an increased or decreased abundance in one of the two copper-enriched fractions or showed no alteration (Supplementary Table 3), indicating that these proteins are not highly important in regulating mitochondrial copper overload in WD. But these proteins are important for maintaining the mitochondrial function as they are responsible for the final assembly of the CcO [118] and the antioxidative function of SOD1 [20].

Out of the 14 identified proteins, the copper chaperone COX17 was found to be the only protein with a known function in copper metabolism [11], suggesting that COX17 is a very important protein for balancing elevated copper loads in liver mitochondria in WD. Within the IMS, COX17 is partially oxidised, binds one copper ion between the two cysteine residues localised at the N-terminal domain [122, 135, 136, 290], and each four partially oxidised COX17 molecules build a tetramer [123, 136, 291, 292]. The higher abundance of COX17 in *Atp7b*$^{-/-}$ rats was confirmed on the level of isolated liver mitochondria using immunoblot analysis (Figure 3-20) and on the level of rat liver tissue using immunohistochemistry staining for COX17 (Figure 3-21, result received from Dr. Michaela Aichler and Dr. Annette Feuchtinger). COX17 amount increased in parallel with disease progression and rising mitochondrial copper loads of *Atp7b*$^{-/-}$ rats. The analysis of liver mitochondria from WD patients extended these results (Figure 3-20). Protein level of COX17 in untreated WD patients was comparable to diseased *Atp7b*$^{-/-}$ rats. WD patients that received unsuccessful D-PA treatment before liver transplantation displayed decreased COX17 comparable to the level of affected *Atp7b*$^{-/-}$ rats, which can be explained by reduced mitochondrial copper concentrations (Figure 3-1). A comparable scenario was found at the cell culture level. Treatment of human hepatocytes (HepG2 cells) with increasing Cu-His concentrations raises cellular copper load and COX17 amount to approximately 38- and threefold, respectively (Figure 3-24A, Figure 3-25A). Treating HepG2 cells with 15 µM Cu-His increased mitochondrial copper load approximately twelvefold (Figure 3-24B) and COX17 level approximately 2.5-fold compared to control cells (Figure 3-25B), being comparable to the levels of diseased *Atp7b*$^{-/-}$ rats (Figure 3-1, Figure 3-20). An increase in COX17 protein levels in copper-treated cells was not only detected in HepG2 cells (this study), but also in human umbilical vein endothelial cells (HUVEC) [293, 294]. A decrease in the copper load in HUVEC is paralleled by a decrease in COX17 protein level [294]. Thus, an increasing copper load in mitochondria from *Atp7b*$^{-/-}$ rats, WD patients and HepG2 and other cells is paralleled by elevated COX17 amounts. Consequently, increasing the amount of COX17 might be a mechanism by which mitochondria deal with rising copper loads. Possibly, due to mitochondrial copper accumulation, COX17 import into mitochondria increases. Within the mitochondria, two pathways for copper direction are feasible: First, copper is translocated into the matrix and bound to the copper ligand. Excess mitochondrial copper that is not needed for enzymatic activities is stepwise transferred back into the IMS, bound to COX17 and exported into the cytosol. As reported by Wang *et al.*, *COX17* knockdown leads to an increase in the mitochondrial copper load [137], promoting the hypothesis that COX17 is involved in copper export from the mitochondria to the cytosol [137]. Second, copper that is taken up into the IMS is directly bound to COX17. In both cases, COX17 would bind and thereby detoxify copper [58] that would otherwise induce oxidative damage. This hypothesis is supported by the result that liver mitochondria from affected and disease onset *Atp7b*$^{-/-}$ rats present with slight structural impairments compared to mitochondria from diseased *Atp7b*$^{-/-}$ rats, indicating that a mitochondrial copper load up to 7 nmol copper per mg mitochondrial protein [58] is balanced. When this mitochondrial copper load is exceeded, copper binding and export by COX17 might be saturated or failing, leading to massive mitochondrial impairments. Whereas copper load in liver homogenate is nearly identical among the three disease states from *Atp7b*$^{-/-}$ rats (approximately 1.2–1.4 µg copper per mg protein), mitochondrial copper load progressively increases (affected: 0.37 µg copper per mg protein, disease onset: 0.52 µg copper per mg protein, diseased: 1.24 µg copper per mg protein). This finding again emphasises the decisive role of the mitochondrial copper state for WD progression.

In this context, questions of further interest are:

1) How is COX17 translocated to the IMS? The unfolded cytosolic conformation of COX17 can be transported into the IMS via channels located in the MOM, probably by TOM complexes (translocase of the outer membrane) [122, 295]. The C-terminal IMS targeting signal (ITS) of COX17 interacts with MIA40 (mitochondrial intermembrane space import and assembly protein 40, CHCHD4) [296]. Binding between these two proteins leads to the formation of the inner disulfide bond of COX17, to a conformational change and folding, stabilising the first disulfide bond [297]. The formation of the outer disulfide bond leads to the final folding of COX17 and

the release from MIA40 [297]. The formation of the two disulfide bonds is paralleled by partial oxidation of COX17, retaining this protein within the IMS [123, 295]. This leads to the hypothesis that rising mitochondrial copper load as in WD leads to an upregulation of MIA40 to improve COX17 uptake into mitochondria. Indeed, the abundance of MIA40 was increased in proteomic analysis in copper-rich mitochondrial subfractions from *Atp7b*$^{-/-}$ rats compared to *Atp7b*$^{+/-}$ rats (Table 3-3), supporting the hypothesis of an increased uptake of COX17 into mitochondria. Increased amounts of MIA40 remain to be proved using other methods, such as immunoblot analysis of liver mitochondria or immunohistochemistry staining of liver tissue from *Atp7b*$^{-/-}$ rats. Alternatively, as shown in the present study, treatment of HepG2 cells with Cu-His increases mitochondrial copper load and COX17 levels. This model can further be used to analyse MIA40 expression on mRNA and protein level.

2) Electron-dense deposits were detected within the IMS of liver mitochondria from diseased *Atp7b*$^{-/-}$ rats (Figure 3-4, Figure 3-16, Figure 3-18). As the mitochondrial copper load was increased in these rats and COX17 is located within the IMS, these deposits are potentially copper-COX17 complexes. Moreover, a possible copper export function of COX17 [137] would support the hypothesis of copper-COX17 complexes within the IMS. This can be examined using immunogold antibodies [298] for COX17 and elemental analysis [299] for copper. Cells with COX17 overexpression and treated without and with copper could be analysed regarding such deposits and could confirm the theory of copper-COX17 complexes.
3) Is COX17 upregulation in copper-loaded mitochondria protective or damaging? This question was addressed in section 3.4 and is discussed in the next section.

### 4.3.2 Upregulation of *COX17* protects HepG2 cells towards Cu-His-induced damage

To analyse whether the increased mitochondrial COX17 abundance (due to increased mitochondrial copper load) is protective for mitochondria and cells, a cell culture model was established using copper-histidine (Cu-His) treated HepG2 cells. Using this cell culture model, *COX17* expression was down- and upregulated by genetic interference to analyse the susceptibility of these cells towards Cu-His.

*COX17* knockdown reduced proliferation and vitality of HepG2 cells at standard subcultivation conditions by 10–21% (Table 3-5). Downregulation of *COX17* increased the susceptibility of these cells towards millimolar Cu-His concentrations and 15 µM Cu-His impaired cellular proliferation by 37%. These results are in line with the finding that knockdown of *COX17* in several other organsims (yeast, HeLa cells) lead to proliferation impairments [11, 118, 124]. Most importantly, knockout of *COX17* in mice is embryonically lethal [116]. There are two possible reasons for these negative effects: First, COX17 is a copper-binding protein that is essential for the assembly of the copper-dependent cytochrome c oxidase (CcO) [116, 118-120, 123, 124]. Due to knockdown of *COX17*, CcO assembly and, as a result, mitochondrial respiration is impaired [11, 118, 124]. Second, due to Cu-His treatment, copper accumulates within mitochondria. As less COX17 is available in these knockdown cells, copper could not be removed from the mitochondria, leading to the production of reactive oxygen species promoting mitochondrial impairments [146, 148]. At present, no information is available about the mitochondrial copper load and function (complex IV activity, MMP stability, ATP production) in 15 µM Cu-His treated COX17- cells. Because of technical reasons (large amounts of transfection reagent are necessary to induce a 95% reduction of *COX17* expression in a low amount of HepG2 cells), mitochondria cannot be isolated from these minute amounts of cells in sufficient yield for downstream analyses.

HepG2 cells with upregulated *COX17* showed no altered sensitivity to 24 hour treatment with rising Cu-His concentrations compared to the empty vector control (Table 3-5). After 48 hours of treatment with 15 µM Cu-His, COX17+ cells presented with an improved vitality. These data strengthen the hypothesis that *COX17* upregulation protects mitochondria from copper overload. Copper toxicity is reduced by COX17, possibly by promoting export of excess copper from mitochondria or by stably binding excess copper. At standard cultivation conditions (no additional copper) cellular proliferation of COX17+ cells is improved. Beers *et al.* showed that due to COX17 overexpression, COX17 levels mainly increase in whole cells (approximately 100-fold) and to a small extent (approximately eightfold) in mitochondria [133, 300]. This leads to the following hypothesis: At standard subcultivation conditions, COX17 is upregulated in whole COX17+ cells. As mitochondria have a normal copper load, no additional COX17 and no COX17 mediated copper export is needed in mitochondria. Hence, COX17 just slightly increases in mitochondria to maintain CcO assembly and complex IV activity. If treating COX17+ cells with Cu-His, however, copper accumulates in mitochondria, leading to a redistribution of COX17 from the cytosol to the IMS. In this case, COX17 could export excess copper from the mitochondria, protecting them towards copper-induced damages or just bind this excess copper. In the present work, mitochondrial COX17 amount was not analysed in COX17+ cells, as large amounts of transfection reagent are necessary to increase COX17 abundance. As COX17 has two distinct loci [11, 133, 139], in future experiments, the localisation of COX17 could be analysed in COX17+ cells with normal copper load, to clarify the question of whether COX17 is more located in the cellular cytosol or within the mitochondria in COX17+

cells. This can be done using tagged COX17, e.g. biotin tags, or antibodies against COX17 [133]. Cellular and mitochondrial copper load as well as mitochondrial functions, such as ATP production and MMP stability, could also be analysed in HepG2 cells with *COX17* overexpression.

In conclusion, knockdown and knockout of *COX17* has life threating effects in yeast, several human cell lines and mice upon elevated copper exposure [11, 116, 118-120, 123, 124]. These studies as well as the fact that this protein is evolutionary conserved [121] and expressed in all tissues (whereby regulation of expression is tissue-dependent) [301], indicate an essential function of COX17 in all organsims to regulate mitochondrial copper. Further, increased COX17 abundance has a protective effect towards cellular copper challenges by a copper-chelating function and possibly by copper export from mitochondria to the cytosol.

### 4.3.3 Possible interaction partners of COX17 in Wilson disease are involved in maintaining the mitochondrial structure and energy production

Several interaction partners of COX17, e.g. MIA40, are known [295, 296, 302-305]. As COX17 was upregulated in *Atp7b*$^{-/-}$ rat liver mitochondria, it is of interest to determine whether the profile of interaction partners changes upon mitochondrial copper accumulation. Using liver mitochondria isolated from *Atp7b*$^{+/-}$ and diseased *Atp7b*$^{-/-}$ rats, immunoprecipitation [306] of endogenous COX17 followed by proteomic analysis was performed. The proteins ACAD11 and CHCHD6 (MIC25) were identified as enriched mitochondrial interaction partners of COX17 in copper-burdened *Atp7b*$^{-/-}$ rat liver mitochondria (Figure 3-22C). This enhanced interaction of COX17 with ACAD11 and CHCHD6 may possibly lead to an activity change of ACAD11 and CHCHD6, due to a potential mislocalisation or diminished enzymatic activity of these proteins.

An impaired function of ACAD11 reduces fatty acid degradation [307], leading to fat accumulation and steatosis and as a consequence to reduced fatty acid biosynthesis. In agreement, steatosis is frequently observed in WD patients [148]. For future studies, it remains to determine whether an enhanced binding of ACAD11 to COX17 is causative for an altered lipid metabolism in copper-burdened *Atp7b*$^{-/-}$ rat liver mitochondria.

CHCHD6 (MIC25) shows an increased interaction with COX17 in *Atp7b*$^{-/-}$ compared to *Atp7b*$^{+/-}$ rat liver mitochondria. CHCHD6 is part of the mitochondrial contact site and cristae organisation system (MICOS complex) [267, 268]. MICOS is responsible for maintaining the structure of the MIM [142]. Knockdown of CHCHD6 has been shown to induce severe defects in mitochondrial cristae organisation and mitochondrial structure and function [267]. Thus, the enhanced interaction of COX17 and CHCHD6 in *Atp7b*$^{-/-}$ rat liver mitochondria could possibly participate in the observed mitochondrial structural changes upon increasing copper load. Future studies have to validate these hypotheses.

# 5 Conclusions

In this thesis, similar copper loads and structural alterations in liver mitochondria from LPP *Atp7b*$^{-/-}$ rats and human Wilson disease (WD) patients present the *Atp7b*$^{-/-}$ rat as a valid animal model to further analyse mitochondrial impairments in WD. The increasing liver damage markers aspartate aminotransferase and bilirubin define progressing disease states in *Atp7b*$^{-/-}$ rats during which ongoing alterations in the mitochondrial structure, membranes and function can be observed – parameters that are altered in parallel with rising mitochondrial copper loads. Therefore, the prime requirement for an effective treatment of WD is to reduce the mitochondrial copper load by using copper chelating agents.

In 10–50% of WD patients, despite the lifelong treatment with D-penicillamine (D-PA) or trientine (TETA), decoppering of liver mitochondria is ineffective. To optimise mitochondrial decoppering, agents are necessary that have a higher copper affinity than D-PA or TETA. Very promising is the bacterial peptide methanobactin (MB) – produced by *Methylosinus trichosporium* OB3b. Using MB, mitochondrial copper load, structure and function are reversed in *Atp7b*$^{-/-}$ rats more efficiently than using D-PA or TETA. MB is suitable for short, intense treatment cycles during which the mitochondrial copper load is reduced which lasts several weeks. *Atp7b*$^{-/-}$ rats received dosages of 150 mg MB/kg bw, meaning about 24 mg/kg bw in adult WD patients [1, 308]. A similar dosage of desferrioxamine – a bacterial peptide from *Streptomyces pilosus* – is used in patients with iron intoxication [1, 289]. Hence MB could be another candidate in this pharmaceutical class and could be the drug of choice for a more efficient and patient-side treatment of WD [1].

In *Atp7b*$^{-/-}$ rat liver mitochondria, copper load increases with disease progression. Mitochondrial structure and function break down if the copper load exceeds approximately 7 nmol copper per mg mitochondrial protein. Thus, the question is how mitochondria deal with elevated copper loads below this treshold. Proteomic analyses of rat liver mitochondria identified the copper-binding protein COX17 to be upregulated in *Atp7b*$^{-/-}$ rats compared to *Atp7b*$^{+/-}$ rats. COX17 increases in parallel with rising mitochondrial copper loads. Increasing mitochondrial copper loads and COX17 amounts are simulated by treating HepG2 cells with copper-histidine (Cu-His). Knockdown of *COX17* in these cells increases cellular susceptibility towards Cu-His, whereas cells with upregulated *COX17* are less sensitive towards Cu-His, presenting COX17 upregulation to be protective for rising mitochondrial copper load. These data highlight a new mechanism by which liver mitochondria deal with elevated copper loads in HepG2 cells and the WD *Atp7b*$^{-/-}$ rat model.

# 6 References

1. Lichtmannegger, J., et al., *Methanobactin reverses acute liver failure in a rat model of Wilson disease.* J Clin Invest, 2016. **126**(7): p. 2721-35.
2. Ahmed, S., J. Deng, and J. Borjigin, *A new strain of rat for functional analysis of PINA.* Brain Res Mol Brain Res, 2005. **137**(1-2): p. 63-9.
3. Wilson, S.K., *Progressive lenticular degeneration: a familial nervous disease associated with cirrhosis of the liver.* Brain, 1912. **34**: p. 295-507.
4. Bearn, A.G., *Genetic and biochemical aspects of Wilson's disease.* Am J Med, 1953. **15**(4): p. 442-9.
5. Cumings, J.N., *The copper and iron content of brain and liver in the normal and in hepato-lenticular degeneration.* Brain, 1948. **71**(Pt. 4): p. 410-5.
6. Hart, E.B., et al., *Iron in nutrition VII. Copper as a supplement to iron for hemoglobin building in the rat.* Journal of Biological Chemistry, 1928. **77**(2): p. 797--833.
7. Schroeder, H.A., et al., *Essential trace metals in man: copper.* J Chronic Dis, 1966. **19**(9): p. 1007-34.
8. Vander Wende, C. and W.W. Wainio, *The state of the copper in cytochrome c oxidase.* J Biol Chem, 1960. **235**: p. PC11-2.
9. McCord, J.M. and I. Fridovich, *Superoxide dismutase. An enzymic function for erythrocuprein (hemocuprein).* J Biol Chem, 1969. **244**(22): p. 6049-55.
10. Palida, F.A., et al., *Cytosolic copper-binding proteins in rat and mouse hepatocytes incubated continuously with Cu(II).* Biochem J, 1990. **268**(2): p. 359-66.
11. Glerum, D.M., A. Shtanko, and A. Tzagoloff, *Characterization of COX17, a yeast gene involved in copper metabolism and assembly of cytochrome oxidase.* J Biol Chem, 1996. **271**(24): p. 14504-9.
12. Klomp, L.W., et al., *Identification and functional expression of HAH1, a novel human gene involved in copper homeostasis.* J Biol Chem, 1997. **272**(14): p. 9221-6.
13. Rae, T.D., et al., *Undetectable intracellular free copper: the requirement of a copper chaperone for superoxide dismutase.* Science, 1999. **284**(5415): p. 805-8.
14. Roelofsen, H., et al., *Copper-induced apical trafficking of ATP7B in polarized hepatoma cells provides a mechanism for biliary copper excretion.* Gastroenterology, 2000. **119**(3): p. 782-93.
15. Yamada, H. and K.T. Yasunobu, *Monoamine oxidase. II. Copper, one of the prosthetic groups of plasma monoamine oxidase.* J Biol Chem, 1962. **237**: p. 3077-82.
16. Friedman, S. and S. Kaufman, *3,4-dihydroxyphenylethylamine beta-hydroxylase. Physical properties, copper content, and role of copper in the catalytic acttivity.* J Biol Chem, 1965. **240**(12): p. 4763-73.
17. Friedman, S. and S. Kaufman, *3,4-Dihydroxyphenylethylamine Beta-Hydroxylase: A Copper Protein.* J Biol Chem, 1965. **240**: p. PC552-4.
18. Gaetke, L.M. and C.K. Chow, *Copper toxicity, oxidative stress, and antioxidant nutrients.* Toxicology, 2003. **189**(1-2): p. 147-63.
19. Zaba, B.N. and E.J. Harris, *Uptake and effects of copper in rat liver mitochondria.* Biochem J, 1976. **160**(3): p. 707-14.
20. Fujimura, M., et al., *The cytosolic antioxidant copper/zinc-superoxide dismutase prevents the early release of mitochondrial cytochrome c in ischemic brain after transient focal cerebral ischemia in mice.* J Neurosci, 2000. **20**(8): p. 2817-24.
21. Palacios-Callender, M., et al., *Cytochrome c oxidase maintains mitochondrial respiration during partial inhibition by nitric oxide.* J Cell Sci, 2007. **120**(Pt 1): p. 160-5.

22. Li, Y., et al., *Cytochrome c oxidase subunit IV is essential for assembly and respiratory function of the enzyme complex.* J Bioenerg Biomembr, 2006. **38**(5-6): p. 283-91.
23. King, J.C., W.L. Raynolds, and S. Margen, *Absorption of stable isotopes of iron, copper, and zinc during oral contraceptives use.* Am J Clin Nutr, 1978. **31**(7): p. 1198-203.
24. Johnson, P.E., D.B. Milne, and G.I. Lykken, *Effects of age and sex on copper absorption, biological half-life, and status in humans.* Am J Clin Nutr, 1992. **56**(5): p. 917-25.
25. Pena, M.M., J. Lee, and D.J. Thiele, *A delicate balance: homeostatic control of copper uptake and distribution.* J Nutr, 1999. **129**(7): p. 1251-60.
26. Vancampen, D.R. and E.A. Mitchell, *Absorption of Cu-64, Zn-65, Mo-99, and Fe-59 from Ligated Segments of the Rat Gastrointestinal Tract.* J Nutr, 1965. **86**: p. 120-4.
27. Crampton, R.F., D.M. Matthews, and R. Poisner, *Observations on the Mechanism of Absorption of Copper by the Small Intestine.* J Physiol, 1965. **178**: p. 111-26.
28. Gubler, C.J., et al., *Studies on copper metabolism. IX. The transportation of copper in blood.* J Clin Invest, 1953. **32**(5): p. 405-14.
29. Neumann, P.Z. and A. Sass-Kortsak, *The state of copper in human serum: evidence for an amino acid-bound fraction.* J Clin Invest, 1967. **46**(4): p. 646-58.
30. Sarkar, B. and Y. Wigfield, *Evidence for albumin--cu(II)--amino acid ternary complex.* Can J Biochem, 1968. **46**(6): p. 601-7.
31. Nose, Y., B.E. Kim, and D.J. Thiele, *Ctr1 drives intestinal copper absorption and is essential for growth, iron metabolism, and neonatal cardiac function.* Cell Metab, 2006. **4**(3): p. 235-44.
32. Delgado, M., et al., *Early effects of copper accumulation on methionine metabolism.* Cell Mol Life Sci, 2008. **65**(13): p. 2080-90.
33. Roberts, E.A., M.L. Schilsky, and D. American Association for Study of Liver, *Diagnosis and treatment of Wilson disease: an update.* Hepatology, 2008. **47**(6): p. 2089-111.
34. Gitlin, J.D., *Wilson disease.* Gastroenterology, 2003. **125**(6): p. 1868-77.
35. Petris, M.J., et al., *Copper-stimulated endocytosis and degradation of the human copper transporter, hCtr1.* J Biol Chem, 2003. **278**(11): p. 9639-46.
36. Klomp, A.E., et al., *The N-terminus of the human copper transporter 1 (hCTR1) is localized extracellularly, and interacts with itself.* Biochem J, 2003. **370**(Pt 3): p. 881-9.
37. Pushie, M.J., et al., *Model Peptide Studies Reveal a Mixed Histidine-Methionine Cu(I) Binding Site at the N-Terminus of Human Copper Transporter 1.* Inorg Chem, 2015. **54**(17): p. 8544-51.
38. Hassett, R. and D.J. Kosman, *Evidence for Cu(II) reduction as a component of copper uptake by Saccharomyces cerevisiae.* J Biol Chem, 1995. **270**(1): p. 128-34.
39. Hamza, I., et al., *Interaction of the copper chaperone HAH1 with the Wilson disease protein is essential for copper homeostasis.* Proc Natl Acad Sci U S A, 1999. **96**(23): p. 13363-8.
40. Larin, D., et al., *Characterization of the interaction between the Wilson and Menkes disease proteins and the cytoplasmic copper chaperone, HAH1p.* J Biol Chem, 1999. **274**(40): p. 28497-504.
41. Wernimont, A.K., et al., *Structural basis for copper transfer by the metallochaperone for the Menkes/Wilson disease proteins.* Nat Struct Biol, 2000. **7**(9): p. 766-71.
42. Lin, S.J., et al., *A role for the Saccharomyces cerevisiae ATX1 gene in copper trafficking and iron transport.* J Biol Chem, 1997. **272**(14): p. 9215-20.

43. Lorinczi, E., et al., *Delivery of the Cu-transporting ATPase ATP7B to the plasma membrane in Xenopus oocytes.* Biochim Biophys Acta, 2008. **1778**(4): p. 896-906.
44. Gollan, J.L. and T.J. Gollan, *Wilson disease in 1998: genetic, diagnostic and therapeutic aspects.* J Hepatol, 1998. **28 Suppl 1**: p. 28-36.
45. Tao, T.Y. and J.D. Gitlin, *Hepatic copper metabolism: insights from genetic disease.* Hepatology, 2003. **37**(6): p. 1241-7.
46. Das, S.K. and K. Ray, *Wilson's disease: an update.* Nat Clin Pract Neurol, 2006. **2**(9): p. 482-93.
47. Polishchuk, E.V., et al., *Wilson disease protein ATP7B utilizes lysosomal exocytosis to maintain copper homeostasis.* Dev Cell, 2014. **29**(6): p. 686-700.
48. Luza, S.C. and H.C. Speisky, *Liver copper storage and transport during development: implications for cytotoxicity.* Am J Clin Nutr, 1996. **63**(5): p. 812S-20S.
49. Gross, J.B., Jr., et al., *Biliary copper excretion by hepatocyte lysosomes in the rat. Major excretory pathway in experimental copper overload.* J Clin Invest, 1989. **83**(1): p. 30-9.
50. Bull, P.C., et al., *The Wilson disease gene is a putative copper transporting P-type ATPase similar to the Menkes gene.* Nat Genet, 1993. **5**(4): p. 327-37.
51. Tanzi, R.E., et al., *The Wilson disease gene is a copper transporting ATPase with homology to the Menkes disease gene.* Nat Genet, 1993. **5**(4): p. 344-50.
52. Yamaguchi, Y., M.E. Heiny, and J.D. Gitlin, *Isolation and characterization of a human liver cDNA as a candidate gene for Wilson disease.* Biochem Biophys Res Commun, 1993. **197**(1): p. 271-7.
53. Petrukhin, K., et al., *Characterization of the Wilson disease gene encoding a P-type copper transporting ATPase: genomic organization, alternative splicing, and structure/function predictions.* Hum Mol Genet, 1994. **3**(9): p. 1647-56.
54. Thomas, G.R., et al., *The Wilson disease gene: spectrum of mutations and their consequences.* Nat Genet, 1995. **9**(2): p. 210-7.
55. Purchase, R., *The link between copper and Wilson's disease.* Sci Prog, 2013. **96**(Pt 3): p. 213-23.
56. Huster, D., *Wilson disease.* Best Pract Res Clin Gastroenterol, 2010. **24**(5): p. 531-9.
57. Cope-Yokoyama, S., et al., *Wilson disease: histopathological correlations with treatment on follow-up liver biopsies.* World J Gastroenterol, 2010. **16**(12): p. 1487-94.
58. Zischka, H. and J. Lichtmannegger, *Pathological mitochondrial copper overload in livers of Wilson's disease patients and related animal models.* Ann N Y Acad Sci, 2014. **1315**: p. 6-15.
59. Gu, M., et al., *Oxidative-phosphorylation defects in liver of patients with Wilson's disease.* Lancet, 2000. **356**(9228): p. 469-74.
60. Porter, H., *Tissue Copper Proteins in Wilson's Disease. Intracellular Distribution and Chromatographic Fractionation.* Arch Neurol, 1964. **11**: p. 341-9.
61. Frommer, D.J., *Defective biliary excretion of copper in Wilson's disease.* Gut, 1974. **15**(2): p. 125-9.
62. Bowcock, A.M., et al., *Eight closely linked loci place the Wilson disease locus within 13q14-q21.* Am J Hum Genet, 1988. **43**(5): p. 664-74.
63. Roche-Sicot, J. and J.P. Benhamou, *Acute intravascular hemolysis and acute liver failure associated as a first manifestation of Wilson's disease.* Ann Intern Med, 1977. **86**(3): p. 301-3.
64. Schilsky, M.L., I.H. Scheinberg, and I. Sternlieb, *Prognosis of Wilsonian chronic active hepatitis.* Gastroenterology, 1991. **100**(3): p. 762-7.
65. Weiss, K.H. and W. Stremmel, *Evolving perspectives in Wilson disease: diagnosis, treatment and monitoring.* Curr Gastroenterol Rep, 2012. **14**(1): p. 1-7.

66. European Association for Study of, L., *EASL Clinical Practice Guidelines: Wilson's disease.* J Hepatol, 2012. **56**(3): p. 671-85.
67. Starosta-Rubinstein, S., et al., *Clinical assessment of 31 patients with Wilson's disease. Correlations with structural changes on magnetic resonance imaging.* Arch Neurol, 1987. **44**(4): p. 365-70.
68. Aisen, A.M., et al., *Wilson disease of the brain: MR imaging.* Radiology, 1985. **157**(1): p. 137-41.
69. van Wassenaer-van Hall, H.N., et al., *Wilson disease: findings at MR imaging and CT of the brain with clinical correlation.* Radiology, 1996. **198**(2): p. 531-6.
70. Sternlieb, I., *Mitochondrial and fatty changes in hepatocytes of patients with Wilson's disease.* Gastroenterology, 1968. **55**(3): p. 354-67.
71. Sokol, R.J., et al., *Oxidant injury to hepatic mitochondrial lipids in rats with dietary copper overload. Modification by vitamin E deficiency.* Gastroenterology, 1990. **99**(4): p. 1061-71.
72. Sternlieb, I. and G. Feldmann, *Effects of anticopper therapy on hepatocellular mitochondria in patients with Wilson's disease: an ultrastructural and stereological study.* Gastroenterology, 1976. **71**(3): p. 457-61.
73. Mansouri, A., et al., *Premature oxidative aging of hepatic mitochondrial DNA in Wilson's disease.* Gastroenterology, 1997. **113**(2): p. 599-605.
74. Altmann, R., *Die elementarorganismen und ihre beziehungen zu den zellen*1890, Leipzig,: Veit & comp. 4 p.l., 145 p.
75. Palade, G.E., *The fine structure of mitochondria.* Anat Rec, 1952. **114**(3): p. 427-51.
76. Karnkowska, A., et al., *A Eukaryote without a Mitochondrial Organelle.* Curr Biol, 2016. **26**(10): p. 1274-84.
77. Mereschkowsky, C., *Über Natur und Ursprung der Chromatophoren im Pflanzenreiche*1905.
78. Whatley, F.R., *The establishment of mitochondria: Paracoccus and Rhodopseudomonas.* Ann N Y Acad Sci, 1981. **361**: p. 330-40.
79. Freeman, J.A., *THE ULTRASTRUCTURE OF THE DOUBLE MEMBRANE SYSTEMS OF MITOCHONDRIA.* J Biophys Biochem Cytol, 1956. **2**(4): p. 353-354.
80. Dempsey, E.W., *Variations in the structure of mitochondria.* J Biophys Biochem Cytol, 1956. **2**(4 Suppl): p. 305-12.
81. Palade, G.E., *An electron microscope study of the mitochondrial structure.* J Histochem Cytochem, 1953. **1**(4): p. 188-211.
82. Zick, M., R. Rabl, and A.S. Reichert, *Cristae formation-linking ultrastructure and function of mitochondria.* Biochim Biophys Acta, 2009. **1793**(1): p. 5-19.
83. Hackenbrock, C.R., *Ultrastructural bases for metabolically linked mechanical activity in mitochondria. I. Reversible ultrastructural changes with change in metabolic steady state in isolated liver mitochondria.* J Cell Biol, 1966. **30**(2): p. 269-97.
84. Colombini, M., *Structure and mode of action of a voltage dependent anion-selective channel (VDAC) located in the outer mitochondrial membrane.* Ann N Y Acad Sci, 1980. **341**: p. 552-63.
85. Berthet, J., et al., *Tissue fractionation studies. II. The nature of the linkage between acid phosphatase and mitochondria in rat-liver tissue.* Biochem J, 1951. **50**(2): p. 182-9.
86. Werkheiser, W.C. and W. Bartley, *The study of steady-state concentrations of internal solutes of mitochondria by rapid centrifugal transfer to a fixation medium.* Biochem J, 1957. **66**(1): p. 79-91.
87. O'Brien, R.L. and G. Brierley, *Compartmentation of heart mitochondria. I. Permeability characteristics of isolated beef heart mitochondria.* J Biol Chem, 1965. **240**(11): p. 4527-31.
88. Pfaff, E., et al., *[Correlation of the unspecific permeable mitochondrial space with the "intermembrane space"].* Eur J Biochem, 1968. **5**(2): p. 222-32.

89. Colombini, M., *A candidate for the permeability pathway of the outer mitochondrial membrane.* Nature, 1979. **279**(5714): p. 643-5.
90. Zalman, L.S., H. Nikaido, and Y. Kagawa, *Mitochondrial outer membrane contains a protein producing nonspecific diffusion channels.* J Biol Chem, 1980. **255**(5): p. 1771-4.
91. Mitchell, P., *Coupling of phosphorylation to electron and hydrogen transfer by a chemi-osmotic type of mechanism.* Nature, 1961. **191**: p. 144-8.
92. Glynn, I.M., *Involvement of a membrane potential in the synthesis of ATP by mitochondria.* Nature, 1967. **216**(5122): p. 1318-9.
93. Kennedy, E.P. and A.L. Lehninger, *Oxidation of fatty acids and tricarboxylic acid cycle intermediates by isolated rat liver mitochondria.* J Biol Chem, 1949. **179**(2): p. 957-72.
94. Schneider, W.C. and V.R. Potter, *Intracellular distribution of enzymes; the distribution of oxalacetic oxidase activity in rat liver and rat kidney fractions.* J Biol Chem, 1949. **177**(2): p. 893-903.
95. Lehninger, A.L., *Water uptake and extrusion by mitochondria in relation to oxidative phosphorylation.* Physiol Rev, 1962. **42**: p. 467-517.
96. Gazmuri, R.J. and J. Radhakrishnan, *Protecting mitochondrial bioenergetic function during resuscitation from cardiac arrest.* Crit Care Clin, 2012. **28**(2): p. 245-70.
97. Guidotti, G., *Membrane proteins.* Annu Rev Biochem, 1972. **41**: p. 731-52.
98. Comte, J., B. Maisterrena, and D.C. Gautheron, *Lipid composition and protein profiles of outer and inner membranes from pig heart mitochondria. Comparison with microsomes.* Biochim Biophys Acta, 1976. **419**(2): p. 271-84.
99. Capaldi, R.A., *Arrangement of proteins in the mitochondrial inner membrane.* Biochim Biophys Acta, 1982. **694**(3): p. 291-306.
100. Hatefi, Y., et al., *Studies on the electron transport system. XVI. Enzymic oxidoreduction reactions of coenzyme Q.* Biochim Biophys Acta, 1959. **31**(2): p. 490-501.
101. Trumpower, B.L. and R.B. Gennis, *Energy transduction by cytochrome complexes in mitochondrial and bacterial respiration: the enzymology of coupling electron transfer reactions to transmembrane proton translocation.* Annu Rev Biochem, 1994. **63**: p. 675-716.
102. Wikstrom, M., *Two protons are pumped from the mitochondrial matrix per electron transferred between NADH and ubiquinone.* FEBS Lett, 1984. **169**(2): p. 300-4.
103. Cecchini, G., *Function and structure of complex II of the respiratory chain.* Annu Rev Biochem, 2003. **72**: p. 77-109.
104. Hatefi, Y., *The mitochondrial electron transport and oxidative phosphorylation system.* Annu Rev Biochem, 1985. **54**: p. 1015-69.
105. Nicholls, D.G. and V.S. Bernson, *Inter-relationships between proton electrochemical gradient, adenine-nucleotide phosphorylation potential and respiration, during substrate-level and oxidative phosphorylation by mitochondria from brown adipose tissue of cold-adapted guinea-pigs.* Eur J Biochem, 1977. **75**(2): p. 601-12.
106. Nicholls, D.G. and M.W. Ward, *Mitochondrial membrane potential and neuronal glutamate excitotoxicity: mortality and millivolts.* Trends Neurosci, 2000. **23**(4): p. 166-74.
107. Xu, T., V. Pagadala, and D.M. Mueller, *Understanding structure, function, and mutations in the mitochondrial ATP synthase.* Microb Cell, 2015. **2**(4): p. 105-125.
108. Riccio, P., H. Aquila, and M. Klingenberg, *Purification of the carboxy-atractylate binding protein from mitochondria.* FEBS Lett, 1975. **56**(1): p. 133-8.
109. Babot, M., et al., *The transmembrane prolines of the mitochondrial ADP/ATP carrier are involved in nucleotide binding and transport and its biogenesis.* J Biol Chem, 2012. **287**(13): p. 10368-78.

110. Mandel, L.J., *Primary active sodium transport, oxygen consumption, and ATP: coupling and regulation.* Kidney Int, 1986. **29**(1): p. 3-9.
111. Wallimann, T., et al., *Intracellular compartmentation, structure and function of creatine kinase isoenzymes in tissues with high and fluctuating energy demands: the 'phosphocreatine circuit' for cellular energy homeostasis.* Biochem J, 1992. **281 ( Pt 1)**: p. 21-40.
112. Brdiczka, D.G., D.B. Zorov, and S.-S. Sheu, *Mitochondrial contact sites: Their role in energy metabolism and apoptosis.* Biochimica et Biophysica Acta (BBA) - Molecular Basis of Disease, 2006. **1762**(2): p. 148-163.
113. Kim, H.J., et al., *Structure, function, and assembly of heme centers in mitochondrial respiratory complexes.* Biochim Biophys Acta, 2012. **1823**(9): p. 1604-16.
114. Amaravadi, R., D.M. Glerum, and A. Tzagoloff, *Isolation of a cDNA encoding the human homolog of COX17, a yeast gene essential for mitochondrial copper recruitment.* Hum Genet, 1997. **99**(3): p. 329-33.
115. Culotta, V.C., et al., *The copper chaperone for superoxide dismutase.* J Biol Chem, 1997. **272**(38): p. 23469-72.
116. Takahashi, Y., et al., *Mammalian copper chaperone Cox17p has an essential role in activation of cytochrome C oxidase and embryonic development.* Mol Cell Biol, 2002. **22**(21): p. 7614-21.
117. Wintz, H. and C. Vulpe, *Plant copper chaperones.* Biochem Soc Trans, 2002. **30**(4): p. 732-5.
118. Horng, Y.C., et al., *Specific copper transfer from the Cox17 metallochaperone to both Sco1 and Cox11 in the assembly of yeast cytochrome C oxidase.* J Biol Chem, 2004. **279**(34): p. 35334-40.
119. Kako, K., et al., *A selective requirement for copper-dependent activation of cytochrome c oxidase by Cox17p.* Biochem Biophys Res Commun, 2004. **324**(4): p. 1379-85.
120. Leary, S.C., et al., *Human SCO1 and SCO2 have independent, cooperative functions in copper delivery to cytochrome c oxidase.* Hum Mol Genet, 2004. **13**(17): p. 1839-48.
121. Palumaa, P., et al., *Metal-binding mechanism of Cox17, a copper chaperone for cytochrome c oxidase.* Biochem J, 2004. **382**(Pt 1): p. 307-14.
122. Arnesano, F., et al., *Folding studies of Cox17 reveal an important interplay of cysteine oxidation and copper binding.* Structure, 2005. **13**(5): p. 713-22.
123. Voronova, A., et al., *Oxidative switches in functioning of mammalian copper chaperone Cox17.* Biochem J, 2007. **408**(1): p. 139-48.
124. Oswald, C., U. Krause-Buchholz, and G. Rodel, *Knockdown of human COX17 affects assembly and supramolecular organization of cytochrome c oxidase.* J Mol Biol, 2009. **389**(3): p. 470-9.
125. Bombelka, E., et al., *Analysis of the Cu, Fe, and Zn contents in cytochrome C oxidases from different species and tissues by proton-induced X-ray emission (PIXE).* Biochem Biophys Res Commun, 1986. **140**(3): p. 1007-14.
126. Kaim, W. and J. Rall, *Copper—A “Modern” Bioelement.* Angewandte Chemie International Edition in English, 1996. **35**(1): p. 43-60.
127. Steffens, G.C., R. Biewald, and G. Buse, *Cytochrome c oxidase is a three-copper, two-heme-A protein.* Eur J Biochem, 1987. **164**(2): p. 295-300.
128. Cobine, P.A., F. Pierrel, and D.R. Winge, *Copper trafficking to the mitochondrion and assembly of copper metalloenzymes.* Biochim Biophys Acta, 2006. **1763**(7): p. 759-72.
129. Hill, B.C. and C. Greenwood, *The reaction of fully reduced cytochrome c oxidase with oxygen studied by flow-flash spectrophotometry at room temperature. Evidence for new pathways of electron transfer.* Biochem J, 1984. **218**(3): p. 913-21.

130. Wilson, D.F. and S.A. Vinogradov, *Mitochondrial cytochrome c oxidase: mechanism of action and role in regulating oxidative phosphorylation.* J Appl Physiol (1985), 2014. **117**(12): p. 1431-9.
131. Leary, S.C., et al., *Human SCO2 is required for the synthesis of CO II and as a thiol-disulphide oxidoreductase for SCO1.* Hum Mol Genet, 2009. **18**(12): p. 2230-40.
132. Hiser, L., et al., *Cox11p is required for stable formation of the Cu(B) and magnesium centers of cytochrome c oxidase.* J Biol Chem, 2000. **275**(1): p. 619-23.
133. Beers, J., D.M. Glerum, and A. Tzagoloff, *Purification, characterization, and localization of yeast Cox17p, a mitochondrial copper shuttle.* J Biol Chem, 1997. **272**(52): p. 33191-6.
134. Abajian, C., et al., *Yeast cox17 solution structure and Copper(I) binding.* J Biol Chem, 2004. **279**(51): p. 53584-92.
135. Banci, L., et al., *Functional role of two interhelical disulfide bonds in human Cox17 protein from a structural perspective.* J Biol Chem, 2011. **286**(39): p. 34382-90.
136. Banci, L., et al., *A structural-dynamical characterization of human Cox17.* J Biol Chem, 2008. **283**(12): p. 7912-20.
137. Wang, B., D. Dong, and Y.J. Kang, *Copper chaperone for superoxide dismutase-1 transfers copper to mitochondria but does not affect cytochrome c oxidase activity.* Exp Biol Med (Maywood), 2013. **238**(9): p. 1017-23.
138. Banci, L., et al., *Affinity gradients drive copper to cellular destinations.* Nature, 2010. **465**(7298): p. 645-8.
139. Cobine, P.A., et al., *Yeast contain a non-proteinaceous pool of copper in the mitochondrial matrix.* J Biol Chem, 2004. **279**(14): p. 14447-55.
140. Cobine, P.A., et al., *Mitochondrial matrix copper complex used in metallation of cytochrome oxidase and superoxide dismutase.* J Biol Chem, 2006. **281**(48): p. 36552-9.
141. Leary, S.C., D.R. Winge, and P.A. Cobine, *"Pulling the plug" on cellular copper: the role of mitochondria in copper export.* Biochim Biophys Acta, 2009. **1793**(1): p. 146-53.
142. Chojnacka, M., et al., *Cox17 Protein Is an Auxiliary Factor Involved in the Control of the Mitochondrial Contact Site and Cristae Organizing System.* J Biol Chem, 2015. **290**(24): p. 15304-12.
143. Sternlieb, I. and J.E. Berger, *Optical diffraction studies of crystalline structures in electron micrographs. II. Crystalline inclusions in mitochondria of human hepatocytes.* J Cell Biol, 1969. **43**(3): p. 448-55.
144. Sternlieb, I. and I.H. Scheinberg, *Prevention of Wilson's disease in asymptomatic patients.* N Engl J Med, 1968. **278**(7): p. 352-9.
145. Sternlieb, I., *Fraternal concordance of types of abnormal hepatocellular mitochondria in Wilson's disease.* Hepatology, 1992. **16**(3): p. 728-32.
146. Huster, D., et al., *High copper selectively alters lipid metabolism and cell cycle machinery in the mouse model of Wilson disease.* J Biol Chem, 2007. **282**(11): p. 8343-55.
147. Santos, E.M., et al., *Identifying health impacts of exposure to copper using transcriptomics and metabolomics in a fish model.* Environ Sci Technol, 2010. **44**(2): p. 820-6.
148. Lutsenko, S., *Modifying factors and phenotypic diversity in Wilson's disease.* Ann N Y Acad Sci, 2014. **1315**: p. 56-63.
149. Sauer, S.W., et al., *Severe dysfunction of respiratory chain and cholesterol metabolism in Atp7b(-/-) mice as a model for Wilson disease.* Biochim Biophys Acta, 2011. **1812**(12): p. 1607-15.
150. Ott, M., et al., *Mitochondria, oxidative stress and cell death.* Apoptosis, 2007. **12**(5): p. 913-22.

151. Fuentealba, I. and S. Haywood, *Cellular mechanisms of toxicity and tolerance in the copper-loaded rat. I. Ultrastructural changes in the liver.* Liver, 1988. **8**(6): p. 372-80.

152. Zischka, H., et al., *Liver mitochondrial membrane crosslinking and destruction in a rat model of Wilson disease.* J Clin Invest, 2011. **121**(4): p. 1508-18.

153. Saris, N.E. and I.A. Skulskii, *Interaction of Cu+ with mitochondria.* Acta Chem Scand, 1991. **45**(10): p. 1042-6.

154. Tavill, A.S. and M.L. Schilsky, *Wilson's Disease.* Curr Treat Options Gastroenterol, 1999. **2**(1): p. 68-71.

155. Roberts, E.A., et al., *A practice guideline on Wilson disease.* Hepatology, 2003. **37**(6): p. 1475-92.

156. Pfeiffer, R.F., *Wilson's disease.* Handb Clin Neurol, 2011. **100**: p. 681-709.

157. Brewer, G.J., et al., *Does a vegetarian diet control Wilson's disease?* J Am Coll Nutr, 1993. **12**(5): p. 527-30.

158. Walshe, J.M., *Penicillamine, a new oral therapy for Wilson's disease.* Am J Med, 1956. **21**(4): p. 487-95.

159. Schilsky, M.L., *Diagnosis and treatment of Wilson's disease.* Pediatr Transplant, 2002. **6**(1): p. 15-9.

160. Cumings, J.N., *The effects of B.A.L. in hepatolenticular degeneration.* Brain, 1951. **74**(1): p. 10-22.

161. McDonald, I.W., *Effect of BAL-intrav on excretion of copper by the sheep.* Nature, 1946. **157**: p. 837.

162. Mandelbrote, B.M., M.W. Stanier, and et al., *Studies on copper metabolism in demyelinating diseases of the central nervous system.* Brain, 1948. **71**(2): p. 212-28.

163. Walshe, J.M., *Wilson's disease; new oral therapy.* Lancet, 1956. **270**(6906): p. 25-6.

164. Waters, L.L. and C. Stock, *Bal (British anti-lewisite).* Science, 1945. **102**(2658): p. 601-6.

165. Schilsky, M.L., *Treatment of Wilson's disease: what are the relative roles of penicillamine, trientine, and zinc supplementation?* Curr Gastroenterol Rep, 2001. **3**(1): p. 54-9.

166. Walshe, J.M., *Treatment of Wilson's disease with trientine (triethylene tetramine) dihydrochloride.* Lancet, 1982. **1**(8273): p. 643-7.

167. Walshe, J.M., *Management of penicillamine nephropathy in Wilson's disease: a new chelating agent.* Lancet, 1969. **2**(7635): p. 1401-2.

168. Kodama, H., C. Fujisawa, and W. Bhadhprasit, *Inherited copper transport disorders: biochemical mechanisms, diagnosis, and treatment.* Curr Drug Metab, 2012. **13**(3): p. 237-50.

169. Durand, F., et al., *Wilson's disease with severe hepatic insufficiency: beneficial effects of early administration of D-penicillamine.* Gut, 2001. **48**(6): p. 849-52.

170. Weiss, K.H., et al., *Zinc monotherapy is not as effective as chelating agents in treatment of Wilson disease.* Gastroenterology, 2011. **140**(4): p. 1189-1198 e1.

171. Weiss, K.H., et al., *Efficacy and safety of oral chelators in treatment of patients with Wilson disease.* Clin Gastroenterol Hepatol, 2013. **11**(8): p. 1028-35 e1-2.

172. Walshe, J.M., *Copper chelation in patients with Wilson's disease. A comparison of penicillamine and triethylene tetramine dihydrochloride.* Q J Med, 1973. **42**(167): p. 441-52.

173. Neri, I., et al., *Detection of D-penicillamine in skin lesions in a case of dermal elastosis after a previous long-term treatment for Wilson's disease.* J Eur Acad Dermatol Venereol, 2015. **29**(2): p. 383-6.

174. Harpey, J.P., et al., *Lupus-like syndrome induced by D-penicillamine in Wilson's disease.* Lancet, 1971. **1**(7693): p. 292.

175. Siegemund, R., et al., *Mode of action of triethylenetetramine dihydrochloride on copper metabolism in Wilson's disease.* Acta Neurol Scand, 1991. **83**(6): p. 364-6.

176. Dahlman, T., et al., *Long-term treatment of Wilson's disease with triethylene tetramine dihydrochloride (trientine).* QJM, 1995. **88**(9): p. 609-16.
177. Lutsenko, S., *Atp7b-/- mice as a model for studies of Wilson's disease.* Biochem Soc Trans, 2008. **36**(Pt 6): p. 1233-8.
178. Pfeiffer, R.F., *Wilson's Disease.* Semin Neurol, 2007. **27**(2): p. 123-32.
179. Brewer, G.J., *Copper control as an antiangiogenic anticancer therapy: lessons from treating Wilson's disease.* Exp Biol Med (Maywood), 2001. **226**(7): p. 665-73.
180. Hoogenraad, T.U., R. Koevoet, and E.G. de Ruyter Korver, *Oral zinc sulphate as long-term treatment in Wilson's disease (hepatolenticular degeneration).* Eur Neurol, 1979. **18**(3): p. 205-11.
181. Richards, M.P. and R.J. Cousins, *Mammalian zinc homeostasis: requirement for RNA and metallothionein synthesis.* Biochem Biophys Res Commun, 1975. **64**(4): p. 1215-23.
182. Richards, M.P. and R.J. Cousins, *Isolation of an intestinal metallothionein induced by parenteral zinc.* Biochem Biophys Res Commun, 1977. **75**(2): p. 286-94.
183. Menard, M.P., C.C. McCormick, and R.J. Cousins, *Regulation of intestinal metallothionein biosynthesis in rats by dietary zinc.* J Nutr, 1981. **111**(8): p. 1353-61.
184. Waalkes, M.P., M.J. Harvey, and C.D. Klaassen, *Relative in vitro affinity of hepatic metallothionein for metals.* Toxicol Lett, 1984. **20**(1): p. 33-9.
185. Brewer, G.J., V. Yuzbasiyan-Gurkan, and A.B. Young, *Treatment of Wilson's disease.* Semin Neurol, 1987. **7**(2): p. 209-20.
186. Brewer, G.J., et al., *Initial therapy of patients with Wilson's disease with tetrathiomolybdate.* Arch Neurol, 1991. **48**(1): p. 42-7.
187. Alvarez, H.M., et al., *Tetrathiomolybdate inhibits copper trafficking proteins through metal cluster formation.* Science, 2010. **327**(5963): p. 331-4.
188. Ogra, Y., M. Ohmichi, and K.T. Suzuki, *Mechanisms of selective copper removal by tetrathiomolybdate from metallothionein in LEC rats.* Toxicology, 1996. **106**(1-3): p. 75-83.
189. Ogra, Y., H. Chikusa, and K.T. Suzuki, *Metabolic fate of the insoluble copper/tetrathiomolybdate complex formed in the liver of LEC rats with excess tetrathiomolybdate.* J Inorg Biochem, 2000. **78**(2): p. 123-8.
190. DuBois, R.S., et al., *Orthotopic liver transplantation for Wilson's disease.* Lancet, 1971. **1**(7698): p. 505-8.
191. Catana, A.M. and V. Medici, *Liver transplantation for Wilson disease.* World J Hepatol, 2012. **4**(1): p. 5-10.
192. Groth, C.G., et al., *Metabolic effects of hepatic replacement in Wilson's disease.* Transplant Proc, 1973. **5**(1): p. 829-33.
193. Schilsky, M.L., I.H. Scheinberg, and I. Sternlieb, *Liver transplantation for Wilson's disease: indications and outcome.* Hepatology, 1994. **19**(3): p. 583-7.
194. Walshe, J.M., *Cause of death in Wilson disease.* Mov Disord, 2007. **22**(15): p. 2216-20.
195. Nazer, H., et al., *Wilson's disease: clinical presentation and use of prognostic index.* Gut, 1986. **27**(11): p. 1377-81.
196. Walshe, J.M., *The conquest of Wilson's disease.* Brain, 2009. **132**(Pt 8): p. 2289-95.
197. Sarkar, B., et al., *A comparative study of in vitro and in vivo interaction of D-penicillamine and triethylenetetramine with copper.* Proc R Soc Med, 1977. **70 Suppl 3**: p. 13-8.
198. Riha, M., et al., *Novel method for rapid copper chelation assessment confirmed low affinity of D-penicillamine for copper in comparison with trientine and 8-hydroxyquinolines.* J Inorg Biochem, 2013. **123**: p. 80-7.
199. Weiss, K.H. and W. Stremmel, *Clinical considerations for an effective medical therapy in Wilson's disease.* Ann N Y Acad Sci, 2014. **1315**: p. 81-5.

200. Brewer, G.J., et al., *Worsening of neurologic syndrome in patients with Wilson's disease with initial penicillamine therapy.* Arch Neurol, 1987. **44**(5): p. 490-3.
201. Chen, D.B., et al., *Penicillamine increases free copper and enhances oxidative stress in the brain of toxic milk mice.* PLoS One, 2012. **7**(5): p. e37709.
202. Kim, B., S.J. Chung, and H.W. Shin, *Trientine-induced neurological deterioration in a patient with Wilson's disease.* J Clin Neurosci, 2013. **20**(4): p. 606-8.
203. Kim, H.J., et al., *Purification and physical-chemical properties of methanobactin: a chalkophore from Methylosinus trichosporium OB3b.* Biochemistry, 2005. **44**(13): p. 5140-8.
204. Choi, D.W., et al., *Spectral, kinetic, and thermodynamic properties of Cu(I) and Cu(II) binding by methanobactin from Methylosinus trichosporium OB3b.* Biochemistry, 2006. **45**(5): p. 1442-53.
205. Semrau, J.D., A.A. DiSpirito, and S. Yoon, *Methanotrophs and copper.* FEMS Microbiol Rev, 2010. **34**(4): p. 496-531.
206. Semrau, J.D., et al., *Methanobactin and MmoD work in concert to act as the 'copper-switch' in methanotrophs.* Environ Microbiol, 2013.
207. Gu, W., et al., *A TonB-Dependent Transporter Is Responsible for Methanobactin Uptake by Methylosinus trichosporium OB3b.* Appl Environ Microbiol, 2016. **82**(6): p. 1917-23.
208. Kim, H.J., et al., *Methanobactin, a copper-acquisition compound from methane-oxidizing bacteria.* Science, 2004. **305**(5690): p. 1612-5.
209. El Ghazouani, A., et al., *Variations in methanobactin structure influences copper utilization by methane-oxidizing bacteria.* Proc Natl Acad Sci U S A, 2012. **109**(22): p. 8400-4.
210. Summer, K.H., et al., *The biogenic methanobactin is an effective chelator for copper in a rat model for Wilson disease.* J Trace Elem Med Biol, 2011. **25**(1): p. 36-41.
211. Sokol, R.J., et al., *Abnormal hepatic mitochondrial respiration and cytochrome C oxidase activity in rats with long-term copper overload.* Gastroenterology, 1993. **105**(1): p. 178-87.
212. Huster, D., et al., *Consequences of copper accumulation in the livers of the Atp7b-/- (Wilson disease gene) knockout mice.* Am J Pathol, 2006. **168**(2): p. 423-34.
213. Roberts, E.A., B.H. Robinson, and S. Yang, *Mitochondrial structure and function in the untreated Jackson toxic milk (tx-j) mouse, a model for Wilson disease.* Mol Genet Metab, 2008. **93**(1): p. 54-65.
214. ATCC. *Hep G2 [HEPG2] (ATCC® HB-8065™)* 21/05/2104 [cited 2015 05/06/]; Available from: http://www.lgcstandards-atcc.org/Products/All/HB-8065.aspx#generalinformation.
215. Luft, J.H., *Improvements in epoxy resin embedding methods.* J Biophys Biochem Cytol, 1961. **9**: p. 409-14.
216. Schosinsky, K.H., H.P. Lehmann, and M.F. Beeler, *Measurement of ceruloplasmin from its oxidase activity in serum by use of o-dianisidine dihydrochloride.* Clin Chem, 1974. **20**(12): p. 1556-63.
217. Erel, O., *Automated measurement of serum ferroxidase activity.* Clin Chem, 1998. **44**(11): p. 2313-9.
218. Togashi, Y., et al., *D-penicillamine prevents the development of hepatitis in Long-Evans Cinnamon rats with abnormal copper metabolism.* Hepatology, 1992. **15**(1): p. 82-7.
219. Greenman, D.L., et al., *Subchronic toxicity of triethylenetetramine dihydrochloride in B6C3F1 mice and F344 rats.* Fundam Appl Toxicol, 1996. **29**(2): p. 185-93.
220. Repetto, G., A. del Peso, and J.L. Zurita, *Neutral red uptake assay for the estimation of cell viability/cytotoxicity.* Nat Protoc, 2008. **3**(7): p. 1125-31.

221. Riss, T., et al., *CellTiter-Glo luminescent cell viability assay: fast, sensitive and flexible.* Promega Notes Magazine, 2002. **81**: p. 2-5.
222. Hoppe-Tichy, T., et al., *[Manufacturing and stability of copper-histidine solution for treatment of Menkes' Kinky Hair Syndrome].* Pharmazie, 2005. **60**(3): p. 205-7.
223. Close, B., et al., *Recommendations for euthanasia of experimental animals: Part 2. DGXT of the European Commission.* Lab Anim, 1997. **31**(1): p. 1-32.
224. Zischka, H., et al., *Isolation of highly pure rat liver mitochondria with the aid of zone-electrophoresis in a free flow device (ZE-FFE).* Methods Mol Biol, 2008. **424**: p. 333-48.
225. Schulz, S., et al., *A protocol for the parallel isolation of intact mitochondria from rat liver, kidney, heart, and brain.* Methods Mol Biol, 2015. **1295**: p. 75-86.
226. Schmitt, S., et al., *A semi-automated method for isolating functionally intact mitochondria from cultured cells and tissue biopsies.* Anal Biochem, 2013. **443**(1): p. 66-74.
227. Schmitt, S., et al., *Isolation of mitochondria from cultured cells and liver tissue biopsies for molecular and biochemical analyses.* Methods Mol Biol, 2015. **1295**: p. 87-97.
228. Shinitzky, M. and Y. Barenholz, *Fluidity parameters of lipid regions determined by fluorescence polarization.* Biochim Biophys Acta, 1978. **515**(4): p. 367-94.
229. Kinosita, K., Jr., et al., *Dynamic structure of biological membranes as probed by 1,6-diphenyl-1,3,5-hexatriene: a nanosecond fluorescence depolarization study.* Biochemistry, 1981. **20**(15): p. 4270-7.
230. Grebowski, J., A. Krokosz, and M. Puchala, *Membrane fluidity and activity of membrane ATPases in human erythrocytes under the influence of polyhydroxylated fullerene.* Biochim Biophys Acta, 2013. **1828**(2): p. 241-8.
231. Prendergast, F.G., R.P. Haugland, and P.J. Callahan, *1-[4-(Trimethylamino)phenyl]-6-phenylhexa-1,3,5-triene: synthesis, fluorescence properties, and use as a fluorescence probe of lipid bilayers.* Biochemistry, 1981. **20**(26): p. 7333-8.
232. Duportail, G. and A. Weinreb, *Photochemical changes of fluorescent probes in membranes and their effect on the observed fluorescence anisotropy values.* Biochim Biophys Acta, 1983. **736**(2): p. 171-7.
233. Weber, G., *Polarization of the fluorescence of macromolecules. I. Theory and experimental method.* Biochem J, 1952. **51**(2): p. 145-55.
234. Johnson, L.V., M.L. Walsh, and L.B. Chen, *Localization of mitochondria in living cells with rhodamine 123.* Proc Natl Acad Sci U S A, 1980. **77**(2): p. 990-4.
235. Emaus, R.K., R. Grunwald, and J.J. Lemasters, *Rhodamine 123 as a probe of transmembrane potential in isolated rat-liver mitochondria: spectral and metabolic properties.* Biochim Biophys Acta, 1986. **850**(3): p. 436-48.
236. Petit, P.X., et al., *Mitochondria and programmed cell death: back to the future.* FEBS Lett, 1996. **396**(1): p. 7-13.
237. Hunter, D.R., R.A. Haworth, and J.H. Southard, *Relationship between configuration, function, and permeability in calcium-treated mitochondria.* J Biol Chem, 1976. **251**(16): p. 5069-77.
238. Crompton, M., *The mitochondrial permeability transition pore and its role in cell death.* Biochem J, 1999. **341 ( Pt 2)**: p. 233-49.
239. Bernardi, P., et al., *The mitochondrial permeability transition from in vitro artifact to disease target.* FEBS J, 2006. **273**(10): p. 2077-99.
240. Haworth, R.A. and D.R. Hunter, *The Ca2+-induced membrane transition in mitochondria. II. Nature of the Ca2+ trigger site.* Arch Biochem Biophys, 1979. **195**(2): p. 460-7.
241. Skulachev, V.P., *Why are mitochondria involved in apoptosis? Permeability transition pores and apoptosis as selective mechanisms to eliminate superoxide-producing mitochondria and cell.* FEBS Lett, 1996. **397**(1): p. 7-10.

242. Petit, P.X., et al., *Disruption of the outer mitochondrial membrane as a result of large amplitude swelling: the impact of irreversible permeability transition.* FEBS Lett, 1998. **426**(1): p. 111-6.
243. Zamzami, N., D. Metivier, and G. Kroemer, *Quantitation of mitochondrial transmembrane potential in cells and in isolated mitochondria.* Methods Enzymol, 2000. **322**: p. 208-13.
244. Zischka, H., et al., *Electrophoretic analysis of the mitochondrial outer membrane rupture induced by permeability transition.* Anal Chem, 2008. **80**(13): p. 5051-8.
245. Schulz, S., et al., *Progressive stages of mitochondrial destruction caused by cell toxic bile salts.* Biochim Biophys Acta, 2013. **1828**(9): p. 2121-33.
246. Bradford, M.M., *A rapid and sensitive method for the quantitation of microgram quantities of protein utilizing the principle of protein-dye binding.* Anal Biochem, 1976. **72**: p. 248-54.
247. Smith, P.K., et al., *Measurement of protein using bicinchoninic acid.* Anal Biochem, 1985. **150**(1): p. 76-85.
248. seTowbin, H., T. Staehelin, and J. Gordon, *Electrophoretic transfer of proteins from polyacrylamide gels to nitrocellulose sheets: procedure and some applications.* Proc Natl Acad Sci U S A, 1979. **76**(9): p. 4350-4.
249. Kar, P., et al., *A protocol for stripping and reprobing of Western blots originally developed with colorimetric substrate TMB.* Electrophoresis, 2012. **33**(19-20): p. 3062-5.
250. von Toerne, C., et al., *Apoe, Mbl2, and Psp plasma protein levels correlate with diabetic phenotype in NZO mice--an optimized rapid workflow for SRM-based quantification.* J Proteome Res, 2013. **12**(3): p. 1331-43.
251. Hauck, S.M., et al., *Deciphering membrane-associated molecular processes in target tissue of autoimmune uveitis by label-free quantitative mass spectrometry.* Mol Cell Proteomics, 2010. **9**(10): p. 2292-305.
252. Radonic, A., et al., *Guideline to reference gene selection for quantitative real-time PCR.* Biochem Biophys Res Commun, 2004. **313**(4): p. 856-62.
253. Pfaffl, M.W., *A new mathematical model for relative quantification in real-time RT-PCR.* Nucleic Acids Res, 2001. **29**(9): p. e45.
254. Larionov, A., A. Krause, and W. Miller, *A standard curve based method for relative real time PCR data processing.* BMC Bioinformatics, 2005. **6**: p. 62.
255. Finck, H., *Epoxy resins in electron microscopy.* J Biophys Biochem Cytol, 1960. **7**: p. 27-30.
256. Hackenbrock, C.R., *Ultrastructural bases for metabolically linked mechanical activity in mitochondria. II. Electron transport-linked ultrastructural transformations in mitochondria.* J Cell Biol, 1968. **37**(2): p. 345-69.
257. Feuchtinger, A., et al., *Image analysis of immunohistochemistry is superior to visual scoring as shown for patient outcome of esophageal adenocarcinoma.* Histochem Cell Biol, 2015. **143**(1): p. 1-9.
258. Stoner, C.D. and H.D. Sirak, *Osmotically-induced alterations in volume and ultrastructure of mitochondria isolated from rat liver and bovine heart.* J Cell Biol, 1969. **43**(3): p. 521-38.
259. Crompton, M., S. Virji, and J.M. Ward, *Cyclophilin-D binds strongly to complexes of the voltage-dependent anion channel and the adenine nucleotide translocase to form the permeability transition pore.* Eur J Biochem, 1998. **258**(2): p. 729-35.
260. Halestrap, A.P. and A.M. Davidson, *Inhibition of Ca2(+)-induced large-amplitude swelling of liver and heart mitochondria by cyclosporin is probably caused by the inhibitor binding to mitochondrial-matrix peptidyl-prolyl cis-trans isomerase and preventing it interacting with the adenine nucleotide translocase.* Biochem J, 1990. **268**(1): p. 153-60.
261. Halestrap, A.P., *A pore way to die: the role of mitochondria in reperfusion injury and cardioprotection.* Biochem Soc Trans, 2010. **38**(4): p. 841-60.

262. Klein, D., et al., *Dissolution of copper-rich granules in hepatic lysosomes by D-penicillamine prevents the development of fulminant hepatitis in Long-Evans cinnamon rats.* J Hepatol, 2000. **32**(2): p. 193-201.
263. Maftah, A., et al., *10-N nonyl-acridine orange: a fluorescent probe which stains mitochondria independently of their energetic state.* Biochem Biophys Res Commun, 1989. **164**(1): p. 185-90.
264. Xiao, B., et al., *Flow Cytometry-Based Assessment of Mitophagy Using MitoTracker.* Front Cell Neurosci, 2016. **10**: p. 76.
265. Chandok, N. and E.A. Roberts, *The trientine crisis in Canada: a call to advocacy.* Can J Gastroenterol Hepatol, 2014. **28**(4): p. 184.
266. Sturtz, L.A., et al., *A fraction of yeast Cu,Zn-superoxide dismutase and its metallochaperone, CCS, localize to the intermembrane space of mitochondria. A physiological role for SOD1 in guarding against mitochondrial oxidative damage.* J Biol Chem, 2001. **276**(41): p. 38084-9.
267. An, J., et al., *CHCM1/CHCHD6, novel mitochondrial protein linked to regulation of mitofilin and mitochondrial cristae morphology.* J Biol Chem, 2012. **287**(10): p. 7411-26.
268. Ding, C., et al., *Mitofilin and CHCHD6 physically interact with Sam50 to sustain cristae structure.* Sci Rep, 2015. **5**: p. 16064.
269. Ferguson, R.E., et al., *Housekeeping proteins: a preliminary study illustrating some limitations as useful references in protein expression studies.* Proteomics, 2005. **5**(2): p. 566-71.
270. Liu, H., et al., *High-Efficient Transfection of Human Embryonic Stem Cells by Single-Cell Plating and Starvation.* Stem Cells Dev, 2016. **25**(6): p. 477-91.
271. Schilsky, M.L., *Liver transplantation for Wilson's disease.* Ann N Y Acad Sci, 2014. **1315**: p. 45-9.
272. Vincent, O.D., et al., *Fluidity of structure and swiveling of helices in the subunit c ring of Escherichia coli ATP synthase as revealed by cysteine-cysteine cross-linking.* J Biol Chem, 2007. **282**(46): p. 33788-94.
273. Schulz, S.M., *Mitochondrial membranes as target structure for the adaptability of MPT induction*, 2013, Ludwig-Maximilians-Universität München. p. 124.
274. Crompton, M., H. Ellinger, and A. Costi, *Inhibition by cyclosporin A of a Ca2+-dependent pore in heart mitochondria activated by inorganic phosphate and oxidative stress.* Biochem J, 1988. **255**(1): p. 357-60.
275. Schneider, M.D., *Cyclophilin D: knocking on death's door.* Sci STKE, 2005. **2005**(287): p. pe26.
276. McGuinness, O., et al., *The presence of two classes of high-affinity cyclosporin A binding sites in mitochondria. Evidence that the minor component is involved in the opening of an inner-membrane Ca(2+)-dependent pore.* Eur J Biochem, 1990. **194**(2): p. 671-9.
277. Tanveer, A., et al., *Involvement of cyclophilin D in the activation of a mitochondrial pore by Ca2+ and oxidant stress.* Eur J Biochem, 1996. **238**(1): p. 166-72.
278. Giorgio, V., et al., *Cyclophilin D modulates mitochondrial F0F1-ATP synthase by interacting with the lateral stalk of the complex.* J Biol Chem, 2009. **284**(49): p. 33982-8.
279. Giorgio, V., et al., *Dimers of mitochondrial ATP synthase form the permeability transition pore.* Proc Natl Acad Sci U S A, 2013. **110**(15): p. 5887-92.
280. Bernardi, P. and F. Di Lisa, *The mitochondrial permeability transition pore: molecular nature and role as a target in cardioprotection.* J Mol Cell Cardiol, 2015. **78**: p. 100-6.
281. Hosseini, M.J., et al., *Toxicity of copper on isolated liver mitochondria: impairment at complexes I, II, and IV leads to increased ROS production.* Cell Biochem Biophys, 2014. **70**(1): p. 367-81.

282. Krumschnabel, G., et al., *Oxidative stress, mitochondrial permeability transition, and cell death in Cu-exposed trout hepatocytes.* Toxicol Appl Pharmacol, 2005. **209**(1): p. 62-73.
283. Majima, E., et al., *Translocation of loops regulates transport activity of mitochondrial ADP/ATP carrier deduced from formation of a specific intermolecular disulfide bridge catalyzed by copper-o-phenanthroline.* J Biol Chem, 1995. **270**(49): p. 29548-54.
284. Hashimoto, M., et al., *Fluctuation of the first loop facing the matrix of the mitochondrial ADP/ATP carrier deduced from intermolecular cross-linking of Cys56 residues by bifunctional dimaleimides.* Biochemistry, 1999. **38**(3): p. 1050-6.
285. Halestrap, A.P. and C. Brenner, *The adenine nucleotide translocase: a central component of the mitochondrial permeability transition pore and key player in cell death.* Curr Med Chem, 2003. **10**(16): p. 1507-25.
286. Kim, K.K., et al., *Tetrathiomolybdate inhibits mitochondrial complex IV and mediates degradation of hypoxia-inducible factor-1alpha in cancer cells.* Sci Rep, 2015. **5**: p. 14296.
287. Wei, H., et al., *Copper chelation by tetrathiomolybdate inhibits lipopolysaccharide-induced inflammatory responses in vivo.* Am J Physiol Heart Circ Physiol, 2011. **301**(3): p. H712-20.
288. Mills, C.F., T.T. El-Gallad, and I. Bremner, *Effects of molybdate, sulfide, and tetrathiomolybdate on copper metabolism in rats.* J Inorg Biochem, 1981. **14**(3): p. 189-207.
289. Cappellini, M.D., K.M. Musallam, and A.T. Taher, *Overview of iron chelation therapy with desferrioxamine and deferiprone.* Hemoglobin, 2009. **33 Suppl 1**: p. S58-69.
290. Takenouchi, T., et al., *Isolation and characterization of Cox17p from porcine heart by determining its survival-promoting activity in NIH3T3 cells.* Biochim Biophys Acta, 1999. **1472**(3): p. 498-508.
291. Banci, L., et al., *Human Sco1 functional studies and pathological implications of the P174L mutant.* Proc Natl Acad Sci U S A, 2007. **104**(1): p. 15-20.
292. Heaton, D.N., et al., *The mitochondrial copper metallochaperone Cox17 exists as an oligomeric, polycopper complex.* Biochemistry, 2001. **40**(3): p. 743-51.
293. Dong, D., et al., *Disturbance of copper homeostasis is a mechanism for homocysteine-induced vascular endothelial cell injury.* PLoS One, 2013. **8**(10): p. e76209.
294. Dong, D., et al., *Changes in copper concentrations affect the protein levels but not the mRNA levels of copper chaperones in human umbilical vein endothelial cells.* Metallomics, 2014. **6**(3): p. 554-9.
295. Mesecke, N., et al., *A disulfide relay system in the intermembrane space of mitochondria that mediates protein import.* Cell, 2005. **121**(7): p. 1059-69.
296. Sideris, D.P., et al., *A novel intermembrane space-targeting signal docks cysteines onto Mia40 during mitochondrial oxidative folding.* J Cell Biol, 2009. **187**(7): p. 1007-22.
297. Koch, J.R. and F.X. Schmid, *Mia40 combines thiol oxidase and disulfide isomerase activity to efficiently catalyze oxidative folding in mitochondria.* J Mol Biol, 2014. **426**(24): p. 4087-98.
298. Varndell, I.M., et al., *Immunogold staining procedure for the localisation of regulatory peptides.* Peptides, 1982. **3**(3): p. 259-72.
299. Jang, H.J., J.M. Kim, and C.Y. Choi, *Elemental analysis of sunflower cataract in Wilson's disease: a study using scanning transmission electron microscopy and energy dispersive spectroscopy.* Exp Eye Res, 2014. **121**: p. 58-65.
300. Heaton, D., et al., *Mutational analysis of the mitochondrial copper metallochaperone Cox17.* J Biol Chem, 2000. **275**(48): p. 37582-7.
301. Kako, K., et al., *The expression of Cox17p in rodent tissues and cells.* Eur J Biochem, 2000. **267**(22): p. 6699-707.

302. Chacinska, A., et al., *Essential role of Mia40 in import and assembly of mitochondrial intermembrane space proteins.* EMBO J, 2004. **23**(19): p. 3735-46.
303. Stelzl, U., et al., *A human protein-protein interaction network: a resource for annotating the proteome.* Cell, 2005. **122**(6): p. 957-68.
304. Szklarczyk, R., et al., *Iterative orthology prediction uncovers new mitochondrial proteins and identifies C12orf62 as the human ortholog of COX14, a protein involved in the assembly of cytochrome c oxidase.* Genome Biol, 2012. **13**(2): p. R12.
305. Wang, J., et al., *Toward an understanding of the protein interaction network of the human liver.* Mol Syst Biol, 2011. **7**: p. 536.
306. Kutzera, J., et al., *Inferring protein-protein interaction complexes from immunoprecipitation data.* BMC Res Notes, 2013. **6**: p. 468.
307. He, M., et al., *Identification and characterization of new long chain acyl-CoA dehydrogenases.* Mol Genet Metab, 2011. **102**(4): p. 418-29.
308. Reagan-Shaw, S., M. Nihal, and N. Ahmad, *Dose translation from animal to human studies revisited.* Faseb J, 2008. **22**(3): p. 659-61.

# Supplement

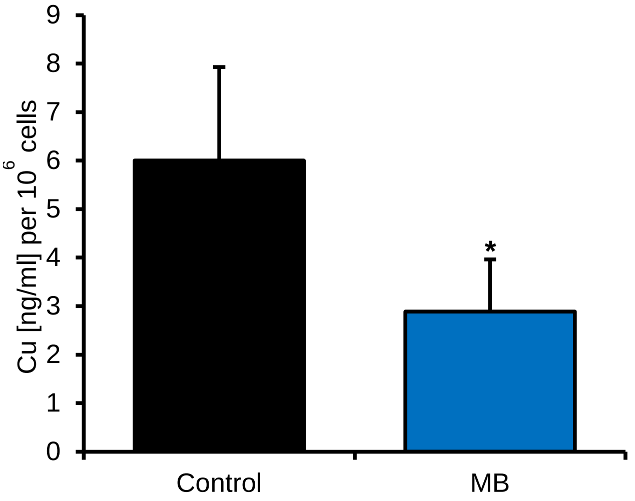

Supplementary Figure 1 Treatment of HepG2 cells with MB reduces cellular copper load for approximately 50% compared to untreated control cells.

*Treating HepG2 cells for 24 hours with 0.5 mM MB reduces cellular copper load for approximately 50% compared to untreated control cells (N=3). Unpaired two-tailed Student’s t-test with Welch’s correction. *Significant to control, *p<0.05.*

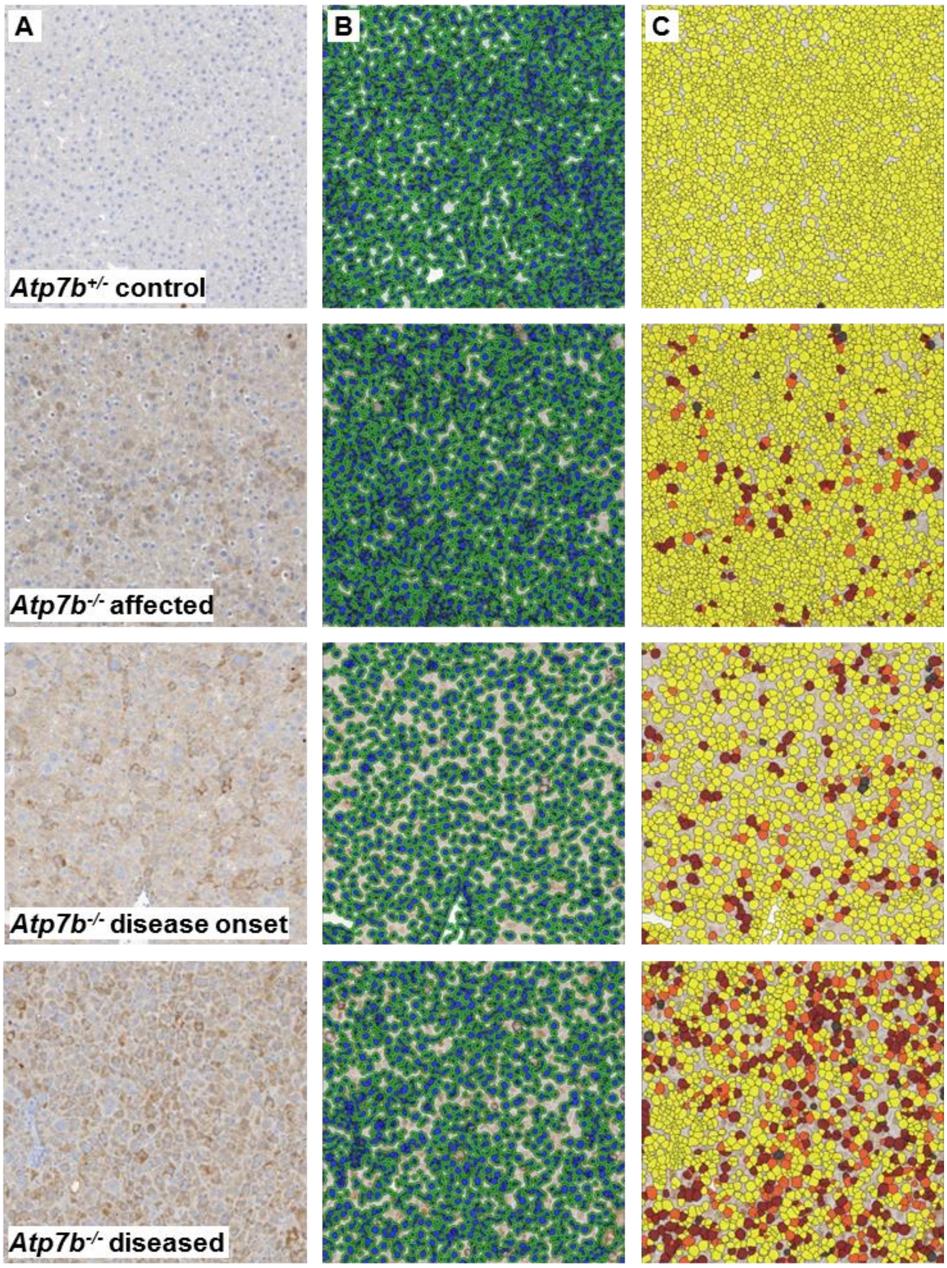
A
B
C
Atp7b+/- control
Atp7b-/- affected
Atp7b-/- disease onset
Atp7b-/- diseased

Supplementary Figure 2 Single cell-based analysis shows an increase of COX17 positive liver cells with disease progression of *Atp7b*$^{-/-}$ rats.

*(A)* *Immunohistochemical staining for* COX17 *of liver tissue from Atp7b*$^{+/-}$ *controls and Atp7b*$^{-/-}$ *rats with progressing disease states. Blue: nuclei; brown:* COX17 *stained cytosol.*

*(B)* *Nuclei (blue) and cellular cytosol (green) is marked.*

*(C)* *Classification of hepatocytes according to the* COX17 *staining signal. White: negative; yellow: weak staining; orange: medium stained; dark red/brown: strong staining; grey: excluded due to artefacts.*

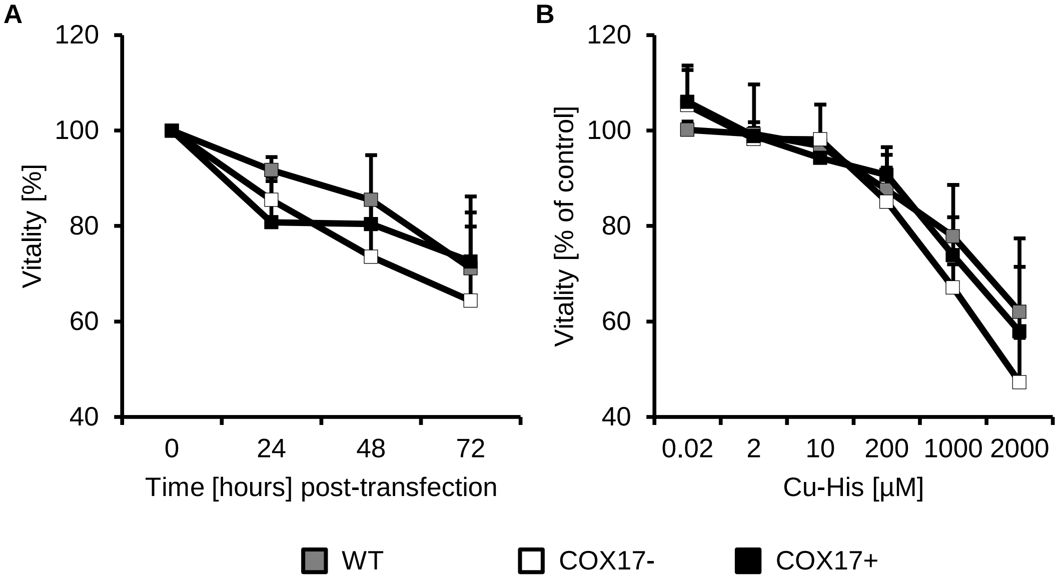

Supplementary Figure 3 COX17- cells are more susceptible towards Cu-His compared to non-transfected HepG2 WT cells and COX17+ cells.

*(A)* *Cellular vitality from non-transfected HepG2 WT cells, COX17- cells and COX17+ cells treated with 15 µM Cu-His 24 hours post-seeding (WT) or post-transfection (COX17-, COX17+). Transfected cells show a 10% reduced vitality 24 hours post-transfection compared to non-transfected WT cells which is due to toxic effects of the transfection reagents. 48–72 hours post-seeding or post-transfection vitality progressively decreases in WT and COX17- cells, whereas it is stabilised in COX17+ cells. N=3. Mean and standard deviation is indicated.*

*(B)* *Neutral red assay was used for the measurement of cellular vitality for WT, COX17- and COX17+ cells treated for 24 hours with increasing Cu-His concentrations. At 2000 µM Cu-His, cellular vitality is reduced for 15% in COX17- cells compared to WT cells. No difference in cellular vitality can be observed for COX17+ cells compared to WT cells. N=3–5, n=6–15. Mean and standard deviation is indicated.*

Supplementary Table 1 Copper concentrations in liver homogenate and liver mitochondria progressively increase with disease progression of *Atp7b*$^{-/-}$ rats.

*Atp7b*$^{-/-}$ *rats with massively increased serum AST and bilirubin values are termed as moribund and die within few days if no treatment takes place. Adapted from Josef Lichtmannegger et al. (2016) Methanobactin reverses acute liver failure in a rat model of Wilson disease. J Clin Invest. 2016 Jul;126(7): p. 2721-35* [1].

| **Group (genotype)**<br>Sex, rats | **Age [days]** | **Weight [g]** | **cp [mU/ml]** | **AST [U/L]** | **Bilirubin [mg/dl]** | **Cu [ng/mg protein]** | |
|---|---|---|---|---|---|---|---|
| | | | | | | Homogenate | Mitochondria |
| **Control (+/-)** | | | | | | | |
| f, N=20 | 82–161 | 175 ± 17 | 225 ± 35 | 113 ± 26 | <0.5 | 14 ± 2 | 27 ± 2 |
| m, N=14 | 75–166 | 295 ± 48 | 141 ± 17 | 122 ± 29 | <0.5 | 15 ± 3 | 42 ± 10 |
| **Affected (-/-)** | | | | | | | |
| f, N=5 | 82–92 | 168 ± 14 | 5 ± 2 | 133 ± 31 | <0.5 | 1266 ± 204 | 392 ± 80 |
| m, N=9 | 66–93 | 254 ± 26 | 0 ± 2 | 146 ± 33 | <0.5 | 1139 ± 144 | 358 ± 60 |
| **Disease onset (-/-)** | | | | | | | |
| f, N=5 | 83–93 | 146 ± 9 | 26 ± 6 | 315 ± 48 | <0.5 | 1477 ± 189 | 556 ± 32 |
| m, N=6 | 80–107 | 275 ± 41 | 7 ± 9 | 244 ± 50 | <0.5 | 1337 ± 141 | 476 ± 145 |
| **Diseased (-/-)** | | | | | | | |
| f, N=1 | 84 | 162 | 35 | 590 | 0.5 | 1389 | 670 |
| m, N=4 | 91–107 | 274 ± 17 | 27 ± 12 | 412 ± 107 | 1.3 ± 1.1 | 1389 ± 69 | 1129 ± 284 |
| **Moribund (-/-)** | | | | | | | |
| f, N=3 | 97–106 | 140 ± 4 | 0 ± 3 | 454 ± 78 | 14.2 ± 4.5 | 1667 ± 391 | 1398 ± 246 |
| m, N=1 | 95 | 255 | 4 | 570 | 8.0 | 1261 | 1602 |

Supplementary Table 2 Different treatment regimens enhance MB-induced mitochondrial decoppering in *Atp7b*$^{-/-}$ rats.

*Short-term treatments of one week by 5x MB i.p. and especially by 16x MB i.p. (one week, twice daily) drastically reduce the mitochondrial copper load.* [a] *Mitochondrial copper depletion relating to the respective untreated group (Supplementary Table 1).* [b] *Abbreviations are (Af) affected Atp7b*$^{-/-}$*, (Do) disease onset Atp7b*$^{-/-}$*, (Di) diseased Atp7b*$^{-/-}$*, (Mo) moribund Atp7b*$^{-/-}$*. Adapted from Josef Lichtmannegger et al. (2016) Methanobactin reverses acute liver failure in a rat model of Wilson disease. J Clin Invest. 2016 Jul;126(7): p. 2721-35* [1].

| **Group (genotype)**<br>Sex, rat | **Age**<br>**[days]** | **Weight**<br>**[g]** | | **AST**<br>**[U/L]** | | **Bilirubin**<br>**[mg/dl]** | | **Cu**<br>**[ng/mg protein]** | | **Mitochondrial Cu depletion**[a] **[%]** |
|---|---|---|---|---|---|---|---|---|---|---|
| | | **Start** | **End** | **Start** | **End** | **Start** | **End** | **Homogenate** | **Mitochondria** | |
| **MB 2x i.p. (+/-)** | | | | | | | | | | |
| f, rat 1 | 89 | 188 | 181 | - | 108 | - | <0.5 | 13 | 26 | 2.6 |
| f, rat 2 | 89 | 170 | 171 | - | 123 | - | <0.5 | 16 | 27 | 0.5 |
| f, rat 3 | 161 | 209 | 212 | - | 139 | - | <0.5 | 11 | 25 | 7.1 |
| f, rat 4 | 161 | 213 | 216 | - | 127 | - | <0.5 | 15 | 27 | -0.2 |
| **MB 3x i.p. (-/-)** | | | | | | | | | | |
| f, rat 1 (Do)[b] | 89 | 144 | 147 | 131 | 215 | <0.5 | <0.5 | 1307 | 525 | 5.5 |
| m, rat 2 (Af) | 88 | 261 | 261 | 192 | 168 | <0.5 | <0.5 | 881 | 335 | 27.8 |
| m, rat 3 (Af) | 88 | 259 | 260 | 106 | 93 | <0.5 | <0.5 | 840 | 215 | 53.7 |
| **MB 5x i.p. (-/-)** | | | | | | | | | | |
| f, rat 1 (Af) | 91 | 157 | 154 | 116 | 87 | <0.5 | <0.5 | - | 205 | 50.7 |
| m, rat 2 (Do) | 90 | 197 | 205 | 480 | 194 | <0.5 | <0.5 | 806 | 321 | 32.4 |
| m, rat 3 (Do) | 90 | 231 | 242 | 270 | 160 | <0.5 | <0.5 | 851 | 251 | 47.2 |
| f, rat 4 (Di) | 95 | 160 | 164 | 369 | 127 | 0.6 | <0.5 | 915 | 432 | 35.6 |
| f, rat 5 (Af) | 89 | 171 | 178 | 83 | 88 | <0.5 | <0.5 | 728 | 197 | 52.6 |
| m, rat 6 (Af) | 89 | 258 | 269 | 97 | 97 | <0.5 | <0.5 | 600 | 177 | 61.9 |
| **MB 16x i.p. (-/-)** | | | | | | | | | | |
| f, rat 1 (Di) | 89 | 148 | 155 | 365 | 182 | 1.0 | <0.5 | 455 | 241 | 64.0 |
| f, rat 2 (Di) | 89 | 144 | 160 | 570 | 178 | 0.9 | <0.5 | 315 | 218 | 67.4 |
| f, rat 3 (Mo) | 90 | 120 | 155 | 610 | 122 | 15.5 | <0.5 | 220 | 203 | 85.5 |
| f, rat 4 (Do) | 90 | 143 | 163 | 273 | 131 | <0.5 | <0.5 | 513 | 206 | 62.9 |

Supplementary Table 3 The copper-binding proteins COX11 and SCO1 are up- or downregulated in one of the two subfractions of rat liver mitochondria.

*Mitochondrial proteins that are identified by proteomic analysis as either upregulated in one of the two fractions, unaltered or downregulated are listed. In the table, the protein names, abundance relative to Atp7b*$^{+/-}$ *rats, their localisation within the mitochondrion as well as their function are listed. Abundance levels were defined as follows: 0–0.5 downregulated in Atp7b*$^{-/-}$ *relative to Atp7b*$^{+/-}$ *(red), 0.5–2.0 unaltered between both groups (yellow), >2.0 upregulated in Atp7b*$^{-/-}$ *(green). Proteins marked in* ***bold*** *have a function in copper metabolism. MIM: mitochondrial inner membrane, IMS: intermembrane space, MOM: mitochondrial outer membrane. Information about localisation and function are obtained from UniProt.*

| **Protein** | **Protein name** | **Accession No.** | **Ratio -/- vs. +/-** | | **Localisation** | **Function** |
|---|---|---|---|---|---|---|
| | | | **IEX_F3** | **IEX_F4** | | |
| ABAT | 4-aminobutyrate aminotransferase | P50554 | 0.97 | 1.57 | Matrix | Conversion of gamma-aminobutyrate and L-beta-aminoisobutyrate to succinate semialdehyde and methylmalonate semialdehyde |
| ACOT2 | Acyl-coenzyme A thioesterase 2 | O55171 | 0.64 | 1.23 | Matrix | Acyl-CoA metabolism, thiolester hydrolase activity |
| ACSM5_RAT | Acyl-coenzyme A synthetase | Q6AYT9 | 1.20 | 1.87 | Matrix | Magnesium ion binding, fatty acid metabolism, ATP binding |
| ADHFE1 | Hydroxyacid-oxoacid transhydrogenase | Q4QQW3 | 0.41 | 0.98 | Mitochondrion | Metal ion binding, reversible oxidation of gamma-hydroxybutyrate (GHB) to succinic semialdehyde (SSA) |
| ADO | 2-amino-ethanethiol (cysteamine) dioxygenase | NP_001101096 | 5.36 | 1.38 | Mitochondrion | Cysteamine dioxygenase activity |
| AIFM1 | Apoptosis-inducing factor 1 | Q9JM53 | 0.66 | 0.76 | MIM | FAD binding, mitochondrial respiratory chain complex I assembly |
| AMACR | Alpha-methylacyl-CoA racemase | P70473 | 0.77 | 0.89 | Mitochondrion | Lipid and fatty acid metabolism |
| ARMC1 | Armadillo repeat-containing protein 1 | NP_001099895 | 2.46 | 1.44 | Mitochondrion | Metal ion binding |
| B0BNM1_RAT | Apolipoprotein A-I-binding protein | NP_001099910 | 2.08 | 1.64 | Mitochondrion | Potassium ion binding |
| BCL2L13 | Bcl-2-like protein 13 | NP_001101355 | 6.96 | 1.07 | Mitochondrion | Regulation of apoptotic process |
| CAR5A | Carbonic anhydrase 5A | P43165 | 1.97 | 1.73 | Mitochondrion | Zinc ion binding, reversible hydration of carbon dioxide |
| CCBL1 | Kynurenine--oxoglutarate transaminase 1 | Q08415 | 1.54 | 1.79 | Matrix | Amino-acid degradation |
| CLU | Clusterin Clusterin beta chain Clusterin alpha chain | P05371 | 2.39 | 1.68 | Membrane | Cell death |
| **COX11** | **COX11 homolog, cytochrome c oxidase assembly protein** | **NP_001103045** | **0.39** | **1.65** | **Mitochondrion** | **Copper ion binding** |
| COX16 | Synaptojanin-2-binding protein | Q9WVJ4 | 0.66 | 1.58 | MOM | Regulates endocytosis of activin type 2 receptor kinases |

Supplementary Table 3 The copper-binding proteins COX11 and SCO1 are up- or downregulated in one of the two subfractions of rat liver mitochondria.

*Mitochondrial proteins that are identified by proteomic analysis as either upregulated in one of the two fractions, unaltered or downregulated are listed. In the table, the protein names, abundance relative to Atp7b*$^{+/-}$ *rats, their localisation within the mitochondrion as well as their function are listed. Abundance levels were defined as follows: 0–0.5 downregulated in Atp7b*$^{-/-}$ *relative to Atp7b*$^{+/-}$ *(red), 0.5–2.0 unaltered between both groups (yellow), >2.0 upregulated in Atp7b*$^{-/-}$ *(green). Proteins marked in* ***bold*** *have a function in copper metabolism. MIM: mitochondrial inner membrane, IMS: intermembrane space, MOM: mitochondrial outer membrane. Information about localisation and function are obtained from UniProt.*

| **Protein** | **Protein name** | **Accession No.** | **Ratio -/- vs. +/-** | | **Localisation** | **Function** |
|---|---|---|---|---|---|---|
| | | | **IEX_F3** | **IEX_F4** | | |
| CPOX | Coproporphyrinogen-III oxidase | Q3B7D0 | 1.49 | 2.12 | IMS | Porphyrin-containing compound metabolism |
| D4A608_RAT | Uncharacterised protein | D4A608 | 1.95 | 1.69 | Mitochondrion | Amino-acid degradation |
| D4A8Y5_RAT | Uncharacterised protein | D3ZH86 | 3.61 | 1.41 | Mitochondrion | nucleic acid binding |
| DHDPSL | Probable 4-hydroxy-2-oxoglutarate aldolase | NP_001099825 | 0.64 | 1.11 | Mitochondrion | Pyruvate biosynthetic process |
| DLAT | Dihydrolipoyllysine-residue acetyltransferase component of pyruvate dehydrogenase complex | P08461 | 4.08 | 1.90 | Matrix | Linkage of the glycolytic pathway to the tricarboxylic cycle |
| DMGDH | Dimethylglycine dehydrogenase | Q63342 | 0.83 | 0.90 | Mitochondrion | Amine and polyamine degradation |
| F1LX89_RAT | Uncharacterised protein | F1LX89 | 2.25 | 1.45 | Mitochondrion | Unknown |
| FDX1L | Adrenodoxin-like protein | NP_001101472 | 0.83 | 1.55 | Mitochondrion | 2 iron, 2 sulfur cluster binding, electron carrier activity |
| FKBP8 | Peptidyl-prolyl cis-trans isomerase FKBP8 | Q3B7U9 | 1.60 | 1.17 | Membrane | Calcium ion binding |
| FXN | Frataxin | D3ZYW7 | 1.86 | 2.07 | Mitochondrion | Assembly and repair of iron-sulfur clusters, negative regulation of mitochondrial fusion |
| GFER | FAD-linked sulfhydryl oxidase ALR | Q63042 | 1.68 | 1.63 | IMS | Protein disulfide oxidoreductase activity |
| ISCA1 | Iron-sulfur cluster assembly 1 homolog | Q80W96 | 1.30 | 0.78 | Mitochondrion | Maturation of mitochondrial 4Fe-4S proteins |
| LACTB2 | Beta-lactamase-like protein 2 | Q561R9 | 2.10 | 1.81 | Mitochondrion | Unknown |
| LIAS | Lipoyl synthase | Q5XIH4 | 2.01 | 1.01 | Mitochondrion | Protein modification |
| LOC100361841 | Kynurenine--oxoglutarate transaminase 3 | NP_001015037 | 0.82 | 0.91 | Mitochondrion | Pyridoxal phosphate binding |
| MSRA | Peptide methionine sulfoxide reductase | Q923M1 | 1.18 | 2.13 | Mitochondrion | Repair enzyme for proteins that have been inactivated by oxidation |
| MSRB2 | Methionine-R-sulfoxide reductase B2 | Q4FZX5 | 1.25 | 2.07 | Mitochondrion | Zinc ion binding, reduction of ROS |

Supplementary Table 3 The copper-binding proteins COX11 and SCO1 are up- or downregulated in one of the two subfractions of rat liver mitochondria.

*Mitochondrial proteins that are identified by proteomic analysis as either upregulated in one of the two fractions, unaltered or downregulated are listed. In the table, the protein names, abundance relative to Atp7b$^{+/-}$ rats, their localisation within the mitochondrion as well as their function are listed. Abundance levels were defined as follows: 0–0.5 downregulated in Atp7b$^{-/-}$ relative to Atp7b$^{+/-}$ (red), 0.5–2.0 unaltered between both groups (yellow), >2.0 upregulated in Atp7b$^{-/-}$ (green). Proteins marked in* ***bold*** *have a function in copper metabolism. MIM: mitochondrial inner membrane, IMS: intermembrane space, MOM: mitochondrial outer membrane. Information about localisation and function are obtained from UniProt.*

| Protein | Protein name | Accession No. | Ratio -/- vs. +/- | | Localisation | Function |
|---|---|---|---|---|---|---|
| | | | IEX_F3 | IEX_F4 | | |
| NLN | Neurolysin | P42676 | 0.69 | 1.06 | IMS | Zinc ion binding |
| NME1 | Nucleoside diphosphate kinase A | Q05982 | 2.01 | 0.92 | MOM | Cellular response to fatty acid |
| NME2 | Nucleoside diphosphate kinase B | P19804 | 0.82 | 0.67 | Membrane | Magnesium ion binding, synthesis of nucleoside triphosphates other than ATP |
| NME3 | Nucleoside diphosphate kinase 3 | NP_445959 | 1.21 | 0.71 | Mitochondrion | ATP binding |
| PEBP1 | Phosphatidylethanolamine-binding protein 1 | P31044 | 0.77 | 0.93 | MOM | Binds ATP, opioids and phosphatidylethanolamine |
| PROSC | Proline synthase co-transcribed bacterial homolog protein | NP_001100790 | 1.98 | 1.72 | Mitochondrion | Pyridoxal phosphate binding |
| REXO2 | Oligoribonuclease | Q5U1X1 | 1.67 | 1.41 | Mitochondrion | 3'-5' exonuclease activity |
| RGD1307465 | Similar to RIKEN cDNA | NM_001009655 | 0.68 | 0.53 | Mitochondrion | Probably involved in mitochondrial DNA repair |
| RGD1564560 | Similar to RCK | NM_001109292 | 0.21 | 0.20 | Mitochondrion | ATP binding, nucleic acid binding |
| SCAND3 | Zinc finger BED domain-containing protein 5 | NP_001099394 | 0.34 | 1.79 | Mitochondrion | Nucleic acid binding |
| **SCO1** | **SCO cytochrome oxidase deficient homolog 1** | **NP_001166845** | **1.74** | **3.27** | **MIM** | **Copper ion homeostasis, complex IV assembly** |
| SDHAF2 | Succinate dehydrogenase assembly factor 2 | Q5RJQ7 | 2.11 | 1.66 | Mitochondrion | Mitochondrial electron transport |
| **SOD1** | **Superoxide dismutase [copper-zinc dependent]** | **P07632** | **0.72** | **1.65** | **Mitochondrion** | **Copper ion binding, zinc ion binding, destroys radicals which are normally produced within the cells and which are toxic to biological systems** |
| SUOX | Sulfite oxidase | Q07116 | 2.61 | 1.28 | IMS | Energy metabolism; sulfur metabolism |
| TXN1 | Thioredoxin | P11232 | 1.83 | 1.54 | Mitochondrion | Protein disulfide oxidoreductase activity |

# List of publications

First author:

1. J. Lichtmannegger*****, **C. Leitzinger***, R. Wimmer, S. Schmitt, S. Schulz, Y. Kabiri, C. Eberhagen, T. Rieder, D. Janik, F. Neff, B. K. Straub, P. Schirmacher, A. A. DiSpirito, N. Bandow, B. S. Baral, A. Flatley, E. Kremmer, G. Denk, F. P. Reiter, S. Hohenester, F. Eckardt-Schupp, N. A. Dencher, J. Adamski, V. Sauer, C. Niemietz, H. H. Schmidt, U. Merle, D. N. Gotthardt, G. Kroemer, K. H. Weiss, H. Zischka. Methanobactin reverses acute liver failure in a rat model of Wilson disease. J Clin Invest (2016) 126(7):2721-35.
   ***Both authors share first authorship.**

Co-author:

1. S. Schulz, J. Lichtmannegger, S. Schmitt, **C. Leitzinger**, C. Eberhagen, C. Einer, J. Kerth, M. Aichler, H. Zischka. A protocol for the parallel isolation of intact mitochondria from rat liver, kidney, heart, and brain. Methods Mol Biology (2015) 1295:75-86.
2. E. Bader, A. Migliorini, M. Gegg, N. Moruzzi, J. Gerdes, S. S. Roscioni, M. Bakhti, E. Brandl, M. Irmler, J. Beckers, M. Aichler, A. Feuchtinger, **C. Leitzinger**, H. Zischka, R. Wang-Sattler, M. Jastroch, M. Tschöp, F. Machicao, H. Staiger, H.-U. Häring, H. Chmelova, J. A. Chouinard, N. Oskolkov, O. Korsgren, S. Speier, H. Lickert. Identification of proliferative and mature β-cells in the islets of Langerhans. Nature (2016) 535(7612):430-4.
3. V. Chubanov, S. Ferioli, A. Wisnowsky, D. G. Simmons, **C. Leitzinger**, C. Einer, W. Jonas, Y. Shymkiv, H. Bartsch, A. Braun, B. Akdogan, L. Mittermeier, L. Sytik, F. Torben, V. Jurinovic, E. van der Vorst, C. Weber, Ö. A. Yildirim, K. Sotlar, A. Schürmann, S. Zierler, H. Zischka, A. G. Ryazanov, T. Gudermann. TRPM6 activity in the intestine is a longevity determinant in mice. **Manuscript submitted.**
4. C. Einer, S. Hohenester, R. Wimmer, L. Wottke, R. Artmann, S. Schulz, C. Gosmann, M. Seifert, A. Simmons, **C. Leitzinger**, C. Eberhagen, S. Schmitt, S. Hauck, C. von Toerne, M. Jastroch, E. Walheim, C. Rust, A. L. Gerbes, B. Popper, D. Mayr, A. M. Vollmar, G. Denk, H. Zischka. Mitochondrial adaptation counterbalances steatosis. **Manuscript in preparation.**

# Contributions

The present work was directly supervised by PD Dr. Hans Zischka, guided by apl. Prof. Dr. Dr. Jerzy Adamski and Prof. Dr. Dirk H. Busch, and assisted by:

Dr. Michaela Aichler, Alan A. DiSpirito, Carola Eberhagen, Dr. Annette Feuchtinger, Peter Grill, Josef Lichtmannegger, Brigitte Megerle, Gabriele Mettenleiter, Claudia-Mareike Pflüger, Dr. Bastian Popper, Tamara Rieder, Claudia Schönichen, Dr. Karl Kenji Schorpp, Dr. Sabine Schulz, Dr. Christine von Törne, Dr. Michelle Vincendeau, Anita Wagner and PD Dr. Karl-Heinz Weiss.

In detail, their assistance refers to:

| | |
|---|---|
| Adamski, Jerzy: | Advisory supervision and examiner of the Technical University Munich. |
| Aichler, Michaela: | Introduction into electron microscopy and support on immunohistochemistry. |
| Busch, Dirk: | Advisory supervision of the Technical University Munich. |
| DiSpirito, Alan A.: | Isolation of MB from *Methylosinus trichosporium* OB3b. |
| Eberhagen, Carola: | Support on electron microscopy and cell culture experiments. Introduction into isolation of mitochondria from cell culture. |
| Feuchtinger, Annette: | Analysis of immunohistochemistry stainings for COX17 of rat liver tissue. |
| Grill, Peter: | Determination of copper concentrations in animal and cell culture samples. |
| Lichtmannegger, Josef: | Support on animal handling and care, isolation of mitochondria from rat liver and measurement of ATP production, and support on subfractionation of isolated rat liver mitochondria. |
| Megerle, Brigitte: | Support on rat handling and breeding. |
| Mettenleiter, Gabriele: | Introduction into electron microscopy. |

Pflüger, Claudia-Mareike: Immunohistochemistry staining for COX17.

Popper, Bastian: Support on electron microscopy.

Rieder, Tamara: Support on rat handling, care and genotyping.

Schönichen, Claudia: Bachelor student of the AG Zischka: established knockdown of *COX17* in HepG2 cells.

Schorpp, Karl Kenji: Introduction into analysis of immunofluorescence staining of HepG2 cells using Operetta system.

Schulz, Sabine: Introduction into the simultaneous measurement of the mitochondrial transmembrane potential, mitochondrial permeability transition and polarisation experiments.

Törne, Christine von: Mass spectrometry of isolated rat liver mitochondria.

Vincendeau, Michelle: Supervision of knockdown and overexpression of *COX17* in HepG2 cells.

Wagner, Anita: Introduction into immunoprecipitation of COX17 from isolated rat liver mitochondria.

Weiss, Karl-Heinz: Provided human WD liver tissue samples.

Zischka, Hans: Advisory supervision in all aspects of the manuscripts as well as of this thesis.

# Proof of figures and tables taken from published articles

### Figure 1-1

Taken from Gitlin, JD (2003) Wilson disease. Gastroenterology, 2003. 125(6): p. 1868-77, with kind permission. License number: 3892880516121 and 3892880095081.

### Figure 1-3

Taken from Gazmuri RJ, Radhakrishnan J. (2012) Protecting mitochondrial bioenergetic function during resuscitation from cardiac arrest. Critical care clinics. 2012 Apr;28(2):245-70, with kind permission. License number: 3917811434269.

### Figure 1-4

Taken from Cobine PA, Pierrel F, and Winge DR, (2006) Copper trafficking to the mitochondrion and assembly of copper metalloenzymes. Biochim Biophys Acta, 1763(7): p. 759-72, with kind permission. License number: 3892900543024.

### Figure 3-5A

Adapted from Grebowski J, Krokosz A, and Puchala M, (2013) Membrane fluidity and activity of membrane ATPases in human erythrocytes under the influence of polyhydroxylated fullerene. Biochim Biophys Acta, 1828(2): p. 241-8.

### Figure 3-2 – Figure 3-5, Figure 3-7 – Figure 3-11, Figure 3-13 – Figure 3-18, Table 3-2, Supplementary Table 1, Supplementary Table 2

In parts taken and adapted from Lichtmannegger J, **Leitzinger C**, Wimmer R, Schmitt S, Schulz S, Kabiri Y, Eberhagen C, Rieder T, Janik D, Neff F, Straub BK, Schirmacher P, DiSpirito AA, Bandow N, Baral BS, Flatley A, Kremmer E, Denk G, Reiter FP, Hohenester S, Eckardt-Schupp F, Dencher NA, Adamski J, Sauer V, Niemietz C, Schmidt HH, Merle U, Gotthardt DN, Kroemer G, Weiss KH, Zischka H. (2016) Methanobactin reverses acute liver failure in a rat model of Wilson disease. J Clin Invest (2016) 126(7):2721-35, with kind permission. License number: 3962931389301.

# Acknowledgements

Most notably, I would like to thank all my advisors for their great support and discussion of this thesis.

Special thanks to PD Dr. Hans Zischka who gave me the opportunity to do my PhD with this very interesting topic in his group. Further, I would like to thank him for getting the possibility to collect experience in animal handling and to get more insight into toxicology by taking part in the “Weiterbildung zur Fachtoxikologin der Deutschen Gesellschaft für Pharmakologie und Toxikologie”.

I would like to thank apl. Prof. Dr. Dr. Jerzy Adamski and Prof. Dr. Dirk H. Busch for their productive discussions during the thesis committee meetings. Thanks to apl. Prof. Dr. Dr. Jerzy Adamski and Prof. Dr. Martin Klingenspor for the examination my thesis.

Special thanks to all members of the working group: Josef Lichtmannegger and Carola Eberhagen for guiding my first steps in the lab of the AG Zischka and their gorgeous support on animal and cell culture experiments as well as electron microscopy; Claudia Einer, Sabine Schulz, Sabine Schmitt and Tamara Rieder for their great assistance on long days of animal experiments and discussions of my thesis, and Claudia Schönichen for her support on COX17 experiments. I really enjoyed working with you!

Further thanks to all collaboration partners: Dr. Michaela Aichler, Dr. Annette Feuchtinger, Gabriele Mettenleiter, Claudia-Mareike Pflüger and Dr. Bastian Popper for their support on electron microscopy and immunohistochemistry staining and evaluation for COX17; Alan A. DiSpirito for providing methanobactin; Dr. Christine von Törne for proteomic analyses of isolated rat liver mitochondria; Dr. Michelle Vincendeau for her great supervision on *COX17* studies; PD Dr. Karl-Heinz Weiss for providing human patient liver samples; Peter Grill for measurement of metal content in several samples; and Anita Wagner, Dr. Simone Woods and Dr. Karl Kenji Schorpp for scientific support. In place of all colleagues who supported animal handling, I would like to say thank you to Brigitte Megerle.

Finally, very special thanks to my family for believing in me, supporting me all the time and for relaxing in the right moments. Especially, thank you: Stephan, for the great distraction from mitochondria during our wonderful weekends, trips and holidays and your assistance and suggestions for Microsoft Office issues. Most importantly, I thank Marcel and Stephan for their patience to read this work!